Multiscale Corner Detection Based on Wavelet Transform and Scale-space Theory

Gao Xinting

School of Electrical & Electronic Engineering

A thesis submitted to the Nanyang Technological University
in fulfillment of the requirement for the degree of
Doctor of Philosophy

2007

Statement of Originality

I hereby certify that the work embodied in this thesis is the result of original research done by me and has not been submitted for a higher degree to any other University or Institute.

....

Date Gao Xinting

Acknowledgements

First and foremost, I would like to express my sincere appreciation to my supervisor, Dr. Farook Sattar, and co-supervisor, Dr. Ronda Venkateswarlu, for their guidance, encouragement and support at every stage of my Ph.D study. I would also like to thank NTU for providing me the scholarship and the nice facilities and environment to do the research.

I am grateful to my first year examination panels, Dr. Yoon Soon Fatt, Dr. Alex Chichung Kot, Dr. Chau Lap Pui and Dr. Leedham Braham for their contributing useful discussion regarding the topic of my Ph.D project. I would like to thank Dr. Yu Zhuliang, Dr. Azhar Quddus, Dr. Eric Sung, Dr. Yap Kim Hui and Dr. Jiang Xudong for their supports and encouragements on my research.

It's my pleasure to thank all the staffs and labmates in Workstation Resource Lab and Media Technology Lab for providing continuous assistance and friendly research environment. I would like to take this opportunity to thank Dr. Yu Dan, Dr. Moe Pwint, Dr. Gan Lu, Dr. Gan Tong, Dr. Wei Yongmei, Mr. Jin Guosheng, Mr. Zhang Wenbo, Mr. Kong Hui, Dr. Liu Mingchun, Ms. Yan Hong and Ms. Wang Zheng for their friendships and helps during my whole graduate studies. A special thank goes to my friends whom I call "lunch group" members: Dr. Wang Haiyun, Mr. Qiu Gang, Dr. Zhang Jianguo, Mr. Lian Naixiang, Mr. Tian Jing, Ms. Wu Kui, Mr. He Yu, Mr. Zhu Jiaqi and Ms. Li Zhenyan. Thank them for the happy lunch time and encouragement they have given to me.

Appreciation is also extended to all my friends for their friendship and care.

If I forget to mention the names that should appear here, please forgive me. I put all my efforts in writing this thesis these days. I will remember all of you along my life.

Last but not least, I would like to thank my families, my parents, my brother, my husband and my son, whose love and support are always the greatest inspiration for me. I began my Ph.D study when my son was less than nine months. Without my parents' help on caring him, I cannot imagine the appearance of this thesis today. This thesis is dedicated to them.

Summary

Being the front-end processing of a large amount of computer vision and image processing systems, corner detection is useful and important in the sense that it has a great impact on the following processing and consequently the performance of the whole system. In this thesis, we focus our research on the *contour based corner detection* (CCD) methods and *direct intensity computation based corner detection* (DICD) methods. Five algorithms are proposed, which partially or wholly solve three problems, i.e., (1) incomplete information; (2) delocalization; and (3) multiple responses to higher order structures.

For the CCD methods, the thesis provides an overview of the existing corner detection methods for contour images covering classification, comparison and performance evaluation.

Based on the review, we propose two algorithms of CCD, **Algorithm I**, the global natural scales based method and **Algorithm II**, the local natural scales based method. First, the orientation function of the input contour image is computed. Second, the dyadic *wavelet transform* (WT) are applied to the orientation function. Then the points correspond to *wavelet transform modulus maxima* (WTMM) at different scales are taken as corner candidates.

For the global natural scales based method, all scales are defined as natural scales for corner detection. For each corner candidate, the sum of the corresponding normalized WTMM at all the natural scales is used as significance measure of the "cornerness".

For the local natural scales based method, the scale at which the maximum

value of the normalized WTMM exists is defined as its "local natural scale", and the corresponding modulus is taken as its significance measure.

The utilization of the complete information makes the performance of the proposed detectors independent to the type of input images. The decomposition scales of the WT is restricted by the contour length, which makes the algorithm adaptable for both long contours and short contours. Both subjective and objective evaluation illustrate better performance of the proposed corner detectors compared to the conventional methods.

For the DICD methods, **Algorithm III** solves three problems existing in the well-known Harris detector. First, it works in the scale-space domain, so it detects corners belonging to different scales instead of a certain scale. Second, only one parameter needs to be set instead of three parameters needed in Harris method. Third, delocalization is a well-known inherent drawback of Harris corner operator. And it will increase with the scale at which it operates. The proposed algorithm solves the problem by detecting the corners from small scale to large scale, then track back from large scale to small scale. As the delocalization in the smallest scale can be ignored, the proposed method obtains the accurate localization. This proposed multiscale scheme can also be applied to other spatial corner detectors to improve their performances. The simulation results demonstrate the improved performance of the proposed method compared with Harris detector and SUSAN detector.

WT is a tool that can provide multi-scale analysis while analyzing the local behavior of a signal. Log-Gabor wavelets are known for their good localization and orientation in the time-frequency domain. Furthermore, they provide the shape and orientation information of local structures directly. Two algorithms

based on log-Gabor WT are proposed in this thesis. In the proposed algorithms, the input image is decomposed at multiple scales and along several directions.

For **Algorithm IV**, the sum of the magnitudes at all the decomposed scales are taken as the measurement. The measurement along the direction that is orthogonal to the gradient orientation represents the "cornerness" measurement.

To obtain the isotropic response, we propose **Algorithm V**. After the decomposition of log-Gabor WT, the magnitudes along all decomposed directions and scales are computed into the second moment matrix. Then the smaller eigenvalue of the second moment matrix is taken as the "cornerness" measurement.

The visual evaluation illustrates good performance of the proposed algorithms compared to Harris and Kovesi's detectors.

Finally, the proposed DICD methods (Algorithm III-V) are evaluated in a classical stereo matching system, compared with Harris detector and Kovesi's detector. The proposed Algorithm V achieves the best performance.

Contents

List of Figures

List of Tables

List of Abbreviations

Abbreviations	**Full expressions**
CCD	Contour based corner detection
DICD	Direct intensity computation based corner detection
WT	Wavelet transform
WTMM	Wavelet transform modulus maxima
2D	Two-dimensional
1D	One-dimensional
SVD	Singular value decomposition
Eq.	Equation
Fig.	Figure
Eff	Efficiency
Fid	Fidelity
CWT	Continuous wavelet transform
DWT	Discrete wavelet transform
HVS	Human visual system
SNR	Signal to noise ratio
LGWTOI	Log-Gabor wavelet transform and orientation information (based corner detection)
LGWTSMM	Log-Gabor wavelet transform and second moment matrix (based corner detection)
MWTMM	Modified wavelet transform modulus maxima
ROC	Receiver operating characteristic
ZNCC	Zero-mean normalized cross correlation
RANSAC	Random sample consensus

List of Symbols

Symbols	Meaning
$'$	First derivative
$''$	Second derivative
$\lvert \cdot \rvert$	Norm operator
$\times$	Multiplication
$\sum$	Sum
max	Take the maximum value among the set
tan^{-1}	Arc tangent
$*$	Complex conjugate
$\circledast$	Convolution
$\cdot$	Dot product
Wf	Wavelet transform of f

Chapter 1

Introduction

1.1 Corner detection

"Corner point" has many analogous appellations in the literature, such as "interest point", "dominant point", "salient point", "significant point" and "key point" etc.. As a kind of low level image processing, corner detection is very important in many applications of computer vision and image processing. It usually is a front-end processing in a lot of feature based image understanding systems. Thus, the performance of corner detection has a great effect on the following processing and the whole system.

As a local feature of images, corner points are sparse and robust. Being sparse, they provide useful information and give important clues for shape representation and analysis. The corners indicate the presence and position of objects, narrowing down the search problem and making high-level interpretation of images easier [1]. Being robust, they are invariant to the changes of translation, rotation and scaling. They provide reliable clues regarding objects even

under occlusion and varying background [2, 3]. Since corner points, as a feature, have these good characteristics, corner detection has been paid more and more attention in recent years [4]. It has wide applications such as object recognition, shape representation, image interpretation and motion analysis [2, 4].

Although corner detection has many applications and have been studied for years, no mathematical or strict definition exists for "corner points" up till now. We select two typical definitions.

- High curvature points on the contour or junction of two or more straight-line edges;
- High intensity variation points [5].

From the above two definitions, we can see the difference. The first definition simplifies the 2D feature points (corner points) detection into 1D computation problem. It depends on the segmentation or edge detection. There is one kind of contour images that are directly suitable for this definition. For the second definition, it defines the corner points as the 2D features. The corners in the second definition may not belong to an edge, e.g., the single points or the high textured points. As a result, the second definition includes more points than the first one.

We categorize the existing corner detection algorithms into three types: template based corner detection, *contour based corner detection* (CCD) and *direct intensity computation based corner detection* (DICD). The first two types of methods are generally based on the first definition, while the third type of methods is based on the second definition.

- **Template based corner detector**

For the template based corner detectors such as in [6, 7], mathematical models for corner structures are set up first, then correlations between the models and the image are used to detect the corners. As the models cannot cover all types of corners that have different orientations and subtended angles, the performance is not satisfactory in practical applications. Consequently, this type of detectors is not explored in this thesis.

- **CCD methods**

A lot of researchers study the CCD methods. In this kind of methods, the input image is the contour image. For the gray level images, the preprocessing includes the segmentation, contour extraction and boundary tracking. Hence, the performance depends on the prior segmentation. But under the premise of perfect segmentation, this type of algorithms simplifies the following calculation and detection. Furthermore, it has some direct applications in computer graphics [8, 9]. We overview this type of algorithms in chapter 2, section 2.1. Based on the survey, **Algorithm I** and **Algorithm II** using *Wavelet Transform* (WT) is proposed in chapter 3.

- **DICD methods**

We call the third type as direct intensity computation based corner detection because this type of detectors does not depend on the edge detection or the mathematical templates that are necessary for the CCD methods and template based methods, respectively. It detects corner points directly from some computations. Usually, computations are based on the first or second derivative of the image, or the structure characteristics. This type of methods does not have the limitations of the other two types as described above. Besides the corners detected on edges, it also detects key points such as single impor-

tant points or high textured points. The existing state-of-the-art methods are reviewed in chapter 2, section 2.2. To solve the problems existing in the well-known Harris algorithm, we propose **Algorithm III** based on the scale-space theory in chapter 4. Utilizing the good localization and orientation properties of log-Gabor wavelets, **Algorithm IV** and **Algorithm V** based on log-Gabor WT is proposed in chapter 5.

As there is no strict mathematical definition for the corners, no unique performance evaluation method exists for corner detection algorithms. Besides the visual comparison, we adopt some objective evaluation for each detector. For the CCD methods, Rosin's evaluation method [10] is adopted to evaluate the proposed CCD methods, which takes the global optimal solution of the polygonal approximation as the ground-truth. For the DICD methods, we apply the proposed methods, Harris detector and Kovisi's method to the same stereo matching system [11] to evaluate the performance objectively in chapter 6.

As a summary, corner detection of still images is investigated in a multiscale frame in this thesis. Four algorithms based on WT and one based on scale-space theory is proposed. All the methods are evaluated visually first. For the CCD methods, Rosin's method is adopted to obtain the objective evaluation. The simulation results show the better performance of the two proposed CCD algorithms. For the three DICD methods, the application based evaluation is adopted to compare the performance of the proposed methods, Harris detector and Kovesi's detector. Each of the methods is put in a stereo matching system as a front-end processing. The results of the stereo matching system based on different corner detection algorithms are compared. Simulation results show the improved performance of the proposed methods.

1.2 Motivations

A good corner detector should make robust performance under the following criteria [12, 13].

- Completeness: the rate of the correct detections should be high, i.e., both the sharp corners and the subtle corners should be detected.
- Correctness: the rate of the false detections should be low.
- Single response: each corner should be detected only once.
- Localization: corner points should be well localized as close as possible to their true locations.
- Robustness: the corner detector should be effective with respect to noise.
- Easy setting of parameters: given a new task, it should be easy to tune the parameters to this task. Ideally, different categories of shapes should be correctly processed with no need to significantly modify the parameters.
- Low complexity: the fast computation makes it more practical in large image database applications.

Although many methods have been developed for corner detection, users are still eager for detectors with better performance. To achieve the above objectives, different algorithms are proposed in the literature. However, there are still some problems in the existing algorithms that limit the performance. There are three main problems investigated and solved in this thesis.

Problem I: Incomplete information

In the literature, most of the detection is based on the incomplete information. In practice, an image usually contains important details belonging to a range of scales [14]. Furthermore, between images of the same scene, they are usually related by the affine transform locally, and scaling is an important factor of the affine transform. Consequently, multiscale analysis is indispensable. However, in the existing multiscale methods, the detection either operates on one certain scale, or operates only based on the location information of the measurement in the scale-space domain. When the detection operates on a certain scale, some corners that are far away from the selected scale will not be detected. Moreover, the delocalization is usually severe when the selected scale is large. When the detection is only based on the location information of the measurement, the magnitude information of the measurement is wasted, which limits the performance of the detection. Therefore, we will explore better multiscale based algorithms in this thesis.

Problem II: Delocalization

Delocalization is a notorious problem, particularly for the best corner detector, Harris detector, operated at higher scales. It directly affects the performance of the following process. For the severe delocalization situation, the third problem (i.e., multiple responses to higher order structures) can not be avoided, even if post processing (i.e., non-maximum suppression) is adopted.

Problem III: Multiple responses to higher order structures

For the digital signal processing, the discretization and smoothing operations cause multiple responses even for the simplest corner structure (first order structure, e.g., "L" corners). To remove the multiple responses, non-maximum suppression is adopted as the post processing. However, for the higher order

structure of corners, e.g., "T","X" corners, the multiple responses will remain even after the post processing step. For example, Harris detector detects "L" corners only. For the higher order structures, e.g., "T", "X", it is found that Harris detector will process these structures as 2 and 4 "L" corners respectively. Combined with the delocalization effect, the multiple responses can not be avoided completely.

1.3 Objectives and contributions

In this thesis, we surveyed many of the existing corner detection methods of still images. For the CCD methods, the classification and comparison among various existing corner detection methods have not been addressed before. This thesis provides an overview of the existing CCD methods for contour images covering classification, comparison and performance evaluation. The advantages and disadvantages of each type of CCD method are also discussed. From this review, we can conclude that there are three important factors in contour corner detection which are inter-linked: the curvature estimation, the natural scale determination and the appropriate smoothing selection. Appropriate smoothing is necessary when determining the natural scale. The curvature estimation should be done at the natural scale with appropriate smoothing.

To solve the problem mentioned in the previous section, five algorithms are proposed in this thesis. **Algorithm I & II**: WT based corner detection on contour images using global natural scales (Algorithm I), and local natural scales (Algorithm II). These two algorithms belong to CCD methods. They solve the first problem, i.e., the incomplete information. **Algorithm III**: multiscale corner detection of gray level images based on scale-space theory. It is an improvement of the famous Harris detector. This algorithm solves the first two problems. **Algorithm IV & V**: log-Gabor WT based corner detection of gray level images. Algorithm IV detects corners based directly on the orientation information of the log-Gabor WT. In Algorithm V, the second moment matrix of the log-Gabor WT decomposition is constructed. Corners are detected using the computation of the second moment matrix. Algorithm IV and V solves all the three problems.

Algorithm I & II: Multiscale corner detection on contour images based on WT

We propose two algorithms of CCD: the global natural scales based method and the local natural scales based method. First, the orientation function of the input contour image is computed. Second, the dyadic WT are applied to the orientation function. Then the points corresponding to *wavelet transform modulus maxima* (WTMM) at different scales are taken as corner candidates.

For the global natural scales based method, all scales are defined as natural scales for corner detection. For each corner candidate, the sum of the corresponding normalized WTMM at all the natural scales is used as the significance measure of the "cornerness".

For the local natural scales based method, the scale at which the maximum value of the normalized WTMM exists is defined as the "local natural scale", and the corresponding modulus is taken as the significance measure.

The utilization of the complete information makes the performance of the proposed detectors independent to the type of input images. The decomposition scales of the WT is restricted by the contour length, which makes the algorithm adaptable for both long contours and short contours. Both subjective and objective evaluation illustrate better performance of the proposed corner detectors compared to the conventional methods.

Algorithm III: Multiscale corner detection of gray level images based on scale-space theory — an improvement of Harris detector

Algorithm III solves three problems existing in the well-known Harris detector. First, it works in the scale-space domain, so it detects corners belonging

to different scales instead of a certain scale. Second, only one parameter needs to be set instead of three parameters needed in the Harris method. Third, delocalization is a well-known inherent drawback of Harris corner operator. And it will increase with the scale at which it operates. The proposed algorithm solves the problem by detecting the corners from small scale to large scale, then track back from large scale to small scale. As the delocalization in the smallest scale can be ignored, the proposed method obtains the accurate localization. The proposed multiscale scheme can also be applied to other spatial corner detectors to improve their performances. The simulation results demonstrate the improved performance of the proposed method compared with Harris detector and SUSAN detector.

Algorithm IV & V: Multiscale corner detection of gray level images based on log-Gabor WT

WT is a tool that can provide multi-scale analysis while analyzing the local behavior of a signal. Log-Gabor wavelets are known for their good localization and orientation in the time-frequency domain. Furthermore, they provide the shape and orientation information of local structures directly. Two algorithms based on log-Gabor WT are proposed in this thesis. In the proposed algorithms, the input image is decomposed at multiple scales and along several directions.

For Algorithm IV, the sum of the magnitudes at all the decomposed scales are taken as the measurement. The measurement along the direction that is orthogonal to the gradient orientation represents the "cornerness" measurement.

To obtain the isotropic response, we propose Algorithm V. After the decomposition of log-Gabor WT, the magnitudes along all decomposed directions and scales are computed into the second moment matrix. Then the "cornerness"

measurement based on the second moment matrix is used to detect corners.

The proposed log-Gabor WT based algorithms improve the performance while solving the problems mentioned in the previous section: (1) detection based on incomplete information; (2) delocalization; (3) multiple responses to higher order structures. Algorithm IV is simpler and has lower computational load than Algorithm V, and the orientation information of the corners are obtained simultaneously. However, due to the isotropic response, the second moment matrix based method obtains the best performance among all the methods. The comparison with Harris detector and Kovesi's detector demonstrates the good performance of the proposed algorithms.

To give an objective evaluation, the proposed DICD methods (Algorithm III-V) are evaluated in a classical stereo matching system, compared with Harris detector and Kovesi's detector. The proposed Algorithm V achieves the best performance.

1.4 Organization of the thesis

The rest of the thesis is organized as follows.

Chapter 2 overviews most of the existing CCD and DICD algorithms. For CCD methods, the thesis classifies the existing methods based on the developing trends and characteristics of the algorithms into five types: (1) single scale based methods; (2) methods based on support region; (3) methods based on smoothing; (4) multiscale corner detection methods; and (5) methods that combine corner detection and polygonal approximation. The advantages and disadvantages of each type are discussed. Rosin's evaluation method is adopted to show the performance of the typical algorithms. For DICD methods, most of the state-of-the-art algorithms are surveyed.

In Chapter 3, the proposed two multiscale WT based corner detection algorithms for contour images are presented. A proposed boundary tracking is described first. Then the theoretical background of 1D WT and the fast implementation algorithm of dyadic WT is presented. The existing WT based corner detection technique is investigated in the following. After that, the proposed global natural scales based method and local natural scales based method is presented. The subjective comparison with the existing methods are presented. The quantitative evaluation using Rosin's method demonstrates the better performance of the proposed algorithms.

In Chapter 4, the multiscale corner detection is proposed based on scale-space theory. The scale-space theory is introduced first. The "cornerness" measurement based on the second moment matrix is computed in the scale-space domain. Then, a new thresholding scheme which based on the number of

detected corners at each scale is proposed to simplify the proposed algorithm. To solve the delocalization problem, we propose a tracking scheme. The corners are detected from small scale to large scale. Finally, for the corners that are detected at scales other than the first scale, we track back to the first scale. The subjective comparison between the proposed algorithm, SUSAN detector, and Harris detector is presented at last.

In Chapter 5, the log-Gabor WT is employed to decompose the gray level image at multiple scales and along several directions due to its good localization and orientation properties.

We first present the basic theory of the log-Gabor WT and its properties. In the following, the methodologies of the two proposed algorithms are described in detail. The comparison with Harris and Kovesi's detectors are shown finally.

In Chapter 6, we put each of the proposed algorithms for gray level images, Harris detector and Kovesi's detector in the same stereo matching system. The normalized 8-point algorithm given by Hartley and Zisserman is adopted [11] to compute the fundamental matrix. The results of the system demonstrate the performance of each corner detection method from the stereo matching application point of view.

The conclusion and discussions are given in Chapter 7.

Chapter 2

An Overview of Corner Detection Methods

We categorize the existing corner detection methods into three types: template based corner detection, *contour based corner detection* (CCD) and *direct intensity computation based corner detection* (DICD). As stated earlier, the template based methods is not practical. Thus, our review focuses on the CCD methods and DICD methods. Fig. 2.1 shows the categories of the existing methods.

In this chapter, section 2.1 is the review on the CCD methods. We present the review of DICD methods in section 2.2. Finally, a conclusion is given in section 2.3.

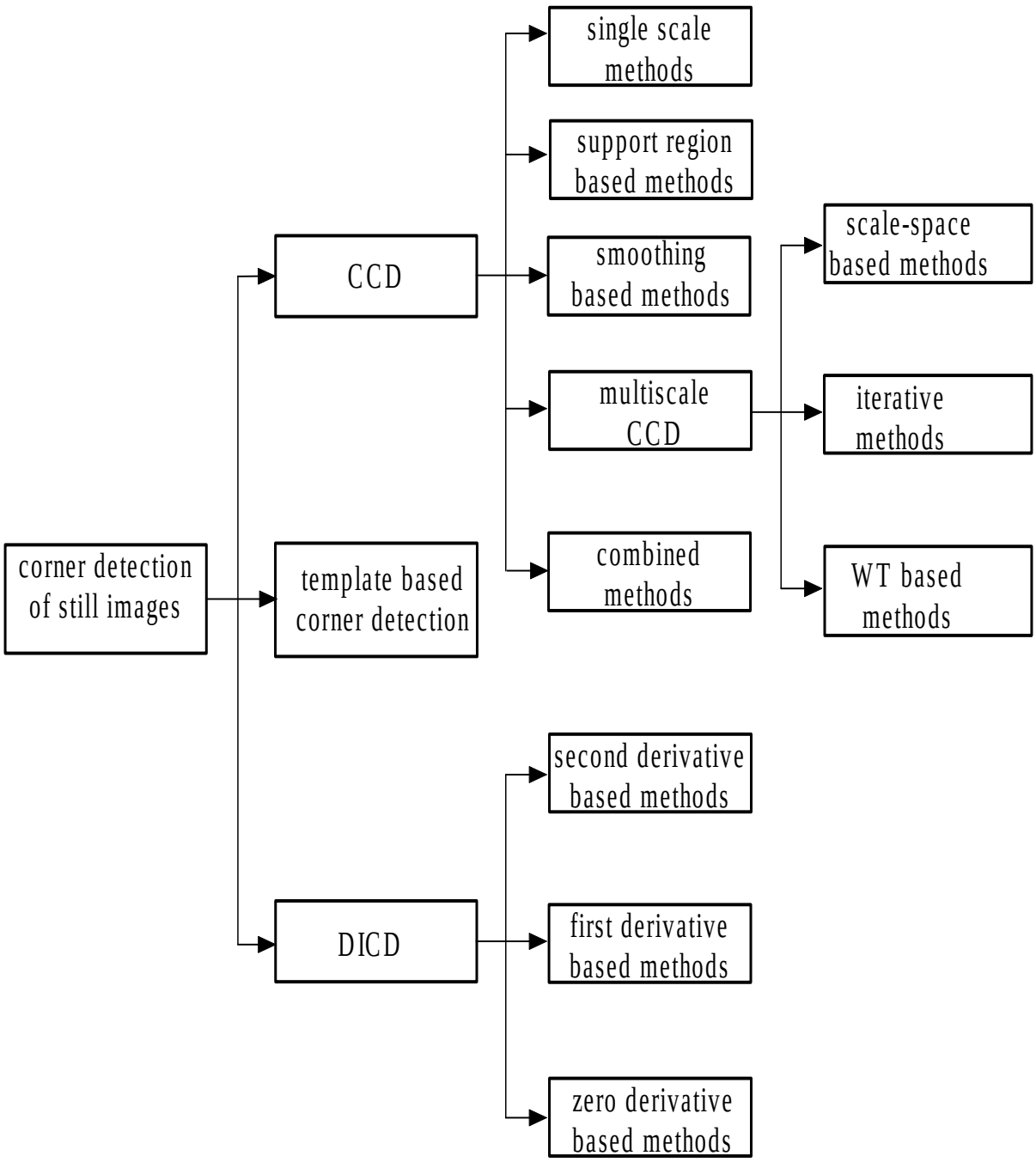

Figure 2.1: The proposed classifications of the existing corner detection methods of still images.

2.1 A review of contour based corner detection (CCD) methods

Although corner detection is an important issue in computer vision and image processing, the classification and comparison among various existing corner detection methods on contour images have not been addressed before. This section provides an overview of the existing corner detection methods for contour images covering classification, comparison and performance evaluation. The advantages and disadvantages of each type of methods are also discussed. From the review, we can conclude that there are three important factors in CCD which are inter-linked: the curvature estimation, the natural scale determination and the appropriate smoothing selection. Appropriate smoothing is necessary when determining the natural scale. The curvature estimation should be done at the natural scale with appropriate smoothing.

2.1.1 Introduction

In the seminal work [15], Attneave reaches the famous conclusion that information is concentrated along contours and further concentrated on the peaks of curvature points. Attneave's work motivates the research on CCD. Corners are defined as high curvature points along the contour. The local maxima of the absolute curvature are selected as corner points. As corners are sufficient to characterize a contour [16], the data are reduced enormously. Connecting the detected points by segments, the original contours can be approximated while very few points need to be saved.

Corner points are local features that can represent 2D shapes well. There

are two ways to represent shapes: region-based methods and boundary-based methods. The boundary-based methods have two advantages. Firstly, human visual system can recognize an object from the shape of its boundary since information of a shape is concentrated along contours [15]. Consequently, the boundary-based representation is concise and sufficient. Secondly, The information is further concentrated on the peaks of curvature points, i.e., corner points. The representation based on corners works well even under partially occluded situations. Consequently, corner points representation is more suitable for 2D shape analysis. 2D shape analysis is an important and difficult task in computer vision and image processing. It has many applications such as object matching, recognition, data compression and characterization of biological shapes etc. [17, 18, 2, 19, 20, 21, 22, 23]. Therefore, CCD is important and useful.

Corner detection and polygonal approximation are two ways to obtain the dominant points of contours. Polygonal approximation uses a number of piecewise segments to approximate the original curves. The approximation is subjected to certain constraints on the goodness of fit [24]. The vertices of the polygon are the dominant points. However, the result is usually dependent on the setting of initial points [25] or the expected number of corners. Dominant points obtained by polygonal approximation methods are usually not high-curvature points [26]. Thus they are sensitive to orientation and scaling [27, 28]. On the other hand, the dominant points obtained through corner detection are more robust representation of the 2D curves. Generally speaking, polygonal approximation methods require large memory and are computational prohibitive [29]. They may not work well for a smooth or curved boundary because so many segments are needed [30]. In this thesis, we investigate the corner detection meth-

ods for the contour images while ignore the polygonal approximation methods.

As no strictly mathematical definition of curvature exists in the discrete domain and quantization error affects the estimation, the performance of corner detection relies on the accuracy of both the curvature estimation and the scale estimation. A good curvature estimation should be measured in the spatial extent corresponding to its scale. The appropriate smoothing is necessary to remove the quantization error and noise while estimating the curvature and scale. In the review, we will see that every method tries to optimize some or all of the three factors: curvature estimation, scale determination, and smoothing factor estimation.

In this section, we survey most of the typical existing CCD methods and classify them into five types: (1) single scale based methods; (2) methods based on support region; (3) methods based on smoothing; (4) multiscale corner detection methods; and (5) methods that combine corner detection and polygonal approximation. The state-of-the-art methods of each type are introduced. Their advantages and disadvantages are discussed in the following. Rosin's evaluation method [10] is adopted to show the performance of the typical algorithms.

The rest of the section is organized as follows. In subsection 2.1.2, the related background is given. The existing methods are divided into five types and discussed respectively in subsection 2.1.3-2.1.7. Subsection 2.1.8 gives an evaluation of some typical methods of each type using Rosin's measurement. The summary is given in subsection 2.1.9.

2.1.2 Related topics

Definition of the curvature

Although the curvature has a clear definition in the continuous domain, no strictly mathematical definition can be found in the discrete domain. Different types of definitions in the continuous domain are used to estimate the curvature in the discrete domain. As in [31], there are three ways to calculate the curvature in the continuous domain. These definitions are as follows, where k represents the curvature of the curve, $f(t) = (x(t), y(t))^T$, with the path-length parameter, t.

1. Orientation based curvature.

$$k(t) = \theta'(t) \tag{2.1}$$

where θ is the angle between the tangential line and the x-axis.

2. Path based curvature.

$$k(t) = \begin{cases} +|f''(t)| & : \quad contour\ locally\ convex, \\ -|f''(t)| & : \quad contour\ locally\ concave. \end{cases} \tag{2.2}$$

where $|\cdot|$ represents the norm operator. For the general case, replace the parameter t with the arbitrary variable u.

$$k(u) = \frac{x'(u)y''(u) - x''(u)y'(u)}{(x'(u)^2 + y'(u)^2)^{3/2}}. \tag{2.3}$$

3. Osculating circle based curvature.

$$k(t) = \begin{cases} +\frac{1}{r(t)} & : \quad contour\ locally\ convex, \\ -\frac{1}{r(t)} & : \quad contour\ locally\ concave. \end{cases} \tag{2.4}$$

Here, r is the radius of the osculating circle that touches $f(t)$ at t.

Since the definition 3 is only suitable for the curves whose arcs are large and of constant radius [31], it is not widely used in contour corner detection. A large number of corner detection methods utilizes either definition 1 or definition 2.

Due to the 4 or 8 connectivity based quantization, the accurate determination of the curvature is not possible in the discrete domain. Therefore, different approaches are applied to improve the estimation accuracy of the discrete curvature.

Natural scales

In [14], Koenderink proposes that the relevant details of images exist only over a range of scales that is restricted by the outer scale (the coarsest scale) and the inner scale (the finest scale). And visual perception treats images on several levels of resolutions simultaneously. The work in [14] motivates the research on multiscale analysis of images. However, on one hand, multiscale representation is usually cumbersome; on the other hand, curves may contain a variety of structures at different scales and most operators work best at the appropriate scales for each of the structures [32]. These problems arouse the research on natural scale analysis of curves [17, 32, 33, 34]. In the literature, natural scales are defined as the scales that contain most or all of the significant information.

In [32], Rosin claims that a local natural scale method works better than a global natural scale method if the curves contain structures of different sizes at different locations. So, it has been proposed in [32] to analyze the curves in the spatial extent that corresponds to the natural scales.

2.1.3 Single scale methods

Denote the input sequence of the contour as follows.

$$p_i = (x_i, y_i) \ , \ i = 1, 2, ..., N.$$

The forward and backward k-vectors at p_i are defined as

$$\vec{a}_{ik} = (x_i - x_{i+k}, y_i - y_{i+k}), \quad \vec{b}_{ik} = (x_i - x_{i-k}, y_i - y_{i-k}). \tag{2.5}$$

In [35], Rosenfeld and Johnston define the k-cosine at p_i as

$$c_{ik} = \frac{\vec{a}_{ik} \cdot \vec{b}_{ik}}{|\vec{a}_{ik}||\vec{b}_{ik}|}. \tag{2.6}$$

Thus, c_{ik} measures the subtended angle between $\vec{a}_{ik}$ and $\vec{b}_{ik}$, i.e., approximates the change of the tangential angle at the ith point.

To select an appropriate value of k, an upper limit, $m = [N/10]$ or $[N/15]$, is set beforehand. For the ith point , k should be

$$c_{im} < c_{i,\ m-1} < \cdots < c_{i,\ k} \geq c_{i,\ k-1}. \tag{2.7}$$

The k-cosine is taken as the significance measure to detect the corner points. The non-maximum suppression is applied adaptively in the post processing according to the support region k .

From the above description, we can see that the support region is determined from large value to small value of the significance measure, c_{ik}, while an upper limit of the support region is set in advance. It may result in the incorrect determination of support region and large support region within the upper limit is preferred. These are the possible reasons why this type of methods are considered as single scale methods in the literature.

In [36], Rosenfeld and Weszka improve Rosenfeld-Johnston's method [35]. The significance measure is estimated from the averaged cosine values in the region $[k/2, k]$. The smoothing process improves the robustness of the algorithm, but the problems with the measure of the support region in [35] still exist in [36].

Freeman and Davis estimate the curvature from the change of the tangential angle by computing the atan or acot from the backward k-vector, where $k = 5$ in [37]. The arms are determined separately and the significance measure includes the effects of the two arms of the angle and the smoothed curvature measurement. In [38], Beus and Tiu improve Freeman-Davis' algorithm by further restricting the upper limit of the two arms as a fraction of the total length of the contour and further smoothing the significance measure. In [39], the change of the angle is calculated from the inscribed triangle. The latter three methods need more than one input parameter.

Some methods apply the statistical and geometrical properties associated with the eigenvalue-eigenvector structure of sample covariance matrices. In [40], Anderson and Bezdek utilize the fact that the principal eigenspace is the unique line of best fit subjected to the least squared error constraint. Furthermore, the principal eigenspace is the tangent line of the curve. The corner detection is based on the change of the tangential angle. Including the threshold that is related to the smallest angle change taken as the corner, this algorithm needs four parameters. The upper limit of the support region, m, is defined in the range $[5, 15]$ in [40]. In [41], Ji and Haralick also apply the least-square line fitting from the covariance matrix of the sample to estimate the two orientations. Then covariance propagation theory is developed to estimate the variances for the estimated line parameter, i.e., the orientation. They further derive a test

statistic to perform the hypothesis testing. This algorithm needs to set the threshold and the context window length in advance. To obtain the statistical testing, the size of the context window can not be too small. This method also can not detect very curved line segments. Tsai *et al.* [42] develop a simple contour corner detector based on the smaller eigenvalue of the covariance matrix. It is observed that the smaller eigenvalue is proportional to the curvature of the curve. In this method, the support region of the covariance matrix is set to be 10. In [43], Yeh utilizes the eigenvector of the covariance matrix to estimate the tangential orientation of the curve. Then 1D *wavelet transform* (WT) is applied to detect the corner points. Although WT is a multiscale scheme to capture the local changes of signals, only the first scale decomposition of the WT is used in [43]. The threshold is determined from the mean and the deviation that are dependent on the complexity of the test objects. All the above covariance matrix based methods are single scale and the computation of the covariance matrix is high, especially when the eigenvalue and eigenvector need to be computed explicitly.

In [44], Wang *et al.* estimate the curvature from the bending value. It is based on the fact that the forward and backward vectors of a non-corner point will cancel each other, while they will enhance each other for the corner points. This algorithm needs to set the support region and the threshold. Basak and Mahata [45] apply a neural network to detect corners based on the information of the neighborhood. In [46], Zhang and Zhao apply a morphological operator to detect corners. Li and Chen [47] classify the points into five types based on the sharpness of the subtended angle and the length and smoothness of its two arms. Then they apply fuzzy reasoning to judge the corners. The support region is limited in a predefined range in [47]. In [48], Fischler and Wolf

systematically analyze the problem of curve partitioning with the reference of human preference. The deviation of the curve from a chord is taken as the significance measurement. The length of the chord is related to a particular scale. Since the length of the chord in [48] is fixed to either 10 or 20, we classify this algorithm into the single scale type.

The common drawback of the above methods is that all of them are single scale methods. The features describing the shape of a curve vary enormously in size and extent. There is seldom a well-defined basis for choosing an appropriate parameter corresponding to a particular feature size [49]. If the support region selected is too small, the algorithm will detect many superfluous corners; while if the support region is too large, some important corners will be missed. To overcome the above problem, two schemes are studied in the literature. One type is based on the support region, while the other one is based on multiscale analysis.

2.1.4 Methods based on the support region

The idea of the support region is first expressed by Langridge in [50]. Langridge points out that each boundary point should have its own view of the curve. A dominant point will have a view which constitutes a meaningful support region of the curve and will block the view of neighboring non-dominant points. In the seminal work [24], Teh and Chin explicitly emphasize the importance of the precise determination of the support region for corner detection. In this algorithm, the support region of a point is determined by the chord length of the support region and the ratio between the perpendicular distance to the chord and the chord length. To prove their idea that the accuracy of the support

region is more important than the accuracy of curvature estimation in corner detection, they compute three curvature measures: k-cosine, k-curvature and 1-curvature in the paper. Although the three curvature estimations obtain nearly the same results in the paper, for the 1-curvature measure, the post processing is quite complex. The most significant characteristic of this algorithm is that it does not need any input parameter, not even a threshold. But it is known that this algorithm is not robust to the noise. The computation load of the perpendicular distance to the chord is heavy. The test images used in the paper are simple and the lengths of the chain codes are short.

In [51], Ray and Ray apply k-cosine to determine the support region. The curvature estimation is the average of the k-cosine within the support region. In [52], Ray and Ray propose the conception of asymmetric support region. The left arm and the right arm of a support region is determined separately by the k-cosine value. This method is called k-l-cosine. The k-l-cosine is used as the curvature estimation. The algorithm tries to determine the support region accurately and naturally. However, the stop criterion is somewhat heuristic. In [27], Cornic observes that the ends of the support region are generally the high curvature points. He determines the support region for each point from the Freeman chain code. The number of times that each point is the left(right) end of the support region of other points are recorded as Left(Right)-Limit. The selection of dominant points is based on the Left(Right)-Limit instead of curvature. In [53, 54, 55], they compare the curve length with the Euclidean distance to determine the support region. In [53], the change of the tangential angle is computed from the support region. The local maxima of the change of the tangential angle are the corner points. In [54], Reche *et al.* determine the left arm and the right arm of the support region respectively. The significance

measure takes the cosine of the subtended angle weighted by the two arm lengths of the support region. In [55], Urdiales *et al.* compute the tangential angle from the support region. They estimate the curvature by the difference of the tangential angle. Wu applies bending value to determine the support region in [56]. The smoothed bending value within the support region is used to estimate the curvature. In [57], Guru and Dinesh apply the small eigenvalue of the covariance matrix to determine the left and right arms of the support region. They compute three features for each pixel: the size of the support region, the curvature that is the reciprocal of the angle constructed by the left and the right arm and the *limit value*, i.e., the number of times that this point is an end point of other pixels' support region. They use these three features to detect the corner points. In [16], Marji and Siy determine the left and right arms of support region separately. The sum of the squared perpendicular distance from all the points to the chord need to be computed, thus the method results in high computational cost. This method utilizes the *limit value* as the measure of corner significance too. The *limit value* measurement prefers long-arm corners. For the sharp but short-arm corners, it may not work well. To overcome this problem, a shape covering procedure is used. In the post processing, collinear points suppression is applied to eliminate the superfluous corner points. In [58], Wu analyzes the drawbacks of the earlier algorithms to determine the support region. In the earlier methods, the local maximum is taken as criterion to determine the support region [24, 51]. This criterion tends to find small support region. Wu proposes that the global maximum instead of the first local maximum should be used as the criterion to determine the support region. This paper can be taken as an improvement of [51]. In [29], Wu improves Teh-Chin's method for determining the support region. The initial length of the

current point's support region is set equal to the length of the support region of the previous break point. The k-cosine is taken as the curvature estimation.

The test data used in this type of methods are simple and short contours. Without smoothing, the estimations of both the support region and the curvature are sensitive to the quantization error or noise.

2.1.5 Methods based on smoothing

Smoothing is necessary to eliminate the false corners caused by the quantization error or noise. But too much smoothing will miss some important features and too little smoothing will result in superfluous corners detected. A few methods are focused on how to determine the appropriate smoothing factor.

In [59], Ansari and Huang analyze the advantages and disadvantages of the algorithms presented in [24] and [60]. They propose an adaptive smoothing method. The support region is determined by using Teh-Chin's method. Then a Gaussian filter with a width proportional to the support region of each point is applied to smooth out the superfluous details. On the smoothed contour, compute the k-cosine as the significance measure for each point. The main contribution of this method is that it applies an adaptive smoothing for each point according to its scale, i.e., support region. In [61], Saint-Marc *et al.* propose an adaptive smoothing scheme. The smoothing is controlled by the functions of gradients. This algorithm preserves the sharpness of the corners in the proposed scale-space. In [62], Chen and Chin apply partial smoothing splines to estimate a noisy boundary. They utilize the generalized cross-validation to determine the smoothing parameter and the corner locations. The statistical properties are extracted from the input sampled data rather than input *a priori*. This

method approximates a noisy boundary while preserving the sharpness of the corners. However, this method is computationally prohibitive. In [30], Sohn *et al.* use the constrained regularization to estimate the smoothing factor. In this method, the noise information must be known in advance. In [63], Sohn *et al.* improve the algorithm in [30]. They apply mean field annealing to remove the noise while preserving the sharpness of corners. However, the noise information is still necessary to be known as *a priori* input. In [64], Cong and Ma theoretically analyze the scale-space causality criterion and the corner enhancement criterion. They obtain a smoothing function that is developed from the integration of an exponential function. In this algorithm, constant deformation is applied to the corner points, while curvature deformation is used to smooth the noise. Thus, this method smoothes the boundary while preserves the sharpness of the corners. In [65], Ray and Pandyan present an adaptive smoothing algorithm based on the roughness of the curve. They start smoothing with the smallest window size and increase the window size until the variance of curvature starts decreasing.

Generally speaking, the determination of the smoothing factor in the above methods is computationally prohibitive.

2.1.6 Multiscale corner detection methods

An alternative approach to detect corners of different arm size and different subtended angle is based on multiscale analysis. There are three types of multiscale corner detection methods including the scale-space based method, the iterative method and the wavelet transform based method.

Scale-space based methods

In [49], Witkin develops the scale-space filtering technique by taking continuous scale parameters. Instead of describing the signal in one scale or in the natural scale, Witkin proposes to describe the signal along the continuous scales. The extrema or zero-crossings of the derivatives of the signal are qualitatively described in an organized way. Consequently, the behavior of the multiscale structures of the signal is characterized. Because of the good properties of the Gaussian function [66], most of the scale-space based methods use Gaussian function as the kernel.

In [67], Asada and Brady define the curvature primal sketch in the scale-space. It is the first time to describe the curvature along the boundary of the planar curve in multiple scales. However, this model based method can not handle well all the cases in practical applications. Mokhtarian and Mackworth utilize the zero-crossings in the curvature scale-space to represent and match planar curves in [28]. In [68] and [69], they further study and develop the renormalized curvature scale-space and resampled curvature scale-space. They analyze the advantages and disadvantages of each type of scale-space and propose the corresponding suitable applications. Since zero-crossings of the curvature only segment the curve into convex and concave parts, this method is not good for the smooth or curved boundary.

In [70], Ansari and Delp use the maxima of the absolute curvature in the scale-space to characterize the curve. Maxima that exist at a common range of scales are defined as the cardinal curvature points, which is often called as *stable criterion*. These points are applied as features in the partially occluded matching. The range of scales is taken as global natural scales in this algorithm.

In [71], Rattarangsi and Chin formulate the scale-space through the maxima of the absolute curvature. They analyze the behavior of the ideal corner models in the curvature scale-space. The scale-space is then transformed into a tree that represents corner points at different scales. A coarse-to-fine tree parsing technique is developed to detect the corner points. This method detect some false corner points due to the quantization error and the other reason that only the locations of the maxima is used. Instead of smoothing the curve to obtain the curvature scale-space, Pei and Lin smooth the curvature to obtain the curvature scale-space in [72]. They take the stable criterion as in [70] to detect the corner points. They also explain clearly how to track from coarse scale to the finest scale to get good localization and a fast convolution algorithm to get the curvature scale-space.

In [73], Ray and Ray improve Rattarangsi-Chin's work in [71] in implementing the scale-space. In [71], the Gaussian filters of different sizes are obtained by self convolution of one Gaussian function. The scale-space is constructed from the convolution of the curve with Gaussian filters of different sizes. Ray and Ray apply the associative property of convolution operation to get the scale-space curves by repeating convolution using a constant size Gaussian filter. This implementation way reduces the computational load of the Gaussian scale-space method. In [74], Xin *et al.* further study Rattarangsi-Chin's curvature scale-space. They utilize the END candidate in the scale-space as the index to guide the termination of the filtering process. The behavior of ARCs and Lines in the scale-space are also studied. However, the termination criterion is heuristic.

In [75], Li applies Fourier analysis to study the curve evolution properties. He proves that a repeated smoothing evolution with any kernel approaches

Gaussian-scale-based curve evolution as the repeated number increases. He further proves that the curve motion due to the exponential-based evolution is equal to the curvatures of the smoothed curve. The evolution number is controlled by the perimeter. The curvature is estimated from the motion in the coarsest scale. Although this method is robust to noise and scaling, it is a single scale method for each curve. In [76], Wang *et al.* utilize the fast B-spline WT to get the curvature scale-space. The corner points are detected at the coarsest scale but localized at the finest scale.

In [12], Mokhtarian and Suomela apply method of the contour corner detection in curvature scale-space on gray level images. They use Canny edge detector and contour tracking as the preprocessing steps. The corner points are detected at the coarse scale. The local maxima whose absolute curvature are above a threshold and twice as much as one of the neighboring local minima are taken as corner points. Then they track back to improve the localization. Although they take the advantages of denoising effect of scale-space, they detect the corners at one single scale for each contour. In [77], Mokhtarian and Mohanna improve the method of [12]. They smooth different length curves with different scales. For short contours, they apply a fine scale; while for the long contours, they use a coarse scale. This method detects different corners at different scales. But no clear criterion to differentiate the long contours from the short contours is presented in the paper. And no clear criterion is shown how to select the scales.

In [78], Fermüller and Kropatsch point out that the continuous scale-space representation is considerable overhead; while the discrete scale-space may lose coarse-scale structures due to the 1D smoothing. The discrete pyramid tech-

niques have limited resolutions and may suffer from the problem of undersampling. To overcome these drawbacks, they propose a hybrid algorithm that utilizes the mathematical relationships of curves in scale-space, while working on a discrete pyramid. The behavior of the corners in the scale-space is analyzed. Although this method is good in the sense of multiscale analysis, both the construction of the pyramid and the process of corner detection are complex and computationally prohibitive.

Iterative algorithms

In [79], each pixel is assigned a value of 0, 1, or -1 according to the type of curvature it has: no curvature, positive curvature and negative curvature respectively. At each iteration, the significance is calculated as the sum of its 8 neighbors and itself. The point that has a maximum value among its 8-neighbor window is taken as a corner candidate. The recursion stops when the number of detected corners are not decreasing. The advantage of this method is that it needs no input parameter.

In [80], Held *et al.* borrow the idea of polygonal approximation to build a hierarchical approximation of the contours. They first spit the curve through evaluating the curvature. The curvature is calculated from a smoothing of the differential of the chain code. In the merging step, they rank all the corner candidates according to the height in the triangle formed by the corner candidate and its two neighbor candidates. The candidate is deleted if its significance is smaller than the threshold. The criterion much resembles human perception in the sense that humans do not try to fulfill a certain error norm but rather attempt to capture the most relevant information. The process is relatively

unaffected by scale and orientation changes. Thus the results obtained by this algorithm much more resemble the results obtained by humans than the results of polygonal approximation do. However, the height of each candidate should be calculated for each iteration in this algorithm as the result is affected by the neighbor candidates. The computation load is heavy for this method.

In [81], Zhu and Chirlian propose several requirements for the corner detectors. They first transfer the contour into polar coordinates. Then the local maxima or minima are determined as "M" points. Between two adjacent "M" points, the distances from the contour to the chord connected by the "M" points are calculated. The local extrema are taken as "Γ" points. The "M" and "Γ" points constitute corner candidates. The significance measure is the area of the triangle formed by the candidate and its two neighbor candidates. A deletion process is utilized recursively according to the significance measure. The simulation on some real complex contour images is shown in the results. The drawback of this method is the high computational cost. Both the transfer of coordinates and the computation of heights are computational complex.

He and Yung propose a novel algorithm in [82]. Canny edge detector is used in the preprocessing steps to obtain the contour image. This method computes the curvature at a fixed low scale. The local extrema are taken as corner candidates. Then dynamic support region is determined to compute the adaptive local threshold to remove round corners. The angle of corner candidate is further calculated to suppress the false corners. The last step is iterated until it converges. The results in the paper are very promising. However, the determination of the fixed scale is not solved. Furthermore, three parameters need to be adjusted in the experiments.

WT based methods

As another multiscale analysis tool, WT analyzes the local properties of the signals well. *Wavelet transform modulus maxima* (WTMM) characterize the irregular structures of the signal. Consequently, it is suitable to detect contour corner points using WT.

In [83], Lee *et al.* analyze the behavior of four types of corner models in the wavelet domain. The orientation function, i.e., the tangential angle of each point, is first computed. Then the WT of the orientation function is performed at four scales. The WTMM is searched and chained together along the scale axis. By analyzing the WTMM, the corner points are finally detected. Both the location and the magnitude of the WTMM are used in the algorithm. This makes the detection more efficient. However, the model-based detection limits the practical applications and increases the computational cost. In [84], Lee *et al.* apply the quadratic spline dyadic WT that can be implemented by a fast algorithm. The point is considered as a corner candidate if its maximum persists from the first scale to the third scale and the magnitude at the third scale is above a threshold. Then each candidate is isolated and the ratio of the WT at another two coarser scales is computed. The corner candidate is confirmed as a corner point if its ratio is close to the ratio of an ideal corner. In this algorithm, the post processing step is somewhat complex. Moreover, all the corner points are detected at the same scales so that some corner points are missed in the results.

In [85] and [86], the properties of corners of 2D shapes are studied through the WT of the tangent orientation function. All the WTMM are taken as the features of detailed patterns in the two papers. This results in superfluous corner

points and high computation in the following learning and matching process. However, the analysis of the properties of corners characterized in the wavelet domain is quite meaningful.

In [17], Antoine *et al.* apply the WT directly to the coordinates of the 2D shape. The coordinates are represented as a complex function. The WTMM indicate the existence of corner candidates. The coarsest scale that an extremum lasts to is defined as its lifetime. They take the lifetime as the significance measure. Consequently, we can say that this method is only based on the position information. In [87], Hua and Liao apply the WT to the x and y coordinates separately. The values of the WTMM at the scale equal to or larger than 2^2 are recorded as the significance measure. We can see all the corners are detected in a single scale in this method. The wavelets with two vanishing moments are used in both [17] and [87]. This agrees with the curvature definition in Eq. (2.2) as the WT is a second order differential operator to a smoothed signal if the wavelet with two vanishing moments is used.

In [88], Quddus and Fahmy apply different wavelets to the orientation function in the contour corner detection. They reach the conclusion that wavelets with one vanishing moment are suitable for orientation based corner detection. Similar as stated earlier, WT is a first order differential operator to a smoothed signal if the wavelet with one vanishing moment is used. The conclusion in [88] agrees with the curvature definition in Eq. (2.1). In [89], Quddus and Fahmy improve the algorithm of [84]. The WT of the orientation function is performed at four scales and the coefficients are normalized to the maximum at each scale. The WTMM at the coarsest scale are taken as corner points if the values are above the first threshold, $\tau 1$. Then those WTMM are also detected as corners

if the values at the coarsest scale are above the second threshold, $\tau 2 (< \tau 1)$, and are increasing as the scales are decreasing. Finally, they check the WTMM at the first scale. The WTMM at the first scale also are recognized as corners if the values are greater than the third threshold, $\tau 3$. Although this method reduces some computation compared to the method in [84], the detection process is quite complex and somewhat heuristic. Although the method detects the corners at multiscales, it limits the detection within four scales, which may not be suitable for all the cases.

In [34], Quddus and Gabbouj propose a novel and efficient corner detection method using WT and *singular value decomposition* (SVD). The WT of the orientation function is performed first. Then SVD is used to detect the global natural scales in the wavelet domain. After that, the largest singular value is used in the reconstruction process and the significance measure is estimated from the average of all the global natural scales. The utilization of WT and SVD makes this method efficient and robust. They apply the method on the real and quite complicated fish contours and obtain satisfactory results in the paper. However, they have not considered the situation where the stop criterion for the selection of natural scales does not work. Moreover, the SVD increases the computational cost.

From the above description and analysis, we can see that most of the multiscale methods are operated on one or several selected global scales.

2.1.7 Methods that combine corner detection and polygonal approximation

As we stated earlier, polygonal approximation methods obtain the good fit of the original curve by connecting the piecewise segments. However, the vertices obtained may not be high curvature points and are sensitive to the initial setting. Although the corner detection methods get high curvature points, the approximation made by connecting the high curvature points may result in large approximation error. To utilize the advantages of both methods and overcome their drawbacks, some researchers apply corner detection as the preprocessing step of the polygonal approximation.

In [90], Leung and Yang fit two strips for each pixel by adjusting the orientation and width of the strips dynamically. The curvature is estimated from the subtended angle of the two strips. The ratio between the length and the width of each strip is computed. The significance is measured by the multiplication of the ratio and the curvature. In [60], two methods are proposed. In the first method, the boundary is smoothed by a Gaussian filter with fixed size. The local extrema of the curvature are used as the initial points of the following split-and-merge polygonal approximation algorithm. This method obtains the result that is insensitive to the orientation. In the second method, the cardinal curvature points that are stable to a range of scales are extracted in the feature extraction step. This method is robust to both orientation and scaling. However, some small desirable details may be deleted by the smoothing. In [18], Garrido *et al.* apply the polygonal approximation to get the corners at their natural scales. In this method, curvature scale-space is first constructed. Then they apply the polygonal approximation based on the corners detected at

the coarse scale. For the part where the error is high, they detect corners at finer scales. Finally, a merging algorithm is used to minimize the number of corners. In [23], an algorithm similar as in [18] is adopted for shape matching. The difference is that the curvature is calculated as the tangential difference. In [26], Horng applies Pei and Lin's algorithm [72] to detect the cardinal curvature points. Then a modified dynamic programming technique of Perez and Vidal's [25] is used to find the globally optimal polygonal approximation and reduces the computational load by searching the one-third of the segments instead of the whole segments. Compared to the algorithm in [18], this algorithm minimizes the fitting error without increasing the number of corners. Compared to the algorithm in [25], the number of vertices is automatically determined by the corner detection step.

The methods described in this subsection have taken the advantages of both corner detection and polygonal approximation. Thus the results keep both the geometric importance and good fitting quality. However, the computation load is prohibitive for all these methods. Another conclusion is that any good corner detection technique can be a good preprocessing step of this type of methods.

2.1.8 Objective comparison using Rosin's method

In this subsection, we apply Rosin's evaluation method [10] to test several typical corner detection algorithms. The chain codes of the test images are given in Appendix A.

There are a few objective evaluation methods for CCD algorithms. Rosin's evaluation method has two advantages compared with the other existing methods. First, it avoids the ground-truth definition. As no strictly mathematical

definition of corners exists, it is difficult to define the ground-truth for test images. Rosin's method takes the optimal results of the polygonal approximation as the reference so that no ground-truth is needed in the evaluation. Second, it formulates the measurements of both the efficiency (compression ratio) and the fidelity (error measurement) in one formula. Generally speaking, there is a trade-off between the efficiency and the fidelity for each algorithm. If we increase the number of corners detected, the efficiency is decreased, while the fidelity is increased and vice versa. Consequently, it is difficult to say which result is good from the two measurements. Rosin's evaluation considers these two measurements simultaneously.

The fidelity is computed as follows.

$$Fidelity = \frac{E_{opt}}{E_{appr}} \times 100 \tag{2.8}$$

where E_{appr} is the error of the polygonal approximation obtained for the detected corners when compared to the original contour, and E_{opt} is the error of the polygonal approximation incurred by the optimal algorithm with the same number of lines as the evaluated algorithm.

The efficiency is computed as follows.

$$Efficiency = \frac{N_{opt}}{N_{appr}} \times 100 \tag{2.9}$$

where N_{appr} is the number of corners detected by the evaluated method, and N_{opt} represents the number of lines that the optimal algorithm would require to produce the same error as the evaluated method does.

The optimal solutions are found using dynamic programming [25] run for all necessary values.

The merit of the corner detection is calculated as follows.

$$Merit = \sqrt{Fidelity \times Efficiency} = \sqrt{\frac{E_{opt}N_{opt}}{E_{appr}N_{appr}}} \times 100. \tag{2.10}$$

In Eqs. (2.8-2.10), the error can have various measures, such as integral square error, E_2; the area between the polygon and the original curve, E_1, and the maximum deviation between the polygon and the original curve, E_∞, etc.. In this paper, we apply the most popular ones of E_2 and E_∞.

$$E_2 = \sum_{i=1}^{n} e_i^2 \tag{2.11}$$

$$E_\infty = \max_{1 \le i \le n} e_i. \tag{2.12}$$

Here, i represents the index of the contour pixel and the error, e_i, is the perpendicular distance from a point of the original curve to the approximating polygon constructed by connecting the corner points.

The measurements of the typical existing good methods of each type using E_2 and E_∞ are listed in Tables 2.1 - 2.4 and Tables 2.5 - 2.8 respectively. In the tables, Eff represents efficiency, and Fid represents fidelity. The $Rank$ means the rank of the performance among the methods evaluated. The corresponding results are illustrated in Figs. 2.2 - 2.5.

From the results, we see that single scale methods do not provide good detection results. The Horng's algorithm [26] applies the Pei-Lin's corner detector [72] as preprocessing. The performance is improved, but it is still dependent on the performance of the Pei-Lin's corner detector. Marji-Siy's method [16] obtains good results, but it has not shown the results for the "figure-8" curve. Quddus-Gabbouj's method [34] also shows good performance except for the "figure-8" curve. The algorithm, used in [34] for selecting the natural scales using SVD, can not work for the "figure-8" curve. The length of the "figure-8" curve is 45

pixels and this may be the possible reason why Quddus-Gabbouj's method fails for this case. Although different methods, such as Cornic's method [27], Ray-Pandyan's method [65] and Pei-Lin's method [72] obtain the best results for a number of test curves, no algorithm can achieve good results for all test curves. He-Yung's method [82] achieves good results for all the curves. However, we need to adjust carefully the three parameters of the algorithm for the "simicir" curve.

2.1.9 Summary

Contour corner detection is an important task for 2D shape analysis. It has many useful applications, such as object matching, recognition, data compression and characterization of biological shapes, etc..

From the above analysis and discussion, we find that single-scale methods are generally simple but not effective. It is difficult to determine the parameters that are related with the scale or the smoothing factor.

The methods based on the support region can be regarded as local natural scale methods. But generally speaking, they are lack of a unified framework and the support region is determined on the raw data that is corrupted by the quantization error and noise. These methods are not robust especially for the complex images.

The methods using smoothing are more robust than the methods based on support regions. Some of the methods determine the global smoothing factor based on the *a priori* information of noise. However, this information is hard to know in practice. Some of the methods determine the smoothing factor

according to the support region. The performance of the latter methods is dependent on the accuracy of the support region.

For the multiscale methods, most of them are based on the global natural scales. They are not optimal for the individual points. Furthermore, the representations in the multiscale methods are generally redundant. Some methods only utilize the position information in the scale-space domain or wavelet domain, such as the life time and the behavior of the maxima lines in the scale-space domain or wavelet domain. Due to its characteristics and its robustness, wavelet should be a good tool for corner detection.

For those methods that combine the corner detection and polygonal approximation approaches, the performance is improved at the expense of huge computation.

From the review, we can say that it is important to estimate both the curvature and the natural scale accurately in contour corner detection. Due to the quantization error, it is necessary to apply appropriate smoothing in the estimation process. As a result, the main important issues involving in contour corner detection are the selection of the smoothing factor, the determination of the natural scale and the estimation of the curvature.

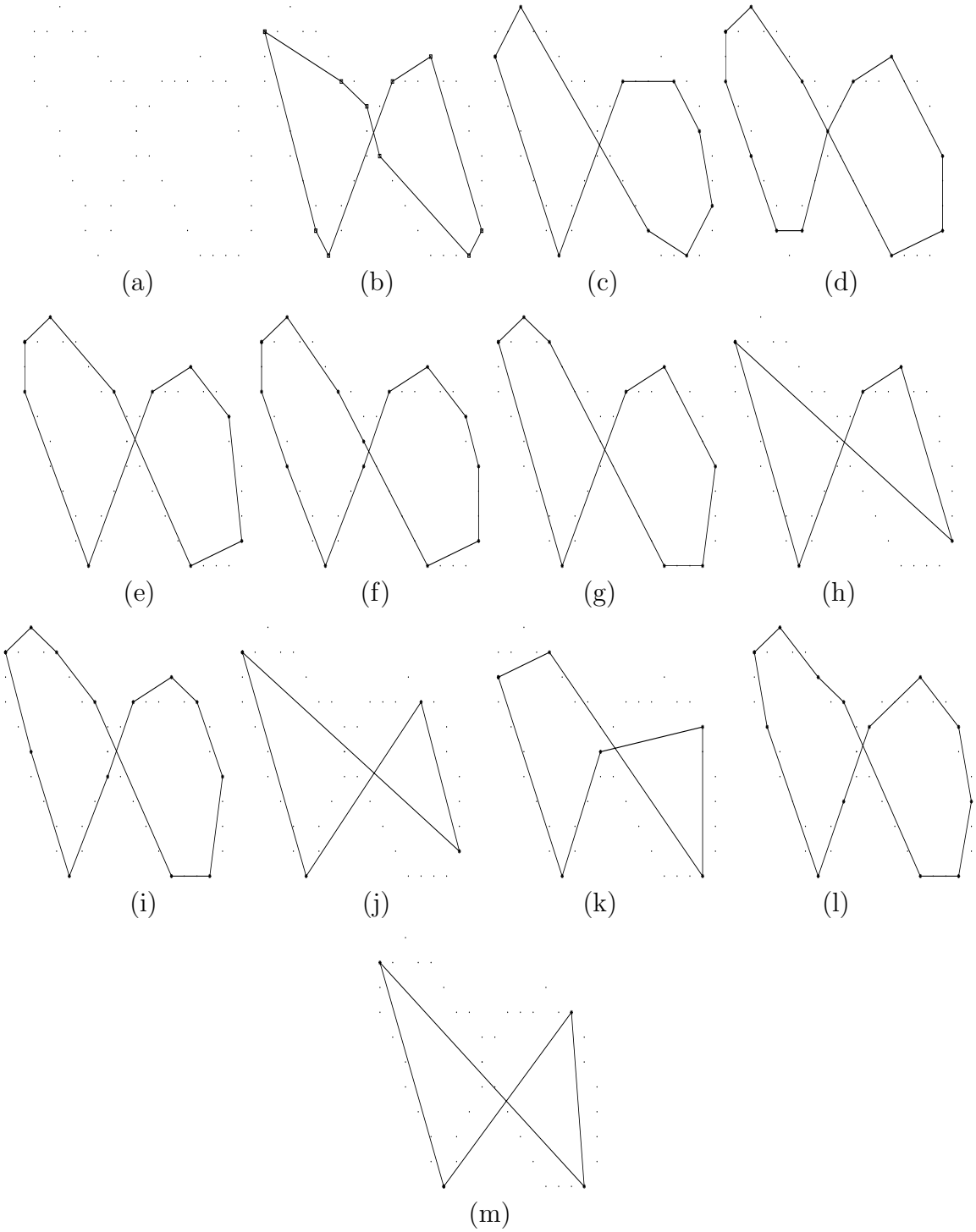

Figure 2.2: The results of the "figure-8" curve. The corners are indicated by '$*$' and connected into polygons. (a) Original curve, (b) Rosenfeld-Johnston73, (c) Anderson-Bezdek84, (d) Teh-Chin89, (e) Conic97, (f) Wu03, (g) Ray-Pandyan03, (h) Rattarangsi-Chin92, (i) Pei-Lin92, (j) Ray-Ray95, (k) Sankar-Sharma78, (l) Horng02, (m) He-Yung04.

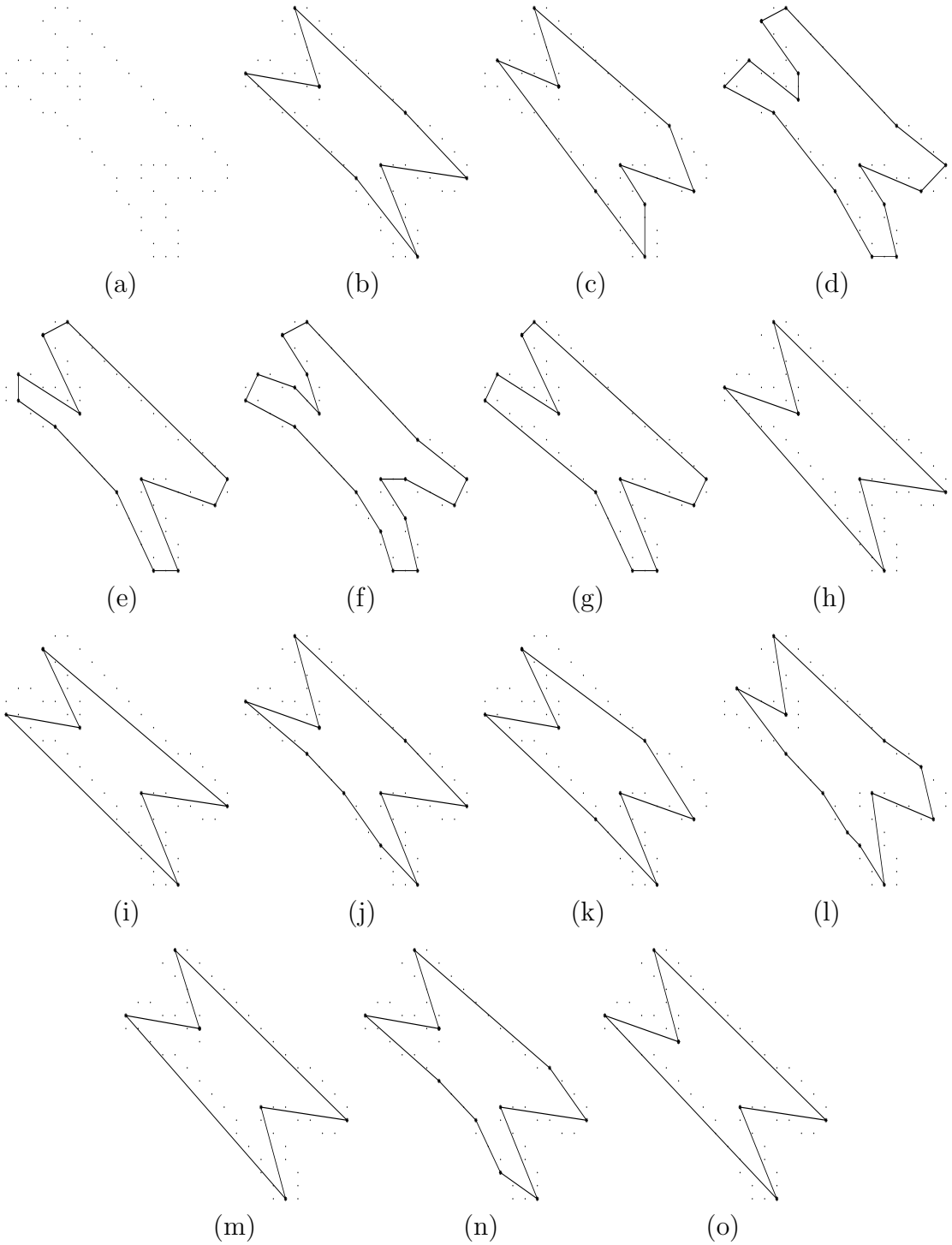

Figure 2.3: The results of the "chromosome" curve. The corners are indicated by '$*$' and connected into polygons. (a) Original curve, (b) Rosenfeld-Johnston73, (c) Anderson-Bezdek84, (d) Teh-Chin89, (e) Conic97, (f) Wu03, (g) Marji-Siy03, (h) Ray-Pandyan03, (i) Rattarangsi-Chin92, (j) Pei-Lin92, (k) Ray-Ray95, (l) Sankar-Sharma78, (m) Quddus-Gabbouj02, (n) Horng02, (o) He-Yung04.

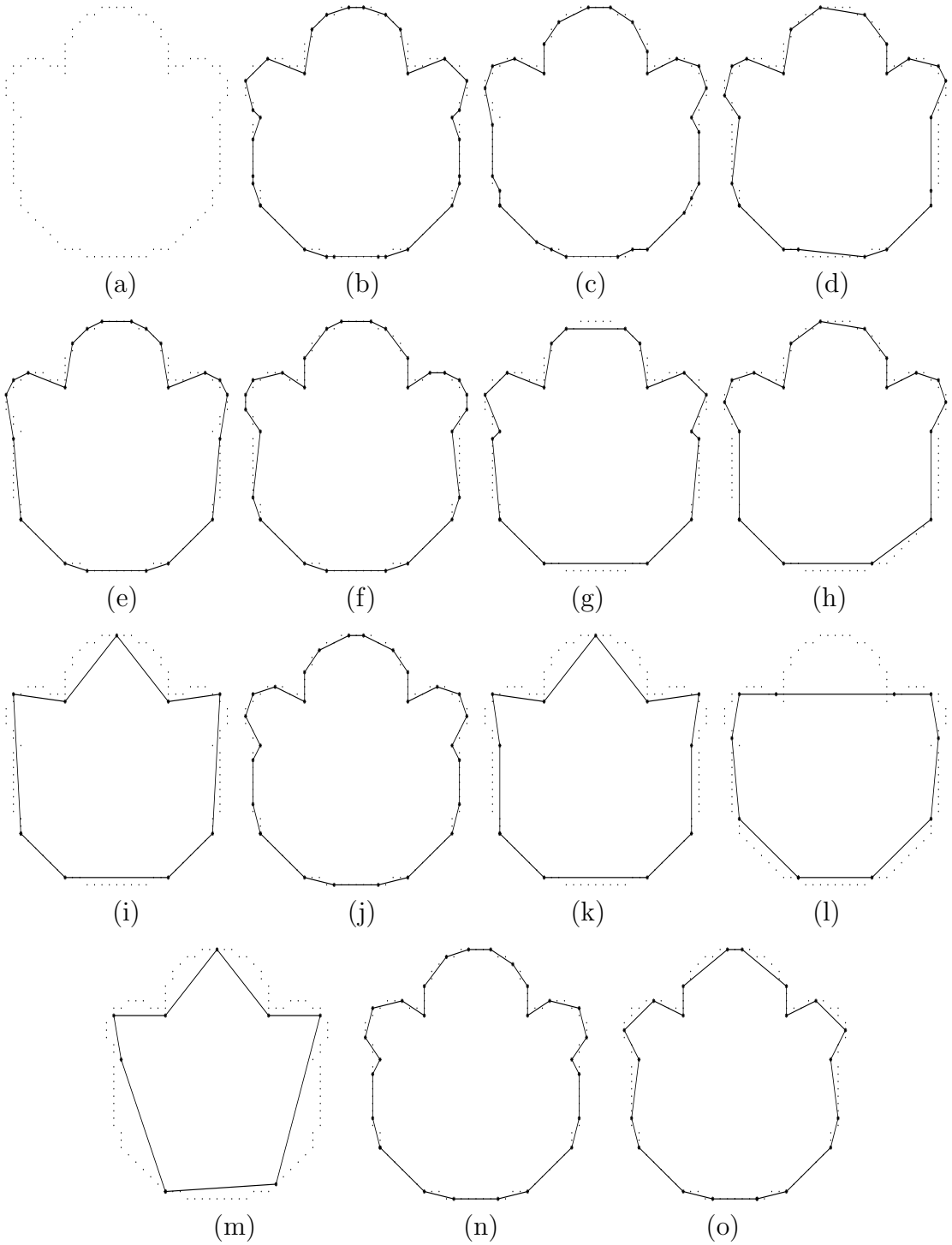

Figure 2.4: The results of the "semicir" curve. The corners are indicated by '$*$' and connected into polygons. (a) Original curve, (b) Rosenfeld-Johnston73, (c) Anderson-Bezdek84, (d) Teh-Chin89, (e) Conic97, (f) Wu03, (g) Marji-Siy03, (h) Ray-Pandyan03, (i) Rattarangsi-Chin92, (j) Pei-Lin92, (k) Ray-Ray95, (l) Sankar-Sharma78 , (m) Quddus-Gabbouj02, (n) Horng02, (o) He-Yung04.

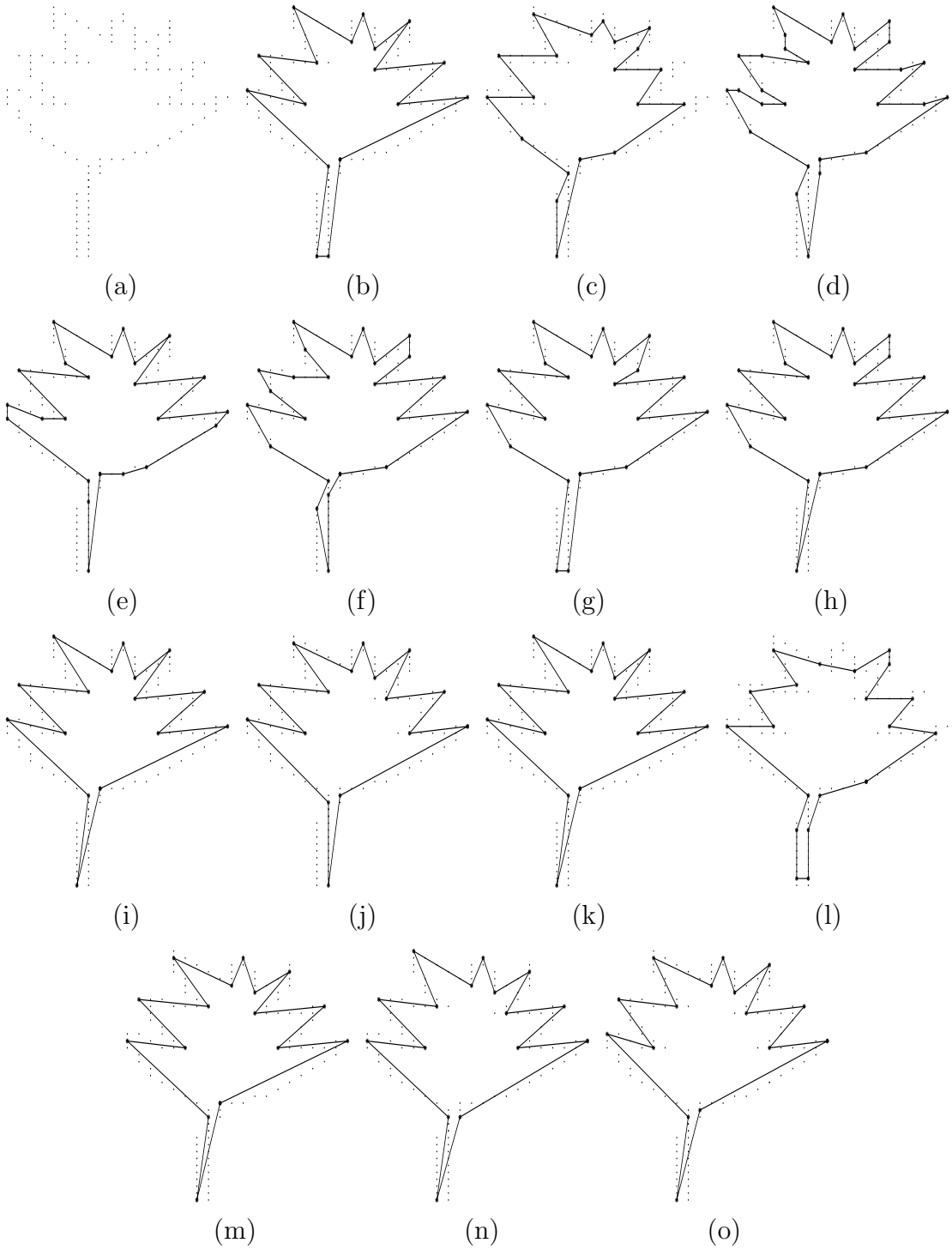

Figure 2.5: The results of the "leaf" curve. The corners are indicated by '$*$' and connected into polygons. (a) Original curve, (b) Rosenfeld-Johnston73, (c) Anderson-Bezdek84, (d) Teh-Chin89, (e) Conic97, (f) Wu03, (g) Marji-Siy03, (h) Ray-Pandyan03, (i) Rattarangsi-Chin92, (j) Pei-Lin92, (k) Ray-Ray95, (l) Sankar-Sharma78, (m) Quddus-Gabbouj02, (n) Horng02, (o) He-Yung04 .

Table 2.1: Quantitative results of the "figure-8" curve using E_2.

Algorithm	N_{appr}	N_{opt}	E_{appr}	E_{opt}	Eff	Fid	$Merit$	$Rank$
Rosenfeld-Johnston [35]	10	5.64	22.83	3.69	56.4	16.2	30.2	12
Anderson-Bezdek [40]	9	6.88	8.97	4.54	76.4	50.6	62.2	7
Teh-Chin [24]	13	7.98	5.93	2.04	61.4	34.4	46.0	11
Cornic [27]	10	9.28	4.30	3.69	92.8	85.8	89.2	1
Wu [29]	14	9.20	4.37	1.81	65.7	41.4	52.2	9
Marji-Siy [16]	-	-	-	-	-	-	-	-
Ray-Pandyan [65]	9	7.71	6.46	4.54	85.7	70.3	77.6	4
Rattarangsi-Chin [71]	5	4.21	49.48	32.21	84.2	65.1	74.0	5
Pei-Lin [72]	13	8.38	5.39	2.04	64.5	37.8	49.4	10
Ray-Ray [73]	4	3.81	72.26	54.18	95.3	75.0	84.5	2
Sankar-Sharma [79]	6	4.71	38.57	17.49	78.5	45.3	59.7	8
Quddus-Gabbouj [34]	-	-	-	-	-	-	-	-
Horng [26]	13	10.14	3.58	2.04	78.0	57.0	66.7	6
He-Yung [82]	4	3.81	72.82	54.18	95.2	74.4	84.2	3

Table 2.2: Quantitative results of the "chromosome" curve using E_2.

Algorithm	N_{appr}	N_{opt}	E_{appr}	E_{opt}	Eff	Fid	$Merit$	$Rank$
Rosenfeld-Johnston [35]	8	6.30	21.94	13.43	78.8	61.2	69.4	7
Anderson-Bezdek [40]	9	5.95	26.50	12.08	66.1	45.6	54.9	11
Teh-Chin [24]	15	10.86	7.20	3.80	72.4	52.8	61.8	8
Cornic [27]	12	9.63	9.57	5.82	80.3	60.8	69.9	6
Wu [29]	18	13.69	4.37	2.83	76.1	64.8	70.2	5
Marji-Siy [16]	11	9.53	9.96	7.06	86.6	70.9	78.4	4
Ray-Pandyan [65]	6	5.84	32.64	23.73	97.3	72.7	84.1	3
Rattarangsi-Chin [71]	6	5.32	61.42	23.73	88.7	38.6	58.5	9
Pei-Lin [72]	10	6.23	22.32	8.07	62.3	36.2	47.5	12
Ray-Ray [73]	8	5.40	56.83	13.43	67.5	23.6	39.9	13
Sankar-Sharma [79]	12	5.91	28.89	5.82	49.3	20.1	31.5	14
Quddus-Gabbouj [34]	6	5.88	30.33	23.73	98.0	78.2	87.6	2
Horng [26]	10	7.16	16.99	8.07	71.6	47.5	58.3	10
He-Yung [82]	6	5.96	26.05	23.73	99.3	91.1	95.1	1

Table 2.3: Quantitative results of the "semicir" curve using E_2.

Algorithm	N_{appr}	N_{opt}	E_{appr}	E_{opt}	Eff	Fid	Merit	Rank
Rosenfeld-Johnston [35]	30	20.16	8.85	2.64	67.2	29.8	44.8	11
Anderson-Bezdek [40]	29	22.69	6.43	3.00	78.2	46.7	60.4	4
Teh-Chin [24]	22	13.03	20.61	7.01	59.2	34.0	44.9	10
Cornic [27]	22	16.36	12.99	7.01	74.4	54.0	63.3	3
Wu [29]	27	19.60	9.42	3.70	72.6	39.3	53.4	7
Marji-Siy [16]	18	12.33	24.24	11.19	68.5	46.2	56.2	6
Ray-Pandyan [65]	18	11.12	31.56	11.19	61.8	35.5	46.8	9
Rattarangsi-Chin [71]	9	6.22	130.13	62.58	69.1	48.1	57.7	5
Pei-Lin [72]	26	24.00	5.32	4.05	92.3	76.1	83.8	2
Ray-Ray [73]	11	5.96	146.00	32.31	54.2	22.1	34.6	12
Sankar-Sharma [79]	10	4.15	769.53	33.92	41.5	5.1	14.5	14
Quddus-Gabbouj [34]	8	4.77	403.51	75.52	59.6	18.7	33.4	13
Horng [26]	26	25.05	4.59	4.05	96.3	88.2	92.2	1
He-Yung [82]	20	12.56	23.06	9.01	62.8	39.1	49.5	8

Table 2.4: Quantitative results of the "leaf" curve using E_2.

Algorithm	N_{appr}	N_{opt}	E_{appr}	E_{opt}	Eff	Fid	$Merit$	$Rank$
Rosenfeld-Johnston [35]	17	14.01	43.42	21.31	82.4	49.1	63.6	9
Anderson-Bezdek [40]	20	14.35	39.18	13.38	71.8	34.2	49.5	12
Teh-Chin [24]	29	19.05	14.96	5.72	65.7	38.2	50.1	11
Cornic [27]	23	16.14	25.84	9.46	70.2	36.6	50.7	10
Wu [29]	24	18.89	15.21	8.64	78.7	56.8	66.9	8
Marji-Siy [16]	21	19.54	14.15	11.91	93.0	84.2	88.5	3
Ray-Pandyan [65]	20	19.20	14.72	13.38	96.0	90.9	93.4	2
Rattarangsi-Chin [71]	16	13.31	46.67	26.60	83.2	57.0	68.9	7
Pei-Lin [72]	16	14.15	41.72	26.60	88.4	63.8	75.1	6
Ray-Ray [73]	16	13.31	46.67	26.60	83.2	57.0	68.9	7
Sankar-Sharma [79]	20	11.61	71.15	13.38	58.1	18.8	33.0	13
Quddus-Gabbouj [34]	16	14.30	39.77	26.60	89.4	66.9	77.3	5
Horng [26]	16	15.89	27.09	26.60	99.3	98.2	98.8	1
He-Yung [82]	16	14.86	32.84	26.60	92.9	81.0	86.7	4

Table 2.5: Quantitative results of the "figure-8" curve using E_∞.

Algorithm	N_{appr}	N_{opt}	E_{appr}	E_{opt}	Eff	Fid	$Merit$	$Rank$
Rosenfeld-Johnston [35]	10	5.12	1.61	0.66	51.2	41.0	45.8	12
Anderson-Bezdek [40]	9	6.70	1.12	0.71	74.4	63.4	68.7	6
Teh-Chin [24]	13	7.00	1.00	0.46	53.8	46.0	49.8	11
Cornic [27]	10	8.89	0.73	0.66	88.9	90.4	89.7	1
Wu [29]	14	8.89	0.73	0.45	63.5	61.6	62.6	8
Marji-Siy [16]	-	-	-	-	-	-	-	-
Ray-Pandyan [65]	9	7.30	0.97	0.71	81.1	73.2	77.1	4
Rattarangsi-Chin [71]	5	3.64	2.61	1.64	72.8	62.8	67.6	7
Pei-Lin [72]	13	8.05	0.89	0.46	61.9	51.7	56.6	10
Ray-Ray [73]	4	3.64	2.61	2.06	91.0	78.9	84.7	2
Sankar-Sharma [79]	6	3.80	2.36	1.40	63.3	59.3	61.3	9
Quddus-Gabbouj [34]	-	-	-	-	-	-	-	-
Horng [26]	13	10.25	0.63	0.46	78.8	73.0	75.9	5
He-Yung [82]	4	3.47	2.87	2.06	86.7	71.8	78.9	3

Table 2.6: Quantitative results of the "chromosome" curve using E_∞.

Algorithm	N_{appr}	N_{opt}	E_{appr}	E_{opt}	Eff	Fid	$Merit$	$Rank$
Rosenfeld-Johnston [35]	8	5.87	1.54	1.15	73.4	74.7	74.0	7
Anderson-Bezdek [40]	9	5.57	2.03	1.13	61.9	55.7	58.7	11
Teh-Chin [24]	15	12.50	0.74	0.63	83.3	85.1	84.2	4
Cornic [27]	12	10.00	1.00	0.77	83.3	77.0	80.1	5
Wu [29]	18	15.00	0.63	0.45	83.3	71.4	77.2	6
Marji-Siy [16]	11	11.00	0.89	0.89	100.0	100.0	100.0	1
Ray-Pandyan [65]	6	5.84	1.58	1.32	97.3	83.5	90.2	3
Rattarangsi-Chin [71]	6	5.41	2.30	1.32	90.2	57.4	71.9	8
Pei-Lin [72]	10	5.84	1.58	1.00	58.4	63.3	60.8	10
Ray-Ray [73]	8	5.41	2.30	1.15	67.6	50.0	58.1	12
Sankar-Sharma [79]	12	5.57	2.03	0.77	46.4	37.9	42.0	13
Quddus-Gabbouj [34]	6	5.88	1.51	1.32	98.0	87.4	92.6	2
Horng [26]	10	6.00	1.32	1.00	60.0	75.8	67.4	9
He-Yung [82]	6	5.84	1.58	1.32	97.4	83.5	90.2	3

Table 2.7: Quantitative results of the "semicir" curve using E_∞.

Algorithm	N_{appr}	N_{opt}	E_{appr}	E_{opt}	Eff	Fid	$Merit$	$Rank$
Rosenfeld-Johnston [35]	30	19.00	0.74	0.45	63.3	60.8	62.1	4
Anderson-Bezdek [40]	29	10.00	1.18	0.45	34.5	38.1	36.3	11
Teh-Chin [24]	22	12.00	1.00	0.66	54.5	66.0	60.0	5
Cornic [27]	22	10.23	1.15	0.66	46.5	57.4	51.7	8
Wu [58]	27	16.20	0.88	0.45	60.0	51.1	55.4	7
Marji-Siy [16]	18	12.00	1.00	0.84	66.7	84.0	74.8	2
Ray-Pandyan [65]	18	12.00	1.00	0.84	66.7	84.0	74.8	2
Rattarangsi-Chin [71]	9	5.31	2.89	1.99	59.0	68.9	63.7	3
Pei-Lin [72]	26	25.00	0.49	0.45	96.2	91.8	94.0	1
Ray-Ray [73]	11	5.31	2.89	1.05	48.3	36.3	41.9	10
Sankar-Sharma [79]	10	3.05	8.00	1.18	30.5	14.8	21.2	12
Quddus-Gabbouj [34]	8	4.69	3.79	2.08	58.6	54.9	56.7	6
Horng [26]	26	25.00	0.49	0.45	96.2	91.8	94.0	1
He-Yung [82]	20	9.71	1.41	0.74	48.6	52.3	50.4	9

Table 2.8: Quantitative results of the "leaf" curve using E_∞.

Algorithm	N_{appr}	N_{opt}	E_{appr}	E_{opt}	Eff	Fid	$Merit$	$Rank$
Rosenfeld-Johnston [35]	17	14.31	1.76	1.00	84.2	56.8	69.2	8
Anderson-Bezdek [40]	20	14.76	1.49	0.89	73.8	59.7	66.4	9
Teh-Chin [24]	29	18.00	0.99	0.56	62.1	56.6	59.3	11
Cornic97 [27]	23	16.05	1.18	0.74	69.8	62.7	66.2	10
Wu [29]	24	18.00	0.99	0.73	75.0	73.7	74.4	7
Marji-Siy [16]	21	20.92	0.78	0.77	99.6	98.7	99.2	1
Ray-Pandyan [65]	20	18.00	0.99	0.89	90.0	89.9	89.9	4
Rattarangsi-Chin [71]	16	14.31	1.76	1.19	89.4	67.6	77.8	6
Pei-Lin [72]	16	15.31	1.30	1.19	95.7	91.5	93.6	3
Ray-Ray [73]	16	14.31	1.76	1.19	89.4	67.6	77.8	6
Sankar-Sharma [79]	20	4.51	3.48	0.89	22.6	25.6	24.0	12
Quddus-Gabbouj [34]	16	14.31	1.76	1.19	89.4	67.6	77.8	6
Horng [26]	16	14.90	1.41	1.19	93.1	84.4	88.7	5
He-Yung [82]	16	15.34	1.30	1.19	95.9	91.8	93.8	2

2.2 A review of direct intensity computation based corner detection (DICD) methods

We call the third type as direct intensity computation based corner detection because this type of detector does not depend on the edge detection or the mathematical models. It detects corner points directly from some computations. Usually, computations are based on the first or second derivative of the image. In [91], they divide this type of algorithms into three kinds: geometry based methods, autocorrelation based methods and structure based methods. The most state-of-the-art methods, Harris detector [92] and SUSAN detector [93], belong to autocorrelation based methods and structure based methods respectively. From another point of view, we can classify the direct intensity computation based algorithms into three different types: second order derivative based methods, first order derivative based methods and zero order derivative based methods. This categorization way is related to the properties and performance of the methods directly and more intuitive. In the earlier stage, a lot of methods based on the second derivative computation are proposed. But the higher the derivative, the more noise exists in the results. Thus, researchers turn to first or zero derivative based methods. Harris detector is the first order derivative based method and SUSAN detector is the zero order derivative based method. However, all the classification are not strict and complete. In this thesis, we will review the state-of-the-art detectors briefly. More information can be found in [91, 94, 95].

In [96], Beaudet derives a corner measurement from the Hessian matrix that needs the second derivative of the image. In [97], Deriche and Giraudon ana-

lyze several existing edge and corner detection algorithms. They use two scale Beaudet's detector to estimate the delocalization and apply the zero-crossing of the Laplacian of Gaussian to get the accurate localization. In [98], Kitchen and Rosenfeld discuss several techniques of corner detection. The most famous one is to multiply the rate of change of gradient direction along an edge by the gradient magnitude to detect corner points. Wu and Rosenfeld further develop this idea in [99]. They project the intensity to x and y axis to select the corner candidates before apply the determination method mentioned in [98].

In [92], Harris and Stephens develop Moravec's idea [100] into the famous Harris corner detector. This method is based on the first derivative quantities. The basic idea of the Harris corner detector is that the difference between the local image and its shift along any direction should be large only at corner points. Noble [101] analyzes the principle behind Harris corner detector and points out that Harris detector can only detect "L" corners. The author further proposes a more complex detector based on the second fundamental form. It characterizes the 2D surface features such as "T", "X" and "L" corners by the differential geometry of a facet model. Zheng *et al.* [13] formulate a gradient-direction corner detector that is developed from the Harris corner detector.

Wavelets are applied to detect corners in [102, 103, 104, 105, 106, 107]. In [102], multi-scale transform information is used to judge corner points. The input image is decomposed using a B-spline wavelet at several scales. The sum of the frequency components from the decomposed low-high, high-low, and high-high subbands is thresholded to obtain the edge map. The corner point is then detected if the high-high component is larger than a threshold and belongs to the edge map. However, in [103], Fransson claims that the high-high subbands

is full of noise in practical applications. He uses the low-high and high-low sub-bands to detect corners. In [104], the first derivative of the Gaussian function is used as the mother wavelet. The ratio of transform moduli of two scales is used to detect the edges and corners. Scale invariant property of corner orientation is applied to detect corner points. In [105], the modified Gabor filter (the difference of two low-pass filters of different bandwidths) is used to filter the input image iteratively. The iteration stops when the change of the output is below a threshold. In [106], the authors apply WT to implement the multiscale Laplacian operator. The zero-crossings are taken as corner candidates. The false corners are removed through the analysis of the luminance profile along the circle centered on the corner itself. However, this post-processing may also remove true corners in the practical application. All the above corner detection algorithms using WT perform well only on simple synthetic images. They are not robust enough for the detection on natural images. In [107], Kovesi detects corners and edges based on the phase congruency of log-Gabor WT. This method tries to provide a contrast invariant way to detect features. However, it needs to estimate the noise at the smallest scale, which adds extra computation.

In [108], the dissimilarity along contour direction is computed to detect corners. In [93], Smith and Brady apply a circular mask to detect corners and this detector is called SUSAN. The SUSAN principle is based on the fact that the center pixel should be a corner point if the number of the pixels that have the same brightness as the center pixel in the circular mask is below a threshold.

Chabat *et al.* exploit the anisotropic intensity pattern to detect corners, and further analyze the corners' arms and histograms to identify the corners' orientation. In [45], the neural network is applied to detect corners. In [109],

gradient covariance matrix and gradient projection are studied and used to detect edge and corner points. Sojka's [110] corner detector measures the variance of directions of the gradient. The weighting coefficients in the measurement function are computed based on Baye's Theorem. Shen and Wang detect corners as the junctions of edges based on the modified Hough transform in [4]. In [111], Hilbert transform is applied to corner detection. Color distribution based corner detection is explored in [112].

Scale-space theory is not only used in the 1D contour image analysis as described in subsection 2.1.6, but also applied in 2D images for corner detection. Alvarez and Morales [113] proposed an affine morphological multiscale analysis based corner detection method. Fidrich and Thirion [114] analyzed the stability of corners in scale-space. Luo and Pycock [115] proposed a multiscale corner detector based on Moments of the Gradient in Scale-space (MoGS). In [116], Lindeberg proposed a feature detection method with automatic scale selection in scale-space framework. Inspired by Lindeberg's work, Mikolajczyk and Schmid proposed scale and affine invariant detector that deals with very large scale changes [117]. However, the computation is very expensive and poor stability for small affine changes [118]. In [118], Lowe proposed a new approach named the Scale Invariant Feature Transform (SIFT). The approach includes both corner points detector and descriptor. It is hard to decouple the above two components to evaluate the performance of the detection. The algorithm for the corner detection is as follows. Lowe applied difference-of-Gaussian function over all scales and locations. The scale-space extrema are taken as corner candidates. As the difference-of-Gaussian operator has a dislocalization problem and has a strong response to edges, a detailed fitting is utilized to improve the localization and remove the low contrast candidates. Hessian matrix is formed

and analyzed to remove the edge points. All the above scale-space methods are very complicated and computationally expensive.

Based on the review, we find that the Harris detector and SUSAN detector have better performances and are widely used in a variety of applications, such as stereo matching, camera calibration etc.. Kovesi's method is multiscale based and proposed recently, thus, we compare the proposed methods with them in this thesis.

2.3 Conclusions

In this chapter, we reviewed most of the state-of-the-art methods of corner detection, especially for CCD and DICD methods. The research in this thesis focuses on these two types of methods. Although a lot of methods are proposed, there still are some problems to be solved. The main issues are the three problems: (1) incomplete information; (2) delocalization; and (3) multiple responses to higher order structures. For the CCD methods, the multiscale detection is mainly based on the incomplete information, which limits the performance and their applications. For the DICD method, the three problems exist in the most commonly used method, Harris detector. Although some methods solve one or several of the three problems, they face other problems. For example, SUSAN detector solves the delocalization problem, but it cannot detect junctions [91]. Furthermore, the detection rate of other detectors are generally lower than that of Harris detector. As a result, we intend to propose some new algorithms in this thesis that partially or wholly solve the three problems while improving the detection rate.

Chapter 3

Multiscale CCD Methods Using Dyadic WT

3.1 Introduction

For the CCD algorithms, one possible application is on the gray level images with some prior segmentation and contour tracking, especially on some cartoon images [8]. Another main usage is in computer graphics field, where the input is contour images [9].

In chapter 2, we have reviewed most of the existing CCD methods. To detect corners of different sizes and extents for contour images, there exist some problems in the two types of commonly used methods: the support region based methods [24] and the multiscale based methods [71, 34]. For the support region based methods, for example, Teh-Chin's algorithm [24], the support region of each point (its natural scale) is determined at individual point. As a result, the natural scale is optimal for the corresponding point. However, the determina-

tion of the support region is based on the raw data which include quantization errors and possible noises. Thus, the methods are not robust. For the multiscale based methods, there exist scale-space based analysis and WT based analysis. Both of them provide a simple hierarchical framework for corner detection, and are robust due to their inherent smoothing property. But there exist some problems for the existing multiscale based methods. For the scale-space based methods, they are computational inefficient because they need to compute at continuous scales. Furthermore, they either utilize information on one or several heuristically selected natural scales [12] or utilize only location information in the transformed domain [71], which limits the performance. Without *a priori* information, no particular scales should be pre-supposed [119]. Thus, the performance of the existing scale-space based methods is not satisfactory for different types of test images. Recently, Quddus and Gabbouj [34] proposed a fast and robust WT based corner detection technique. The technique requires to compute *singular value decomposition* (SVD) of the dyadic WT to estimate natural scales for the contour. However, in a few cases the stop criterion for the selection of natural scales does not work. Moreover, there is some computational overhead to compute SVD.

To overcome the above problems, we propose two new CCD methods using dyadic WT: the global natural scales based method and the local natural scales based method.

For the global natural scales based method, all the possible decomposition scales of the dyadic WT are considered as natural scales for corner detection. For each candidate, the sum of the normalized WTMM from different scales is taken as the significance measure to differentiate the corners from the noise.

For the local natural scale based method, the significance measure of each candidate is considered at all the possible scales. As natural scale should be the scale that contains most or all the important information, for each candidate, the scale at which the maximum value of the normalized WTMM exists is defined as its "local natural scale", and the corresponding measure is taken as the significance measure to differentiate the corners from the noise. Local natural scale is explored in the literature, but the goals are different. It is the first time that local natural scale is applied in contour corner detection in a multiscale framework.

The decomposition scales of the dyadic WT are sparse and complete. Being sparse, it simplifies the following processing. Being complete, the decomposition contains all the important information. The inherent smoothing and localization properties of WT make the proposed methods effective and accurate. In addition, the technique is fast due to the fast implementations of the dyadic WT computations.

The chapter is organized as follows. In section 3.2, we first present a proposed boundary tracking algorithm. Then, the theory of WT and the fast algorithm of the dyadic WT is introduced. The multiscale WT based corner detection technique is summarized at the end of section 3.2. In section 3.3, the proposed algorithm based on global natural scales is presented. The algorithm based on local natural scales is presented in section 3.4. Section 3.5 shows simulation results and performance evaluation. The conclusion is given in section 3.6.

3.2 Fundamentals

3.2.1 A proposed boundary tracking algorithm

In order to compute the orientation profile of the input contour image, we need to find first the chain code of the corresponding contour image. This has been performed using the boundary tracking algorithm as described in the following.

Let us consider that a current contour pixel is detected at (x, y). The neighbor relationship of the current detected contour pixel at (x, y) is shown in Fig. 3.1.

(x-1, y-1)	(x, y-1)	(x+1, y-1)
(x-1, y)	(x, y)	(x+1, y)
(x-1, y+1)	(x, y+1)	(x+1, y+1)

Figure 3.1: The neighbor relationship of the detected contour pixel at (x, y).

According to Fig. 3.1 there will be only three pixels (the center pixel and the two other neighboring pixels among the 8-connectivity neighbors) which belong to the image contour. In practice, there are often more than three pixels due to the noise or any sharp changes. That is the reason that the simple clockwise or anti-clockwise search could not complete the tracking.

We have implemented the boundary tracking algorithm by considering neighboring pixels in different directions (comparing with the detected contour direction) with different priority. On the basis of the given priority along different

directions, we can order the 8-connectivities of the current pixel at (x, y). The pixels that are along or near the detected contour direction should have high priority, so that we can detect those pixels first. Three following situations should be considered to detect the possible contour directions:

a. The detected contour direction is along diagonal axis;

b. The detected contour direction is along horizontal, i.e. x-axis;

c. The detected contour direction is along vertical, i.e. y-axis.

For example (see Fig. 3.2), suppose the previous detected contour pixel is at position with index 7 and the current contour pixel is detected as a contour pixel with index 5. We then give the highest priority towards the pixel with index 3. The next highest priority will be given towards the pixel with index 2 and the pixel with index 6 and the following lower priority is given to the pixels with index 1 and with index 9. The lowest directional priority is given towards the pixels having indices 4 and 8, respectively. In this way, the selection priority for the 8 neighboring pixels with respect to the current pixel at (x, y) will be given according to the pixel index order of $3, 2, 6, 1, 9, 4, 8$. In fact, the order is not unique since the pixels with indices 2 and 6, or 1 and 9, or 4 and 8 are given the same priority.

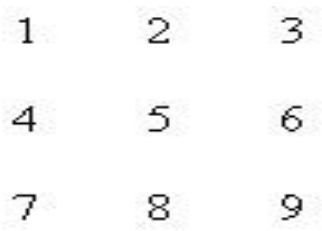

Figure 3.2: The index of the neighboring pixels at the current pixel of (x, y) with index 5.

We search each neighboring pixel in the sequence of their priority until we can find the next true contour pixel. Suppose the number of the neighbors that belong to the contour is two, then we do not need to sort out among the other neighbors. For example, according to Fig. 3.2, when there are just three pixels with index $(3, 5, 7)$ belong to the contour in this figure, say, the current contour pixel is of index 5, the previous contour pixel is of index 7, then the next contour pixel will be the one with index 3 and other pixels having indices $(2, 6, 1, 9, 4, 8)$ do not belong to the contour. For such case, we can increase the processing speed by avoiding the sorting step.

3.2.2 Wavelet transform

Since wavelets are introduced at the beginning of eighties by J. Morlet [120], the theory and applications of WT are studied and developed enormously. WT decomposes signals into different frequency bands with different resolutions. A mother wavelet ψ is a function with finite energy and a zero average.

$$\int dt\ |\psi(t)|^2 < +\infty. \tag{3.1}$$

$$\int dt\ \psi(t) = 0. \tag{3.2}$$

A family of functions $\psi_{u,s}$ called wavelets are derived from the mother wavelet by scaling ψ by s and translating it by u.

$$\psi_{u,s}(t) = \frac{1}{\sqrt{s}}\psi(\frac{t-u}{s}). \tag{3.3}$$

The WT of a function $f(t)$ at scale s and location u is defined as follows.

$$Wf(u,s) = \int dt\ f(t)\frac{1}{\sqrt{s}}\psi^*(\frac{t-u}{s}), \tag{3.4}$$

where $Wf(u,s)$ denotes the WT of the function $f(t)$ and $*$ represents the complex conjugate operation. In this thesis, we denote

$$\overline{\psi}_s(t) = \frac{1}{\sqrt{s}}\psi^*(\frac{-t}{s}), \tag{3.5}$$

then the WT is

$$Wf(u,s) = f \circledast \overline{\psi}_s(u). \tag{3.6}$$

Here, '$\circledast$' represents the convolution operator. In [121], Mallat proves that a wavelet with n vanishing moments can be written as the n^{th} order derivative of a smoothing function ξ. And the resulting WT is a multiscale differential operator.

$$\psi(t) = (-1)^n \frac{d^n \xi(t)}{dt^n}. \tag{3.7}$$

$$\overline{\psi}_s(t) = s^n \frac{d^n \overline{\xi}_s(t)}{dt^n}, \tag{3.8}$$

with $\overline{\xi}_s(t) = s^{-1/2}\xi(-t/s)$.

$$Wf(u,s) = s^n \frac{d^n}{du^n}(f \circledast \overline{\xi}_s)(u). \tag{3.9}$$

$Wf(u,s)$ is the n^{th} order derivative of the smoothed signal $f \circledast \overline{\xi}_s$. If we take $n = 1$, in other words, the wavelet has one vanishing moment, the local maxima of the absolute value of the first derivative are sharp variation points of the smoothed signal, $f \circledast \overline{\xi}_s$ [122].

Wavelet transform modulus maximum (WTMM) is defined as the points that satisfy the following conditions.

$$\begin{cases} |Wf(u_0,s)| > |Wf(u_1,s)| & : \quad u_1 \textit{ is one neighbor of } u_0, \\ |Wf(u_0,s)| \geq |Wf(u_2,s)| & : \quad u_2 \textit{ is the other neighbor of } u_0, \end{cases} \tag{3.10}$$

here $|Wf|$ represent the modulus of Wf. Accordingly, WTMM is any point that its modulus of WT is greater than that of one of its neighbor's and not

less than that of the other neighbor's [123]. The *maxima line* is defined as any connected curve $s(u)$ in the scale-space plane (u, s) along which all points are modulus maxima. In [122], Mallat and Hwang prove that all singularities of the signal $f(u)$ can be located by following the maxima lines when the scale goes to zero.

The WT obtains the details of the signal at different scales. While the approximations of the signal at different scales can be obtained by introducing a scaling function ϕ that is related with the wavelet function ψ. Sometimes, ϕ is called the father wavelet. Denote

$$\phi_s(t) = \frac{1}{\sqrt{s}}\phi(\frac{t}{s}), \tag{3.11}$$

then the approximation of the signal f at the scale s is

$$Sf(u, s) = f \circledast \overline{\phi}_s(u). \tag{3.12}$$

From the filter banks point of view, the details correspond to the output of the high pass filters; while the approximations are the output of the low pass filters.

3.2.3 The dyadic WT and its fast algorithm

Shift invariant representation is necessary in pattern recognition. The *continuous wavelet transform* (CWT) is a shift-invariant representation. Uniformly sampling the translation parameter destroys this property, consequently, the *discrete wavelet transform* (DWT) can not provide such invariance [121].

To keep the shift invariance property while reducing the redundancy of the CWT, the dyadic WT can be used. The dyadic WT samples the scale along a dyadic sequence, i.e. $s = 2^j$ and j is an integer. The dyadic WT is as follows.

$$Wf(u, 2^j) = f \circledast \overline{\psi}_{2^j}(u). \tag{3.13}$$

Another advantage of the dyadic WT is that there is a fast algorithm of it introduced by Holshneider, Kronland-Martinet, Morlet and Tchamitchian. The fast dyadic WT is implemented with the filter bank structure [121].

Suppose the scaling function ϕ and the wavelet ψ are designed with the filters H and G. H_j and G_j are the discrete filters obtained by putting $2^j - 1$ zeros between each of the coefficients of the filters H and G respectively. H_0 and G_0 represent the original filters H and G. In the numerical implementations, the input signal is the sequence of the samples $a_0[n]$ that is the local average of f in the neighbors of $t = n$. The approximation coefficients and the detail coefficients (WT) are denoted as $a_j[n]$ and $d_j[n]$ at the scale 2^j. It is proved that the approximations and the details at each dyadic scale can be obtained by the following equations [121].

$$a_{j+1}[n] = Sf(n, 2^j) = a_j \circledast \overline{H}_j[n]. \tag{3.14}$$

$$d_{j+1}[n] = Wf(n, 2^j) = a_j \circledast \overline{G}_j[n]. \tag{3.15}$$

In the above equations, $\overline{H}_j[n] = H_j[-n]$, $\overline{G}_j[n] = G_j[-n]$. Therefore, the WT of the input signal $a_0[n]$ can be described as the process in Fig. 3.3.

The application of dyadic WT in image processing is motivated by many physiological and computer vision studies [121, 124]. As the decomposition of the dyadic WT is complete, all the information are remained in the decomposition. The scales are also sparse, which simplifies the following processing.

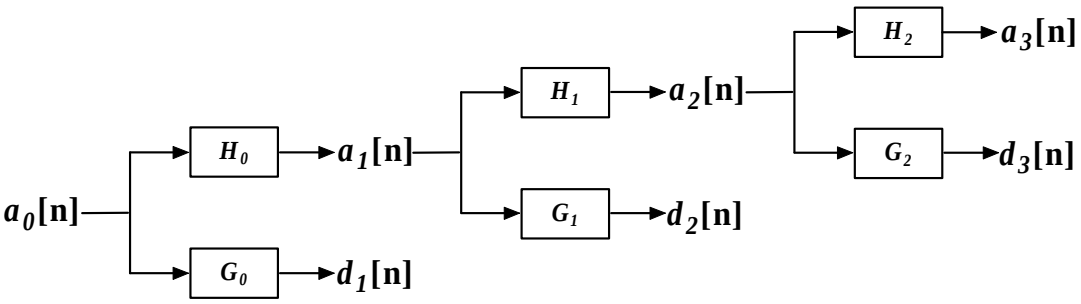

Figure 3.3: The fast implementation of the dyadic WT. The filters H_j and G_j are the discrete filters obtained by putting $2^j - 1$ zeros between each of the coefficients of the filters H and G respectively. H_0 and G_0 represent the original filters H and G. $a_j[n]$ and $d_j[n]$ denotes the approximation coefficients and the detail coefficients obtained at the scale 2^j. The operation of filtering means convolution.

3.2.4 The multiscale WT based corner detection technique

The preprocessing steps (contour extraction, boundary tracking and orientation computation) are the same for all the multiscale WT based corner detection techniques (see [84, 34]).

For these techniques, the contour image is extracted from the gray image first, then the 2D planar curve (or we can call it the boundary) can be expressed as

$$C(t) = (X(t), Y(t)), \tag{3.16}$$

where t is the arc length [125]. The orientation function (the angle between the tangent line and the positive x-axis) of the boundary is defined as

$$f(t) = tan^{-1}\frac{dY/dt}{dX/dt}. \tag{3.17}$$

Instead of using the first order difference with the orientation resolution, $\pi/4$,

we can improve the orientation resolution by defining

$$f(i) = tan^{-1}\frac{Y_{i+d} - Y_{i-d}}{X_{i+d} - X_{i-d}}, \tag{3.18}$$

for $d > 1$. Here, i denotes the index of the chain code. In this context, the chain code can be defined as a 1D sequence that contains relative position information for the pixels of the contour image. According to Eq. (3.18), we can then obtain a smoothed version of the orientation profile.

The WT of the function f at the scale s and position u is then defined by

$$Wf(s,u) = f(u) \circledast \psi_s(u), \tag{3.19}$$

where $\circledast$ denotes the convolution and $\psi_s(u) = s^{-1/2}\psi(u/s)$ is the wavelet function.

The corner points (with high curvature) of the contour image are those points having the large rate of change of the orientation. Here, these points correspond to the WTMM of the orientation profile [84, 34].

3.3 The proposed multiscale CCD algorithm based on dyadic WT and global natural scales

Corners are defined as high curvature points on a contour. To estimate the curvature, we select the dyadic WT using the quadratic spline mother wavelet [121] to decompose the orientation function because it satisfies the following necessary conditions and good properties. Firstly, the dyadic WT is shift invariant, which is a necessary condition for feature extraction. Secondly, the quadratic spline mother wavelet has one vanishing moment, which is a first order differential operator on a smoothed signal. Accordingly, the curvature is approximated when the transformation is applied on the orientation function. Thirdly, the dyadic WT is complete. Thus, it provides the decomposition at a sparse set of appropriate scales, which simplifies the following analysis and computation. Lastly, it has a fast implementation algorithm, which makes the proposed algorithm computationally efficient. The filter coefficients of the quadratic wavelet are in appendix B.

In the proposed algorithm, the preprocessing steps described in 3.2 are adopted to get the orientation function of the contour image. Then dyadic WT is applied to the orientation function to estimate the curvature at all possible scales because no scale should be preferred without *a priori* information.

- **Curvature estimation**

The quadratic spline wavelet $\psi(t)$ is the first derivative of the cubic spline function $\xi(t)$, i.e. $\psi(t) = \xi'(t)$. Consequently, it has one vanishing moment. By

denoting

$$\overline{\psi}_s(t) = \frac{1}{\sqrt{s}}\psi^*\left(\frac{-t}{s}\right), \tag{3.20}$$

the WT of the orientation function f at the scale s and position u can be written as follows.

$$Wf(u,s) = f \circledast \overline{\psi}_s(u) = s\frac{d}{du}(f \circledast \overline{\xi}_s)(u), \tag{3.21}$$

where Wf represents the WT of the orientation function f. Equation (3.21) shows that the WT (with one vanishing moment) of the orientation function is proportional to the curvature of the boundary. It measures the change of the orientation.

- **Determine the range of the decomposition scales**

The range of the decomposition scales, 2^j, for the WT is determined by the inherent property of the dyadic WT and the length of the signal N [121].

$$1 < 2^j \leq N, \quad j = 1, 2, \cdots, J \tag{3.22}$$

where J is the maximum level of the WT. According to (3.22), the decomposition scales of the WT is restricted by the signal length N, which makes the algorithm adaptable for both long contours and short contours.

- **Corner detection**

Subsequently, all the decomposition scales are taken as natural scales for the corner detection. The WTMM are extracted and the points with WTMM are taken as corner candidates. At a certain scale, the candidates with acute angles produce large WTMM, while the candidates with obtuse angles have small WTMM. To make each scale contribute the same to the final significance measure, the values of the WTMM are normalized with the respective maximum value at each scale.

Denote $W_{2^j}f$ as the WTMM of the discrete orientation profile f at the scale 2^j, and $max(W_{2^j}f)$ as the maximum WTMM at that scale. The normalized WTMM is as follows.

$$NW_{2^j}f = \frac{W_{2^j}f}{max(W_{2^j}f)}, \tag{3.23}$$

Although dyadic WT is shift invariant, there is still some shift of the local maxima due to the changes of the local properties caused by the scale changes. To construct the maxima line for each corner candidate along the scale, the tracking is according to the distance criterion. The distance criterion is applicable for both the one-to-one tracking and two-to-one tracking. For an instance, at scale i, there are two local maxima, $p1$ and $p2$, within a range whose positions are $d1$ and $d2$, respectively. At scale $i+1$, there is only one local maximum, $p3$, within the range at the position $d3$ (we assume here, no corresponding local maximum at the outside of the range for these two corner candidates here). If $|d1 - d3| < |d2 - d3|$, $p3$ and $p1$ belong to the same candidate, vice versa.

Then, the values at different scales corresponding to a particular corner candidate are constructed as a WTMM sequence (i.e., the maxima line) along the scales. To detect corners of different subtended angles and sizes, the normalized WTMM values for all natural scales are used to compute the wavelet coefficients as

$$\hat{W}f = \frac{1}{J}\sum_{j=1}^{J} NW_{2^j}f, \tag{3.24}$$

where $\hat{W}f$ denotes the average. This average includes the information considered at all the natural scales. It also suppresses the noise while strengthening the corner points. Finally, the corners are detected by setting a predefined threshold.

- **Process of the proposed algorithm**

The flowchart of the proposed algorithm is shown in Fig. 3.4. The steps of the proposed algorithm are presented as follows.

1. Preprocessing steps as described in [34]

(a) Track the boundary and obtain the chain code of it;

(b) Compute the orientation profile.

2. Determine the natural scales according to the length of the contour image.

3. Compute the WT of the orientation profile at the natural scales.

4. Detect the corner candidates by selecting the WTMM. Normalize the values at each scale.

5. Construct the maxima line for each corner candidate along the scales.

6. Compute the average of the normalized values of WTMM for all natural scales as the significance measure.

7. Normalize the significance measure to the maximum one, thus all the measure values are in the range $[0, 1]$. Then suppress the false corner points by setting a threshold.

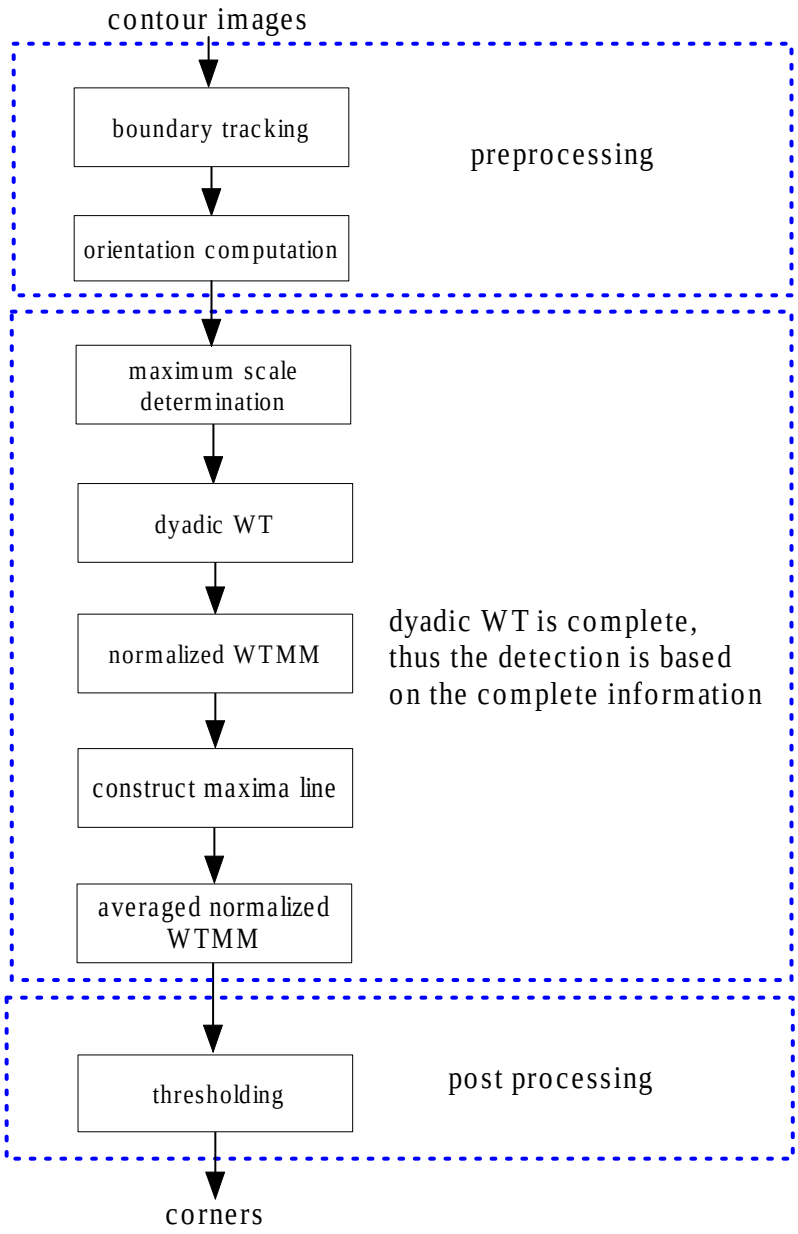

Figure 3.4: The flowchart of the proposed CCD algorithm based on dyadic WT and global natural scales.

3.4 The proposed multiscale CCD algorithm based on dyadic WT and local natural scales

As we concluded in chapter 2, because no strict mathematical definition of the curvature exists in the discrete domain, the performance of corner detection relies on the accuracy of both the curvature estimation and the scale estimation. In other words, a good curvature estimation should be measured in the spatial extent corresponding to its scale. The appropriate smoothing is necessary to remove the quantization error and noise while estimating the curvature and scale.

In the proposed algorithm, the prior five steps described in the global natural scales based algorithm are adopted. The WTMM are extracted and the points with WTMM are taken as corner candidates.

Since the "corner" is a relative conception, it depends on the shape and scale considered in the detection. At any specific scale, obtuse candidates will not be considered if there exist acute candidates. Therefore, we normalize the values of the WTMM at each scale. As a result, the curvature estimation is considered in an uniform manner in the whole framework. For different candidates at the same scale, the candidates with acute angles produce large WTMM, while the candidates with obtuse angles have small WTMM. For each candidate along different scales, the value of the normalized WTMM at a certain scale represents the "cornerity" of the candidate and the maximum value of the WTMM shows that the candidate achieves a strong "cornerity" at the corresponding scale. Consequently, the scale at which the maximum value exists should be defined as its "local natural scale" and the corresponding maximum modulus is taken

as the significance measure.

The flowchart of the proposed CCD algorithm based on local natural scales is illustrated in Fig. 3.5. The detection process of the proposed method is implemented as follows.

Step 1. Detect corner candidates.

The corner candidate is those points with WTMM. The same processing is adopted as described in section 3.3 to obtain the normalized WTMM, $NW_{2^j}f$.

Step 2. Detect corners at their respective natural scales, i.e., "local natural scales".

For each corner candidate, the maximum value among all the normalized WTMM is detected. It is determined as the local natural scale at which the maximum value of the candidate exists, and the corresponding modulus value is taken as the significance measure, i.e.,

$$M_c(\cdot, 2^l) = max\{NW_{2^j}f \ | j = 1, 2, \cdots, J\} \tag{3.25}$$

where $M_c(\cdot, 2^l)$ denotes the significance measure at the natural scale. The scale, 2^l, is the local natural scale for the candidate. The corners are detected at the locations, where the significance measure of the candidates is greater than a predefined threshold.

The corners are detected at different scales due to their different natural scales. The proposed method provides the locations of corners as well as the local natural scale information simultaneously, which is useful for the hierarchical approximation of the original contour.

To illustrate the process, we use the fourth test image of Fig. 3.9 as an example. Fig. 3.6 (a) shows the normalized WTMM of the candidates at each scale. For a clear illustration, Fig. 3.6 (b) shows the normalized WTMM of

the corner points at each scale. The length of each segment in Fig. 3.6 is proportional to the measure of the "cornerity" of the pixel at the corresponding scale. We can see that at certain scales, the acute candidates (or corners) give large values, while the normalized WTMM of different candidates (or corners) change differently along the scales. Fig. 3.7 shows the natural scales of the corners as the scales with the largest normalized WTMM. Referred to the fourth test image in Fig. 3.9, it is found that detected natural scales of corners agree with their support regions, i.e., the points with larger natural scales have larger support regions, and vice versa.

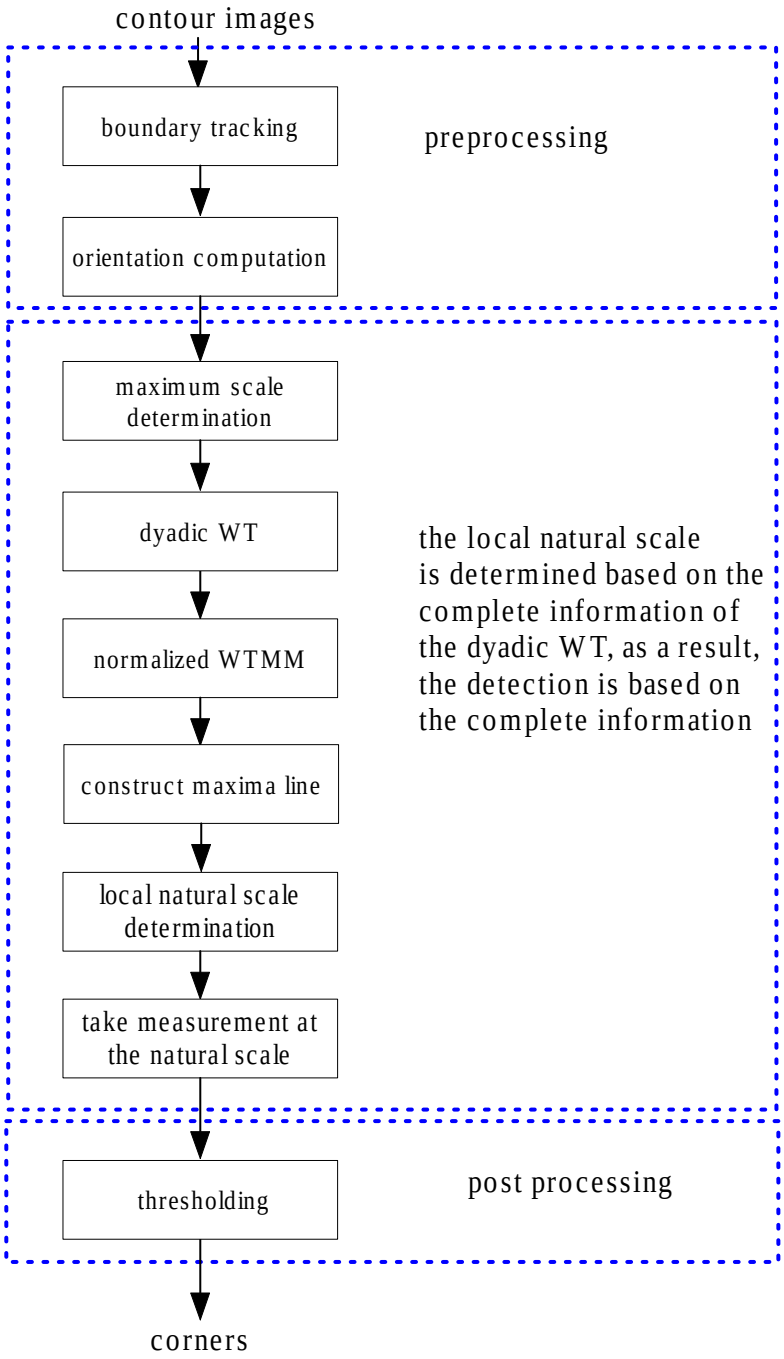

Figure 3.5: The flowchart of the proposed CCD algorithm based on dyadic WT and local natural scales.

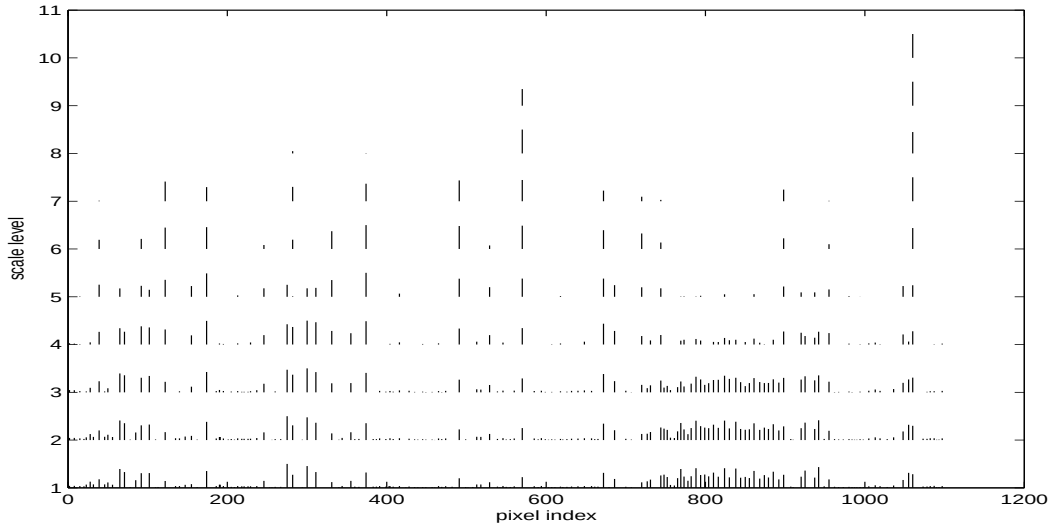

(a)

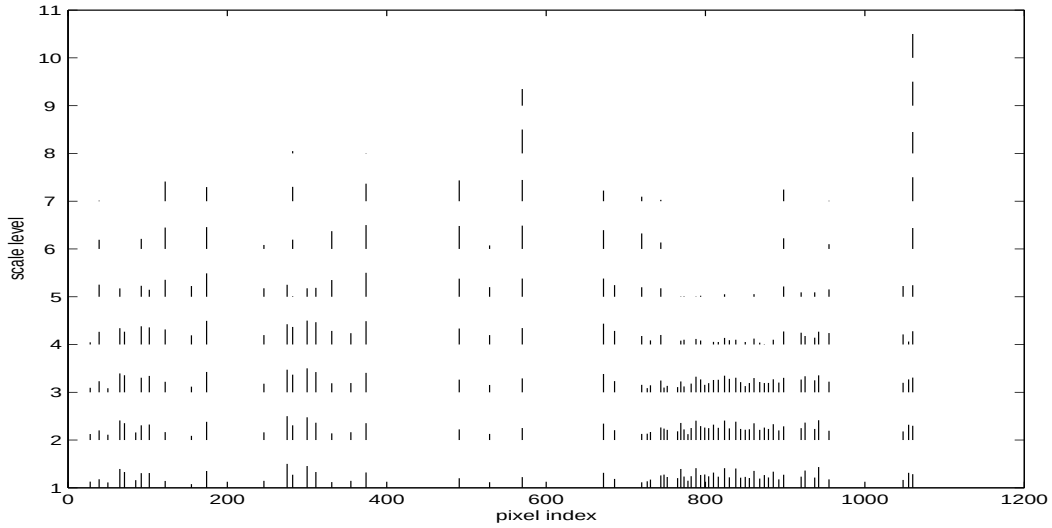

(b)

Figure 3.6: The normalized WTMM of the fourth figure in Fig. 3.9 for (a) corner candidates and (b) corners. The vertical axis represents the logarithm of the scale with base 2, while the horizontal axis is the index of the contour pixel.

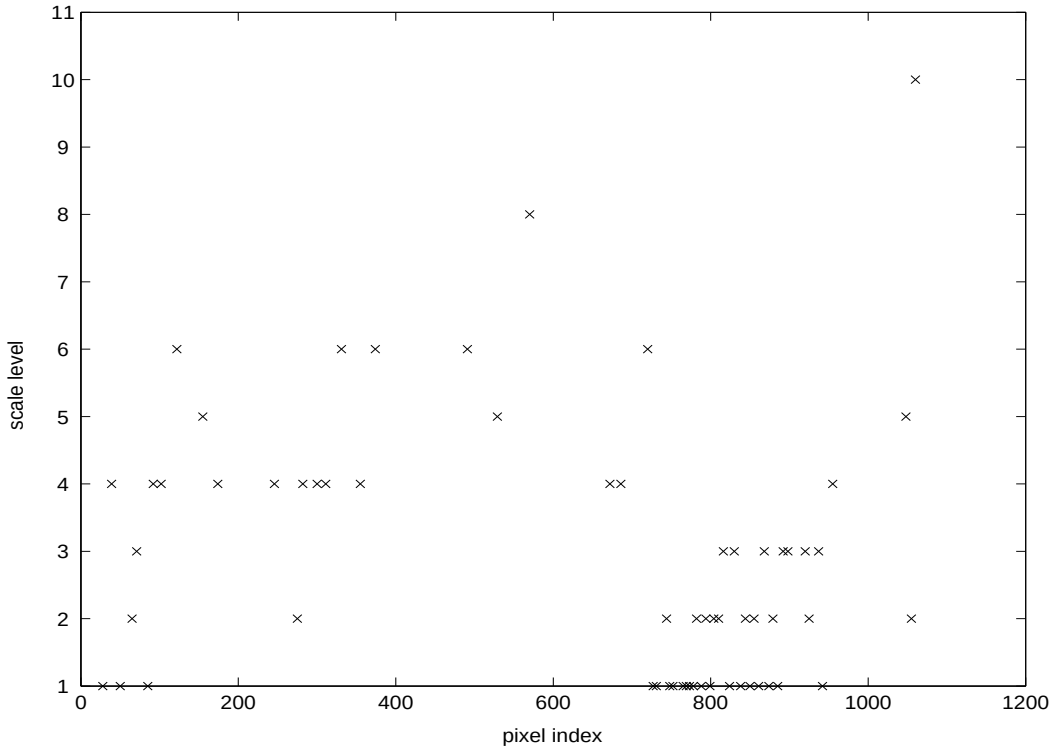

Figure 3.7: The natural scale of each corner point for the fourth figure in Fig. 3.9 as shown by '×'. The vertical axis represents the logarithm of the scale with base 2, while the horizontal axis is the index of the contour pixel.

3.5 Simulation results and performance evaluation

3.5.1 Subjective evaluation

The simulation results of the proposed method based on global natural scales are shown in Fig. 3.8 and Fig. 3.9. The fixed threshold, which is set empirically, is 0.08 for all the simulations shown in this chapter. The corresponding simulation results of the proposed method based on local natural scales are shown in Fig. 3.10 and Fig. 3.11. The threshold is 0.2 for all the simulations shown.The lengths of the curves in Fig. 3.8(a)–3.8(d) are 45, 60, 102, and 120, respectively. The lengths of the curves in Fig. 3.9(a)–3.9(d) are 563, 854, 872 and 1104, respectively. The parameter d in Eq.(3.18) is 2 in the experiments.

The test images in Fig. 3.8 are quite short in length, and consequently, the proposed method detects less corners compared to the results in Fig. 3.9. From the simulation results, we see that the proposed methods provide satisfactory performance for both long contours and short contours. This feature makes them more suitable in practical applications. The local based method even obtains a slightly better performance than the global based method.

Compared the results of the existing methods shown in chapter 2, both the proposed methods achieve better performance. Let us analyze the typical methods mentioned in section 3.1. Teh-Chin's method [24] is based on the support region determination. This method is classical but not so effective compared to the other three methods. It detects more points, including some insignificant points. Rattarangsi-Chin's method [71] is based on scale-space

analysis. The results shown in chapter 2 are good. However, this method only use the location information in the scale-space analysis. In the original paper [71], It shows some false detection on other test images. Recently, Quddus and Gabbouj propose a robust method in [34], which is based on WT. This approach requires to compute SVD of the dyadic WT for the orientation profile of the contour to estimate the global natural scales. It has been applied to test images used in Fig. 3.9 and 3.11, and obtains similar satisfactory results in [34] as the proposed methods do. However, in a few cases the stop criterion for the selection of natural scales does not work, e.g., for "figure-8" curve. Moreover, there is some computational overhead to compute the SVD. The length of "figure-8" curve is 45 pixels and it is relatively short, which might be the possible reason that Quddus-Gabbouj's method fails. The proposed methods overcome the problems of the above methods mentioned in chapter 2, as a result, they achieve the best performance among them.

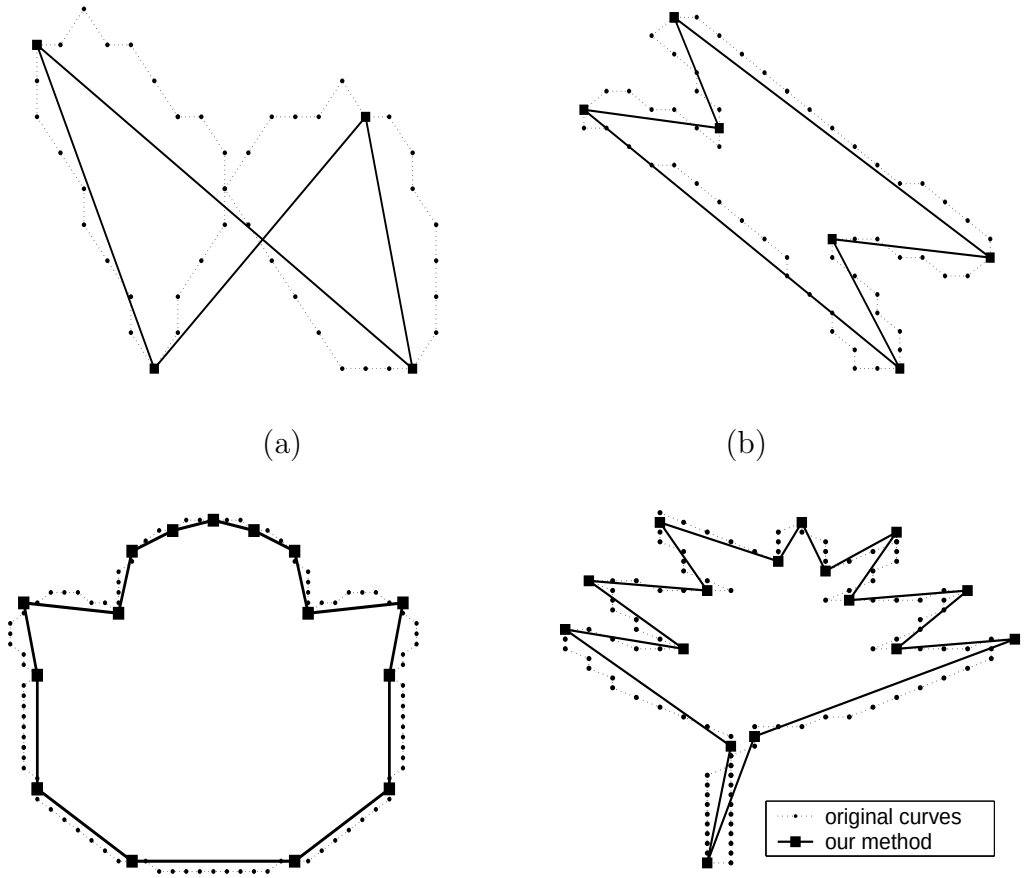

(a) (b)

(c) (d)

Figure 3.8: Results of the proposed method based on the global natural scales. The corners are indicated by '■' and connected into polygons. (a) the "figure-8" curve, (b) the "chromosome" curve, (c) the "semicir" curve, (d) the "leaf" curve.

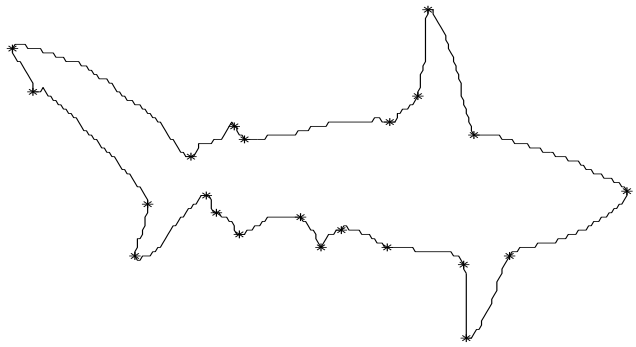

(a)

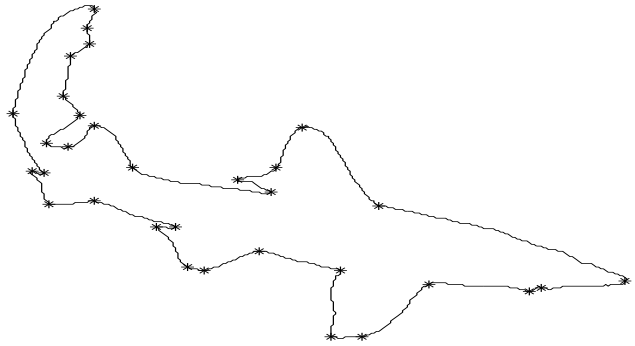

(b)

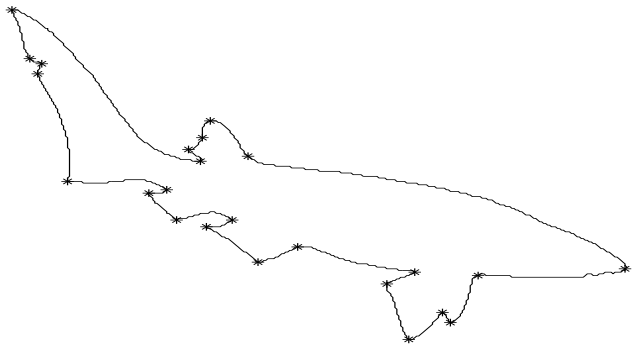

(c)

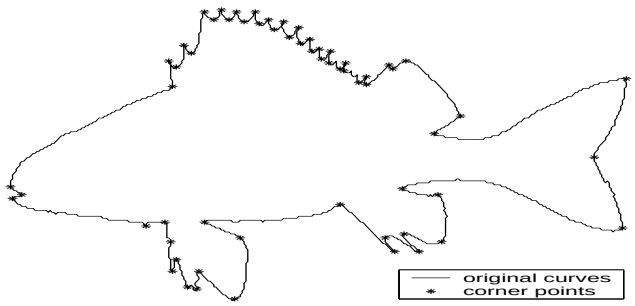

(d)

Figure 3.9: Results of the proposed method based on the global natural scales. The corners are indicated by '$*$'.

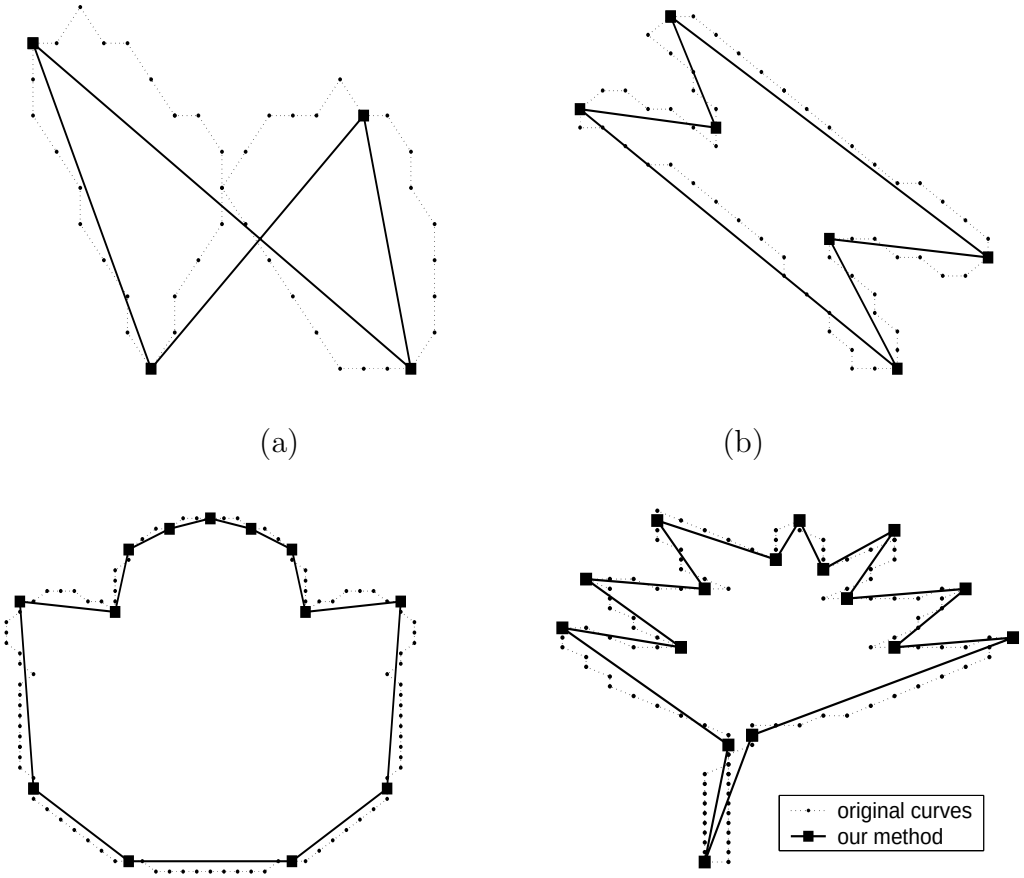

(a) (b)

(c) (d)

Figure 3.10: Results of the proposed method based on the local natural scales. The corners are indicated by '■' and connected into polygons. (a) the "figure-8" curve, (b) the "chromosome" curve, (c) the "semicir" curve, (d) the "leaf" curve.

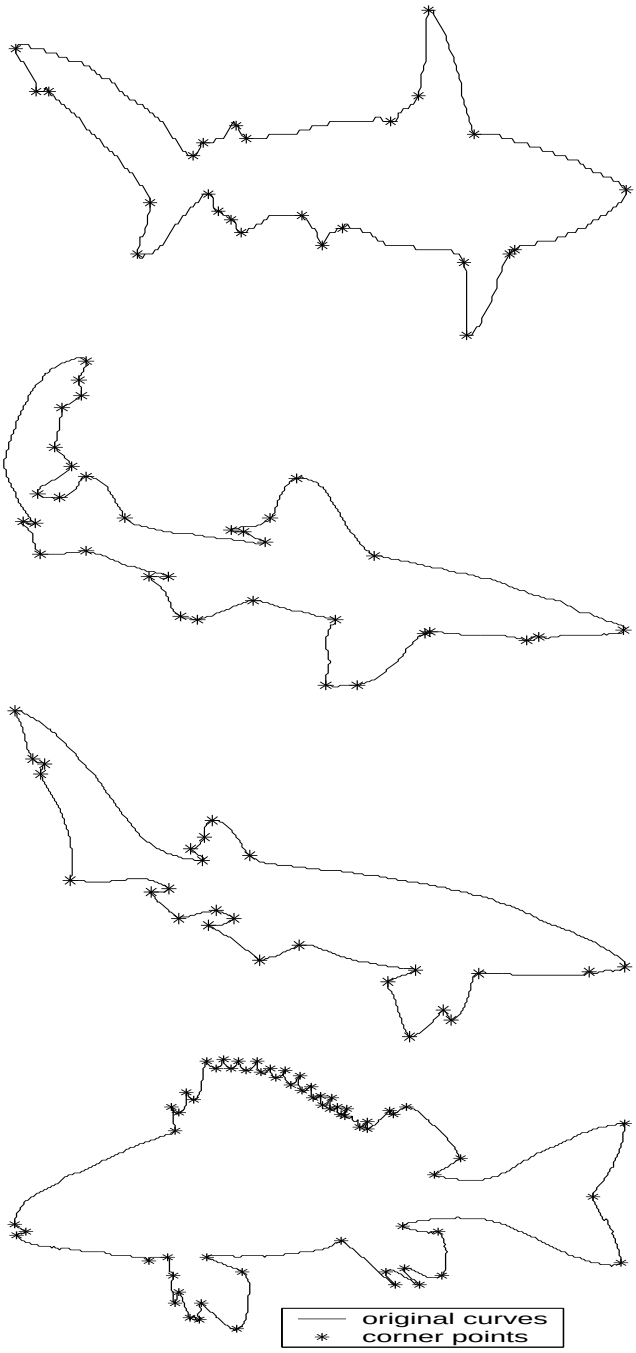

Figure 3.11: Results of the proposed method based on the local natural scales. The corners are indicated by '∗'.

Table 3.1: Quantitative results of the proposed methods using E_2 on test curves shown in Fig. 3.8 and Fig. 3.10.

Test Curves	Methods	N_{appr}	N_{opt}	E_{appr}	E_{opt}	Eff	Fid	$Merit$
figure-8	global	4	3.85	69.09	54.18	96.2	78.4	86.8
	local	4	3.85	69.09	54.18	96.2	78.4	86.8
chromosome	global	6	6.00	23.73	23.73	100.0	100.0	100.0
	local	6	6.00	23.73	23.73	100.0	100.0	100.0
semicir	global	15	8.69	66.56	14.40	58.0	21.6	35.4
	local	13	9.46	51.64	20.72	72.8	40.1	54.0
leaf	global	16	14.84	33.15	26.60	92.7	80.3	86.3
	local	16	14.84	33.15	26.60	92.7	80.3	86.3

3.5.2 Objective comparison using Rosin's method

The quantitative measurement results using Rosin's method (refer to chapter 2) are shown in Table 3.1 and Table 3.2. It shows that the two proposed methods have identical results except for the test image "semicir". The global based method detects two more insignificant points, and consequently, its performance evaluation is a little worse than the local based method. Also, the results of the "semicir" are not very satisfactory despite that the results from the subjective evaluation are good. This may be due to two reasons. Firstly, the gap between the subjective evaluation and the objective evaluation can not be ignored. Secondly, the adopted objective evaluation method evaluates how the curve is fitted by the connected detected corners, which may not measure the merits of corner detection algorithms precisely.

The global natural scales based method is simply denoted as "global", while the local natural scales based method is denoted as "local".

Compared with the results shown in chapter 2, section 1, there are some ex-

Table 3.2: Quantitative results of the proposed methods using E_∞ on test curves shown in Fig. 3.8 and Fig. 3.10.

Test Curves	Method	N_{appr}	N_{opt}	E_{appr}	E_{opt}	Eff	Fid	$Merit$
figure-8	global	4	3.74	2.46	2.06	93.5	83.9	88.6
	local	4	3.74	2.46	2.06	93.5	83.9	88.6
chromosome	global	6	5.94	1.41	1.32	99.1	93.4	96.2
	local	6	5.94	1.41	1.32	99.1	93.4	96.2
semicir	global	15	9.54	1.66	1.00	63.6	64.3	63.9
	local	13	9.54	1.56	1.00	73.4	64.3	68.7
leaf	global	16	15.34	1.30	1.19	95.9	91.8	93.8
	local	16	15.34	1.30	1.19	95.9	91.8	93.8

isting algorithms that can achieve better performance for some curves. Among all the results of performance evaluation, Cornic's algorithm [27] obtains slightly better performance on three results. For most of the other five results, the proposed methods have much better results than it. Marji-Siy [16]'s method shows better performance for five results. However, the results of the proposed algorithms quite approach. Marji-Siy's method has not shown the results for the "figure-8" curve. Moreover, the method are quite complicated and computational expensive as stated in chapter 2, section 1. Horng's algorithm [26] also achieves three better results than the proposed algorithms. However, it uses Pei-Lin's method [72] to detect the initial corner points, and then applies dynamic programming to identify the final location of the corners. Dynamic programming is computationally expensive. Furthermore, it takes the polygonal approximation as the evaluation criterion, thus, the evaluation method adopted here should prefer this method. He-Yung's method achieves good results for all the test images, however, it is necessary to adjust three parameters carefully for the "semicir" curve. While, the proposed algorithms sustain for different curves and achieves good results in the evaluation, which is an advantage in practical

applications.

For the proposed methods, the main computation is spent on the Wavelet Transform. Comparing with the existing methods that use the same transformation tools, the proposed methods are efficient. For example, Quddus-Gabbouj's method need to do SVD at every tranformation scale. Corner detection is a local processing, therefore, parallel processing or hardware (ASIC/ FPGA) implementation can be adopted if it is necessary to speed up the methods.

To further evaluate the performance of the proposed algorithms, human perception based evaluation is tried. The human perception based evaluation shows that the proposed algorithms achieve comparable performance compared to Quddus-Gabbouj's method and He-Yung's method. The detail will be found in Appendix C.1.

3.6 Conclusions

In this chapter, we present two new CCD methods based on dyadic WT of the orientation function of a contour image. The maximum decomposition level of the dyadic WT is imposed by the contour length, which makes the algorithm suitable for both long and short contours. Unlike the existing methods, the information at all dyadic scales have been used for detection, which makes the proposed methods independent to the type of contour images. For the global based method, the average of the measurement at all the decomposed scales is taken as the detection measurement. For the local based method, the local natural scale is determined more accurately and the measurement at the local natural scale is used as the detection measurement. The two methods are also

computationally efficient due to the fast implementation of the dyadic WT. Both subjective and objective evaluation illustrates better performance of the proposed corner detectors compared to the conventional methods.

Chapter 4

Multiscale Corner Detection of Gray Level Images Based on Scale-space Theory

In the review in chapter 2, we find that Harris corner detector achieves the best results and has the widest applications. However, there exist several problems with Harris detector. In this chapter, we present an improved algorithm that solves the existing problems, while enhancing the detection rate.

This chapter is organized as follows. We first give an introduction in section 4.1. The characteristics about the DICD methods and the advantages are analyzed in subsection 4.1.1. In subsection 4.1.2 and 4.1.3, the motivations and objectives of this chapter are presented respectively. Then, in section 4.2, Harris detector is reviewed. Section 4.3 investigates the basic concept of the scale-space theory. In section 4.4, the proposed multiscale corner detection algorithm is presented. Section 4.5 shows the simulation results. The conclusion

is given in section 4.6.

4.1 Introduction

4.1.1 Characteristics of DICD methods

The DICD methods have more applications than the CCD methods. For some high texture images, e.g., trees with a lot of small leaves, the CCD methods nearly fail to do any detection, while the DICD methods still can pick up the high curvature points. Another advantage of the DICD methods is that they can detect more kinds of significant points, including the points that do not belong to edges, for example, single blob.

Corners are the points that have high intensity changes along two orthogonal directions in the images. The derivatives of images detect the changes of the intensity. For the DICD methods, some are based on the second order derivatives, some are based on the first order derivatives, while some are based on structures (zero order derivative) of the images. At first, researchers applied the second order derivative to detect the corners in 70's, e.g., in [96]. But it is found that these methods are sensitive to noise [101] because the noise mainly occurs in the high-frequency component of the images, which corresponds to the derivatives of images. Consequently, the higher the order of derivatives, the more amount of noise exists. Then the first order derivative based methods were proposed in 80's. The representative is the Harris detector [92]. In 90's, structure based methods were developed to improve the performance, for example, the SUSAN detector [93]. However, through simulation and applications, it is found that the Harris detector has a higher detection rate than the SUSAN

detector [95]. Thus, in this chapter, we focus on improving the performance of Harris detector.

4.1.2 Motivations

Although the Harris detector is well-known as the best detector and is used in many applications, there still exist some problems with Harris detector.

- First, it works in the space domain, so it detects corners at a certain scale.
- Second, three parameters need to be set manually for the Harris detector: the threshold, the detection scale, and the size of the non-maximum suppression window.
- Third, delocalization is a major inherent drawback of Harris corner operator, and it will increase with the scale at which it operates.
- Fourth, Harris detector can only detect corners of simple structures, e.g., "L" corners.

There is no strict mathematical definition for corners. Usually, they are taken as the high curvature points on the contour of the image. But this definition is a relative conception that is based on the scale selection. For example, in Fig. 4.1, the parts marked by circles seem to contain corner points when zoomed out, while they do not when zoomed in. We call these points large scale corners. While describing the object by corners, it is important to include these points.

In practice, an image usually contains important details belonging to a range of scales [14]. This makes multiscale analysis necessary. Meanwhile, *Human Visual System* (HVS) has the following two characteristics: first, the visual perception treats images on several scales simultaneously; second, when the

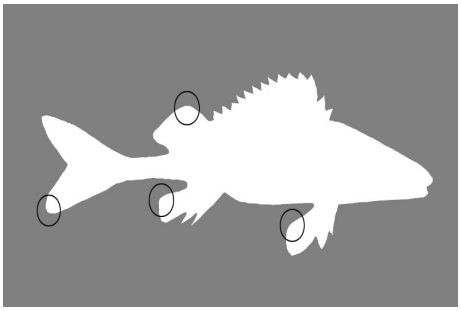

Figure 4.1: Illustration of large scale corners.

SNR (signal to noise ratio) decreases in an image, the HVS automatically increases the scales at which it characterizes the image.

4.1.3 Objectives

Due to the above analysis, it is preferable to detect corners at multiscales. In this chapter, we propose a multiscale corner detector for gray level images based on scale-space theory. Compared to Harris detector, the proposed method solves three problems existing in the Harris detector.

- Using the proposed detector, corners belonging to different scales are detected because it works in the scale-space domain.

- This method avoids the complexity of setting several parameters in the original method. Only one parameter needs to be set in the proposed method.

- The proposed algorithm solves the delocalization problem by detecting the corners from small scale to large scale, then tracking back from large scale to small scale. As the delocalization in the smallest scale can be ignored, the proposed method obtains the accurate localization.

The fourth problem described in subsection 4.1.2 is an inherent shortcoming of Harris detector. The proposed methods described in chapter 5 will solve it.

The multiscale scheme proposed here can also be applied to other spatial corner detectors to improve their performances. Comparisons among the proposed method, Harris corner detector [92] and SUSAN method [93] are also presented. Better results demonstrate the improved performance of the proposed method.

4.2 Scale-space theory

In 1983, Witkin proposes the principal rules of modern scale-space theory [49]. He considers the scale as a continuous parameter and structures of signals at different scales. In the following years, scale-space theory is studied and developed by Koenderink [14], Lindeberg [119] and Florack [126] etc.. They claim that the visual system should sample retinal irradiance with Gaussian apertures of a range of scales and Gaussian kernel is unique for generating the scale-space representation [127, 128, 119, 66].

For 1D continuous signal f, the scale-space representation of the signal is given by convolving the given signal with the Gaussian kernels of different width

$$L(\cdot, \sigma) = g(\cdot, \sigma) \circledast f, \tag{4.1}$$

where '$\circledast$' represents the convolution operator and g is the 1D Gaussian kernel

$$g(x, \sigma) = \frac{1}{\sqrt{2\pi\sigma^2}} \, e^{\frac{-x^2}{2\sigma^2}}. \tag{4.2}$$

The scale-space representation of an image $I(x, y)$ is defined as

$$L(x, y, \sigma) = g(x, y, \sigma) \circledast I(x, y), \tag{4.3}$$

where $g(x, y, \sigma)$ denotes the 2D uniform Gaussian kernel,

$$g(x, y, \sigma) = \frac{1}{2\pi\sigma^2} \, e^{-\frac{x^2+y^2}{2\sigma^2}}. \tag{4.4}$$

Due to the property of the derivative of a convolution, there is the following relationship for the derivative of the scale-space representation,

$$\partial^n L = (\partial^n g(\cdot, \sigma)) \circledast I = g(\cdot, \sigma) \circledast (\partial^n I), \tag{4.5}$$

which can extract various orders of local structures of the scale-space image.

From another point of view, scale-space representation is a special case of continuous wavelet transform, where the kernel (mother wavelet) must be selected as a derivative of the Gaussian function [119].

4.3 Revisit Harris corner detector

Besides the original paper [92] written by Harris and Stephens, we can find many other papers that analyze Harris method such as in [101] and [13]. To present a self-contained chapter, we review the original Harris method here.

In [100], Moravec employs the auto-correlation of an image to detect corners. The basic idea is that the differences between the adjacent pixels along an edge or on a uniform part of the image is small, but at the corner points the difference is high in all directions. The implementation is as follows. Consider a local window $w(u, v)$ centered at (u, v) in the image, shift the window a small amount (x, y) along various directions, then compute the average changes of the image intensity $E(x, y)$ that results from the shifting.

$$E(x, y) = \sum_{u,\ v} w(u, v)|I(x + u, y + v) - I(u, v)|^2, \tag{4.6}$$

where $I(u, v)$ represents the intensity of the image pixel at (u, v). In Moravec's method, $w(u, v)$ is unity within a specified rectangular region, and zero elsewhere. The shifts (x, y) considered by Moravec comprise $(1, 0), (0, 1), (1, 1), (-1, 1)$, i.e., along horizontal, vertical, and diagonal directions. After computing all the changes of E along the four directions, the minimum of E for every point is taken as the "cornerness" measurement. Then the corner points correspond to the local maxima.

In [92], Harris *et al.* make a significant improvement of Moravec's idea. They overcome the shortcomings of Moravec's method and develop the famous Harris corner detector (also called Plessey detector). To be robust to noise, they replace the binary rectangular window with a smooth circular Gaussian window. To be isotropic responses, they perform an analytic expansion about

the shift origin. To be suppressive to the responses to edges, they make use of the variation of E with the direction of shift to judge corners instead of the minimum E only. The derivative process is as follows.

$$\begin{aligned} E(x,y) &= \sum_{u,\ v} w(u,v)|I(x+u,y+v)-I(u,v)|^2 \\ &= \sum_{u,\ v} w(u,v)|xI_x+yI_y+O(x^2,y^2)|^2. \end{aligned} \tag{4.7}$$

Here, I_x and I_y denotes the first derivative of the image along the x and y directions respectively. By considering small shifts and a window of $w(u,v)$ as Gaussian window, i.e.,

$$w(x,y) = g(x,y) = \frac{1}{2\pi\sigma^2}\ e^{-\frac{(x^2+y^2)}{2\sigma^2}}. \tag{4.8}$$

We can approximate Eq. (4.7) as follows.

$$E_{x,y} \approx x^2L_x^2 + y^2L_y^2 + 2xyL_{xy} \tag{4.9}$$

$$= \begin{bmatrix} x & y \end{bmatrix} \begin{bmatrix} L_x^2 & L_{xy} \\ L_{xy} & L_y^2 \end{bmatrix} \begin{bmatrix} x \\ y \end{bmatrix}, \tag{4.10}$$

where

$$L_x^2 = g \circledast I_x^2, \tag{4.11}$$

$$L_y^2 = g \circledast I_y^2, \tag{4.12}$$

$$L_{xy} = g \circledast (I_x \times I_y), \tag{4.13}$$

here, g denotes the 2D Gaussian function. Let M denote the auto-correlation matrix (second moment matrix) in (4.10).

$$M = \begin{bmatrix} L_x^2 & L_{xy} \\ L_{xy} & L_y^2 \end{bmatrix}. \tag{4.14}$$

Through analyzing M, we can get the properties of E. Let α, β be the eigenvalues of M, then they form a rotationally invariant description of M. As M is a real and symmetric matrix, it can be decomposed as follows.

$$M = U \begin{bmatrix} \alpha & 0 \\ 0 & \beta \end{bmatrix} U^T, \tag{4.15}$$

where U denotes the orthogonal matrix that is constituted by the eigenvectors corresponding to the eigenvalues of M and ' U^T ' indicates the transpose of U. Consequently, the measurement E can be represented as follows.

$$E_{x,y} = [x\ y]U \begin{bmatrix} \alpha & 0 \\ 0 & \beta \end{bmatrix} U^T [x\ y]^T. \tag{4.16}$$

As we know that $[x, y]U$ is just the rotation of the coordinate system. Let $[x', y'] = [x, y]U$, then

$$E_{x,y} = [x'\ y'] \begin{bmatrix} \alpha & 0 \\ 0 & \beta \end{bmatrix} [x'\ y']^T \tag{4.17}$$

$$= \alpha x'^2 + \beta y'^2. \tag{4.18}$$

If both α and β are small, then E is small for the shift along arbitrary direction. If only one of them is small, the E is small only along the direction corresponding to the small eigenvalue, i.e., the shift along an edge. If both of the eigenvalues are large, it means that the shifts in any direction cause a large E, i.e., it corresponds to a corner.

To avoid computing the eigenvalues of M, the trace, tr, and the determinant, det, of M are used to measure the "cornerness".

$$tr(M) = L_x^2 + L_y^2, \tag{4.19}$$

$$det(M) = L_x^2 L_y^2 - L_{xy}^2. \tag{4.20}$$

The "cornerness" measurement function is defined as

$$R = \frac{det}{tr} = \frac{L_x^2 L_y^2 - L_{xy}^2}{L_x^2 + L_y^2}. \tag{4.21}$$

Eq. (4.21) should be interpreted in the limit sense when the tr approaches zero.

In [101], Noble analyzes the Harris detector and derives that the measurement of the Harris detector measures the curvature of the local structures of the image. To detect the corners, a commonly used post-processing algorithm, non-maximum suppression [35], is needed to be applied to suppress the multi-responses followed by the use of a preset threshold to delete false corners. Generally speaking, to get the best result, the scale of the Gaussian window, the size of the non-maximum suppression window and the threshold need to be decided by trial and error.

4.4 The algorithm of the proposed scale-space based corner detection

It is known that Harris corner detector has many good properties. Firstly, it is robust to noise because it uses only the first derivative of the image and is smoothed by a circular Gaussian kernel. Secondly, it performs well because of its isotropic response. Thirdly, it is easy to implement in practice. Due to these good properties, Harris corner detector is used very widely in many applications since it is proposed. But there exist some problems in this algorithm as we stated in section 4.3. In the proposed algorithm, we will focus on and solve the following problems.

- Harris method detects the corner points at one single scale, it can rarely capture all the corner points that contain sufficient information of the structures in the image;

- Since it detects the corner points only at one scale, the user needs to try manually at different scales to determine the suitable scale for each specific image. Harris corner detector also needs manually selection of the threshold value and the size of the non-maximum suppression window for each specific image;

- Delocalization is a major problem of Harris detector. In [97], Deriche and Giraudon analyze Harris detector and reach the conclusion that the shift increases with the smoothing scale. Thus, Harris corner detector has a tradeoff between the localization and the scale at which it operates. The larger the scale, the worse the localization.

To address the above problems, we propose a multiscale analysis scheme for

corner detection based on scale-space theory as follows.

We set a range of scales from small scale to large one. The image is transformed into the scale-space domain using Eq. (4.3). Then, the corner measurement is computed at each scale. After detecting the local maxima by a commonly used post-processing algorithm—non-maximum suppression, the false corners are suppressed by setting a threshold.

When the corner detection is completed at all the scales, the final result is obtained by combining the corners detected at each scale. Lastly, a tracking back algorithm is applied to find the accurate localization. For each detected corners, we search its corresponding local maxima in its neighbors from large scale to small scale. Consequently, the accurate localization is obtained at the first scale, i.e., the smallest scale. In the following, we discuss each step of the proposed algorithm in detail.

4.4.1 Scale-space representation of the second moment matrix

Compute the second moment matrix at different scales by varying the standard deviation of the Gaussian window as $\sigma_i = 0.5 : 5$ where the step size for σ_i is 0.5, i.e., $i = 1 : 10$.

$$L_x^2(\sigma_i) = g(\sigma_i) \circledast I_x^2. \tag{4.22}$$

$$L_y^2(\sigma_i) = g(\sigma_i) \circledast I_y^2. \tag{4.23}$$

$$L_{xy}(\sigma_i) = g(\sigma_i) \circledast (I_x \cdot I_y). \tag{4.24}$$

$$\mathbf{M}(\sigma_i) = \begin{bmatrix} L_x^2(\sigma_i) & L_{xy}(\sigma_i) \\ L_{xy}(\sigma_i) & L_y^2(\sigma_i) \end{bmatrix}. \tag{4.25}$$

Here, I_x, I_y are the first derivatives of the image along the x and y directions, $g(\sigma_i)$ is the Gaussian function, and $\mathbf{M}(\cdot, \sigma_i)$ is the second moment matrix at scale σ_i.

4.4.2 Cornerness measurement computation at each scale

Compute the "cornerness" measurement at each scale.

$$R(\cdot, \sigma_i) = \frac{L_x^2(\sigma_i)L_y^2(\sigma_i) - (L_{xy}(\sigma_i))^2}{L_x^2(\sigma_i) + L_y^2(\sigma_i)}. \tag{4.26}$$

Eq. (4.26) should be interpreted in the limit sense when the denominator approaches zero.

4.4.3 Automatic parameter-setting and detection at different scales

For each scale, non-maximum-suppression is applied to suppress the multi-responses. The size of the non-maximum suppression window relates with the size of the Gaussian window. The results obtained here should be stored for the following tracking procedure.

Since in practice, corners often belong to different scales in an image, we replace the threshold at each scale in [92] with the possible number of corners, n_0, which we expect to detect at each scale. Using this scheme, we need not adjust the threshold at each scale manually. This scheme also satisfies the requirements of the applications such as registration, calibration and matching etc. In these applications, sometimes we expect to have more corner points after the front-end processing. By increasing n_0, we may get more corner points

belonging to the large scale besides the small scale corners. This parameter setting agrees with both the definition of the corners and the characteristics of the HVS as stated earlier.

At each scale, the local maxima are sorted in a descending order. The first n_0 points are taken as corners detected at that scale.

4.4.4 Tracking forward and backward to localize the corners

To locate the corners accurately, we propose the following tracking forward and backward techniques.

- **Forward tracking**

From the second scale to the largest scale, find if the corner candidate at the current scale appears at the previous scale. If not, keep it; else, remove it. For example, for each corner detected at the second scale, we will examine the corresponding location at the first scale if there is a corresponding corner detected or not. If not, we keep it as the corner detected at the second scale. Otherwise, we remove it from the corner list of the second scale since it is already in the corner list of the first scale. Thus, the corners detected at the second scale are those that have not been detected at the first scale. This tracking forward procedure guarantees that the corners will be detected at the scale that is as small as possible. Consequently, we obtain the best localization precision for each corner point. Fig. 4.2 shows the results obtained at each scale of Fig. 4.1.

- **Backward tracking**

At last, for the corner points that are not detected at the first scale, we track back from the scale detected to the first scale based on the results obtained by the non-maximum suppression. For example, for the corners that are detected at the second scale, we will examine all the local maxima in the first scale and find the corresponding location for these corners. The size of each searching window should relate with the size of Gaussian window at that scale.

In [97], it is proved that the shift of the detected coordinates is 0.7611σ when the subtended angle is $\pi/2$. As $\sigma_1 = 0.5$, the delocalization can be ignored in the proposed algorithm provided that the tracking operator works efficiently.

The flowchart of the proposed algorithm is shown in Fig. 4.3.

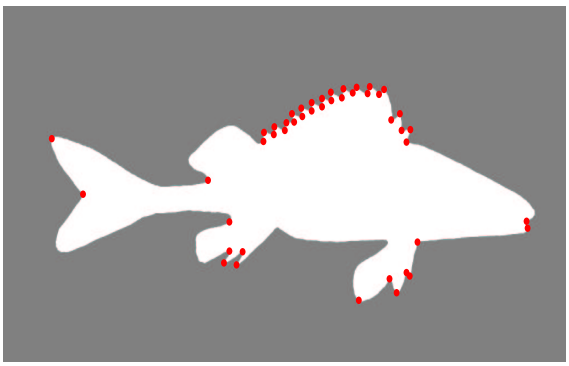

(a)

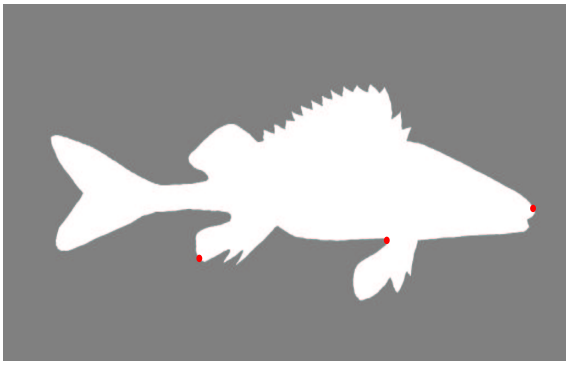

(b)

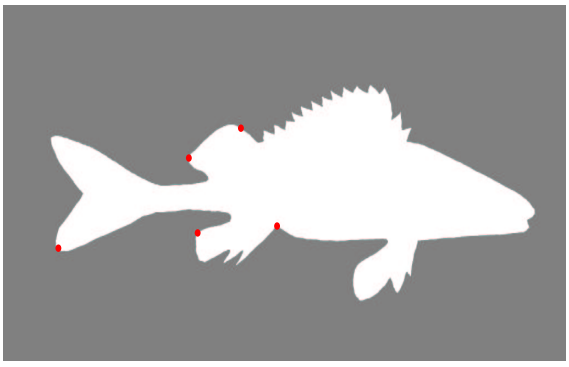

(c)

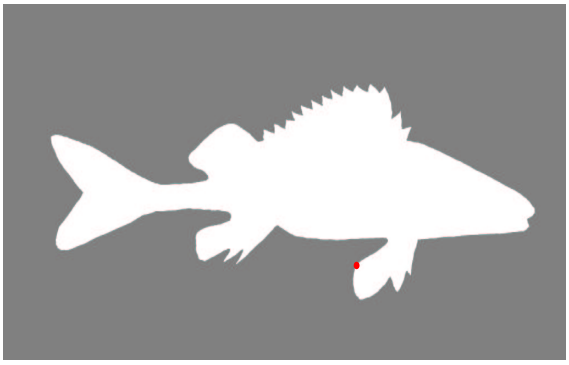

(d)

Figure 4.2: Results of corner detection (a) at level 1 ($\sigma = 0.5$), (b) at level 3 ($\sigma = 1.5$), (c) at level 4 ($\sigma = 2$), (d) at level 10 ($\sigma = 5$).

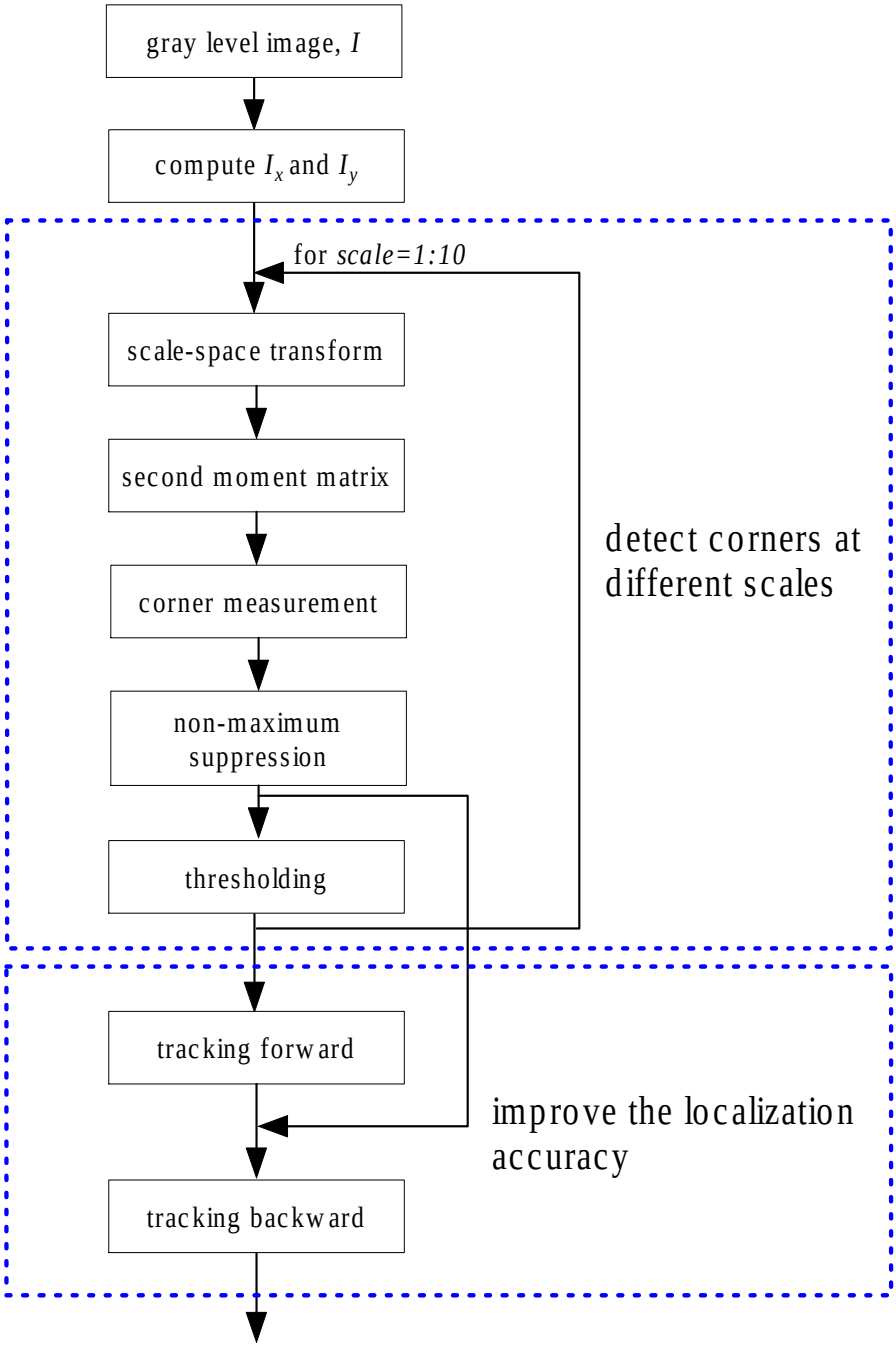

Figure 4.3: The flowchart of the proposed multiscale corner detection algorithm based on the scale-space theory.

4.5 Illustrative results and comparisons

In this section, we have compared the performance of the proposed method with Harris corner detector and SUSAN detector. We adjusted the parameters carefully for each detector to obtain the best results.

In Fig. 4.4 (a), both large scale corners and small scale corners are detected. The simulation results agree with our analysis. The proposed method detects all the corners belonging to different scales. While Harris detector and SUSAN detector cannot detect the large scale corners as marked in Fig. 4.1. SUSAN corner detector even misses some small scale corner points.

Fig. 4.5 is an image of a lab. It is more complex. Among the three method, the proposed method has the best performance. It detects most of the corners while keeping a low rate of false alarm. The detection of Harris corner detector must have a tradeoff between large scale corners and small scale corners. Thus, it detects less corners than the proposed method. SUSAN detector detects even less corner points and detects more false points as well.

The computational load of the proposed detector is higher than Harris detector. However, Harris detector needs a trial and error procedure. The proposed method can be operate more automatically, while providing better results.

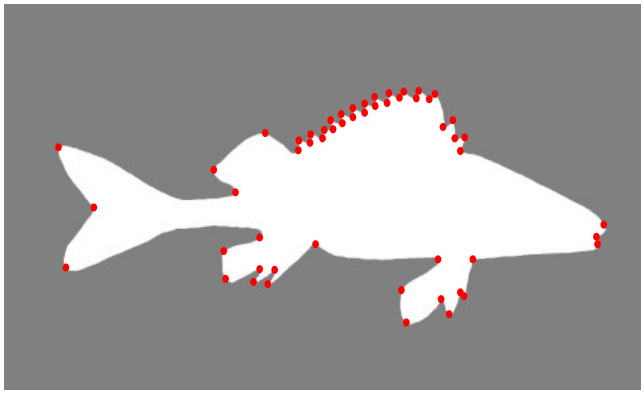

(a)

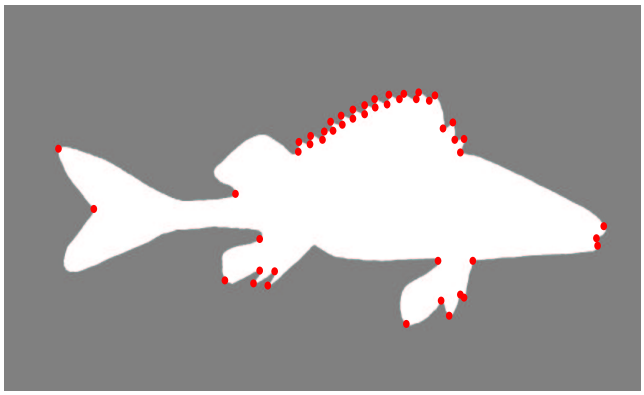

(b)

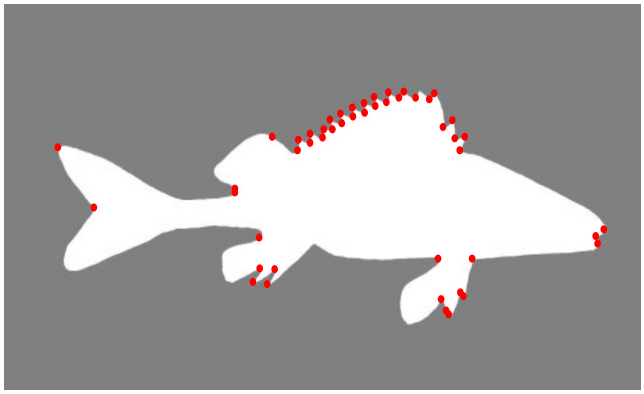

(c)

Figure 4.4: Results of corner detection using (a) proposed multiscale corner detector, (b) Harris detector, (c) SUSAN detector.

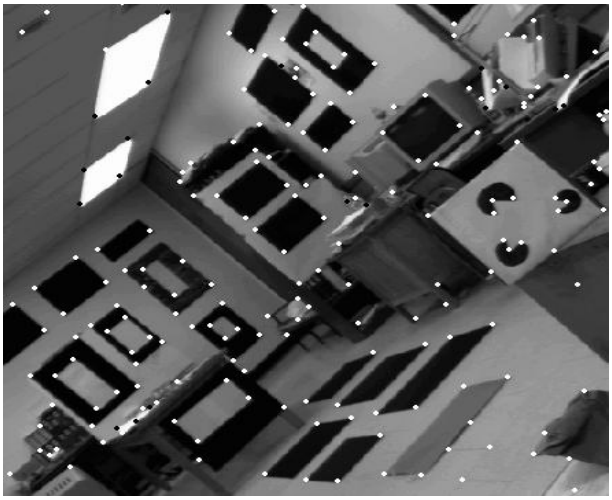

(a)

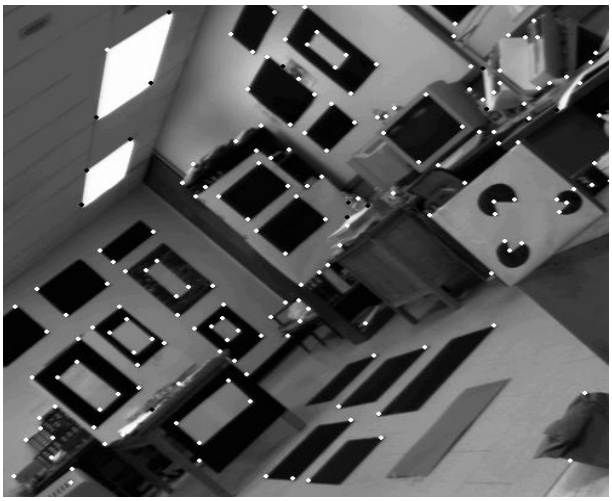

(b)

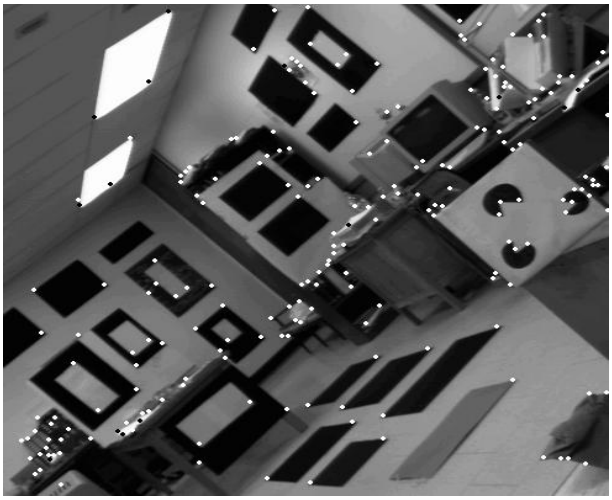

(c)

Figure 4.5: Results of corner detection using (a) proposed multiscale corner detector, (b) Harris detector, (c) SUSAN detector.

4.6 Conclusions

In this chapter, we propose a multiscale corner detection scheme. The proposed algorithm addresses the problems existing in Harris detector.

• The proposed multiscale algorithm detects the corner points at multiscales. At small scales, details of the structures in the image are captured. At large scales, the general feature of the structures is obtained [66]. Thus, the corners detected by the proposed algorithm obtain more complete information of the images.

• The proposed algorithm simplifies the setting of parameters. As the corners are detected at different scales, we can set the size of the non-maximum suppression window according to the size of the Gaussian kernel used in scale-space transformation. The number of corners expected to be detected at each scale is used as the threshold.

• To address the delocalization problem, we detect the corners from small scale to large scale. Corners detected at small scale have relatively better localization. After all the detections, we track back from large scale to small scale to obtain the accurate localization.

Experimental results show that this new method is efficient. It also simplifies the parameter setting and solves the delocalization problem existed in Harris detector. Moreover, this proposed scheme can be applied to other spatial corner detection methods to improve their performances as well.

Chapter 5

Multiscale Corner Detection of Gray Level Images Based on Log-Gabor WT

The main issue of this thesis is to solve the existing three problems of corner detection, i.e., (1) incomplete information based detection, (2) delocalization problem, and (3) multiple responses to higher order structures. For the contour based corner detection methods, it mainly has the first problem. Accordingly, in chapter 3, we proposed two new CCD methods that solve the first problem. However, the contour based method has its inherent shortcomings (e.g., it depends on the prior segmentation and boundary tracking), which limit its performance and applications. Thereafter, in chapter 4, we propose an improved algorithm based on Harris detector, which solves the first and second problems. The original Harris detector has the drawback of the third issue, and so does the improved algorithm proposed in chapter 4. In this chapter, we propose two

methods that solve all the three existing issues. As a result, these two methods obtain the best performance. The first method is a simple algorithm that is based on the *log-Gabor WT and orientation information* (LGWTOI). The second method is an algorithm that is based on the *log-Gabor WT and second moment matrix* (LGWTSMM).

The rest of this chapter is organized as follows. In section 1, we give an introduction of this chapter. Section 2 is the theory background of Gabor wavelets and log-Gabor wavelets. In section 3, the simple algorithm based on LGWTOI is described in detail. The algorithm based on LGWTSMM is presented exhaustively in section 4. Section 5 shows the simulation results of the two proposed methods, compared with the results of Harris and Kovesi's detectors. We draw the conclusion in section 6.

5.1 Introduction

Generally speaking, corner points have the following characteristics. First, they are local features of an image. Second, they may belong to structures of different sizes in an image. On the other hand, wavelet transform (WT) is a tool that can provide multi-scale analysis while analyzing the local behavior of a signal. Due to the above analysis, it is attractive to apply WT in corner detection. Because different wavelets have different properties, the selection of wavelet bases is of great importance.

As there is no strict mathematical definition for corners, the judgement of a corner point is subjective. Thus, it is suitable to detect corners using filters that agree with the *human visual system* (HVS). Gabor wavelets are such filters. Furthermore, Gabor wavelets have the optimal localization in time-frequency plane. They transform the input images along multi-orientations. The magnitudes along the orientations provide more intuitive and useful information to describe the shape of the 2D structures. However, the maximum bandwidth of it is limited to approximately one octave. Furthermore, Gabor wavelets are not optimal for broad spectral information with maximal spatial localization. In [124], Field proposed the log-Gabor WT that is an improvement of Gabor WT. Log-Gabor wavelets can be constructed with arbitrary bandwidth and the bandwidth can be optimized to produce a filter with minimal spatial extent. Consequently, we can expect to detect and localize corners accurately using log-Gabor wavelets.

In this chapter, we first propose a novel corner detection algorithm using log-Gabor WT and its orientation information. In the proposed algorithm, the input image is decomposed at several wavelet scales and along several direc-

tions. The magnitude along the direction that is orthogonal to the gradient orientation represents the "cornerness" measurement. Using this detector, corners are detected and localized accurately. Meanwhile, this method provides us the magnitudes and orientations along the principal axes corresponding to the directions of the eigenvectors of the local changes. The information is useful when we deal with the affine transform applications in matching problems.

The second proposed method is based on log-Gabor wavelets and second moment matrix. The input image is decomposed by the Log-Gabor wavelets at multiscales along multi-orientations. Then the components at different scales and orientations are projected onto the x-axis and y-axis and formulated into the second moment matrix. Finally, the smaller eigenvalue of the second moment matrix is used to detect corner points.

Comparisons among the proposed methods, Harris corner detector [92] and Kovesi's method [107] are presented. The results demonstrate the good performance of the proposed methods.

5.2 Gabor wavelets and log-Gabor wavelets

As log-Gabor wavelet is an improvement of Gabor wavelet, let us start the description from the Gabor wavelet whose theory is easier to be understood.

5.2.1 Gabor wavelets

1D Gabor wavelet is constructed with modulating the Gaussian window to a certain frequency [129].

$$\psi(x) = g(x)\ e^{i2\pi\eta x}, \tag{5.1}$$

where

$$g(x) = \frac{1}{\sqrt{2\pi\sigma_x^2}}\ e^{-\frac{x^2}{2\sigma_x^2}}. \tag{5.2}$$

Here, σ_x controls the width of the region over which most of the energy of $\psi(x)$ is concentrated, and η is the frequency parameter. It is proved that the Gabor kernel is the optimal one in the sense that it simultaneously locates accurately in both the frequency domain and the space domain [121].

The 2D Gabor wavelets are known to give a good fit to the behavior of the receptive field of simple cells in mammals' primary visual cortex [121, 130, 131]. A 2D Gabor function is obtained with a Gaussian window $g(x, y)$ modulated by a sinusoidal wave:

$$\psi(x, y) = g(x, y)\ e^{i2\pi\eta x} = \frac{1}{2\pi\sigma_x\sigma_y}\ e^{-\frac{1}{2}\left[\frac{x^2}{\sigma_x^2}+\frac{y^2}{\sigma_y^2}\right]}\ e^{i2\pi\eta x}. \tag{5.3}$$

In Eq. (5.3), $g(x, y)$ is the 2D Gaussian function, and i refers to the imaginary notation. The Fourier transform of the Gabor function is:

$$\Psi(u, v) = \ e^{-\frac{1}{2}\left[\frac{(u-\eta)^2}{\sigma_u^2}+\frac{v^2}{\sigma_v^2}\right]}, \tag{5.4}$$

where, $\Psi(u, v)$ is the Fourier transform of $\psi(x, y)$ and $\sigma_u = 1/(2\pi\sigma_x)$, $\sigma_v = 1/(2\pi\sigma_y)$.

The 2D Gabor wavelets are obtained by rotating and dilating the mother wavelet [131].

$$\psi_{mn}(x, y) = a^{-m}\psi(x', y'). \tag{5.5}$$

In Eq. (5.5),

$$x' = a^{-m}(x\cos\theta + y\sin\theta). \tag{5.6}$$

$$y' = a^{-m}(-x\sin\theta + y\cos\theta). \tag{5.7}$$

Here, $\theta_n = n\pi/K$ is the orientation for $n = 1, 2, \cdots, K$, where K is the total number of orientations. $a^{-m}, m = 0, 1, \cdots, S-1$ is the scale factor.

Gabor wavelets have the optimal energy concentration in the time and frequency plane [121]. Furthermore, they provide multi-scale and multi-orientation information of the input image. Fig. 5.1 shows a cover of the frequency plane by such Gabor wavelets.

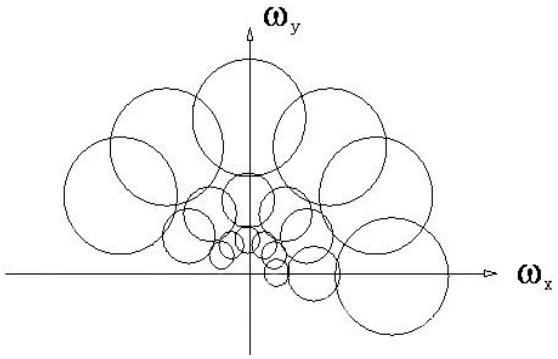

Figure 5.1: Illustration of the frequency supports of 2D Gabor wavelets.

5.2.2 Log-Gabor wavelets

Although Gabor wavelets obtain the optimal localization in spatial and frequency domains simultaneously, the maximum bandwidth of a Gabor filter is limited to one octave. Otherwise, the zero frequency (low frequency) component is not small. In [124], Field proposes the log-Gabor wavelets that solve the problems existing in Gabor wavelets. Log-Gabor filters can be constructed with arbitrary bandwidth and the bandwidth can be optimized to produce a filter with minimal spatial extent [132].

Gabor functions have Gaussian transfer functions when viewed on the linear frequency scale. While log-Gabor functions have Gaussian transfer functions when viewed on the logarithmic frequency scale. Log-Gabor function has the following transfer function if viewed in the linear frequency scale.

$$G(f) = e^{-\frac{(log(f/f_0))^2}{2(log(\sigma/f_0))^2}}, \tag{5.8}$$

where, f_0 is the filter's center frequency. σ/f_0 controls the shape ratio of the filter. Fig. 5.2 illustrates the difference between Gabor and log-Gabor transfer functions in the frequency domain.

2D log-Gabor filters can be constructed in the frequency domain around some central frequency (f_i, θ_i), where θ_i is the orientation angle of the filter, and f_i is the central radial frequency [133, 134]:

$$G(f, \theta) = e^{-\frac{(log(f/f_i))^2}{2(log(\sigma_{f_i}/f_i))^2}} e^{-\frac{(\theta-\theta_i)^2}{2\sigma_{\theta_i}^2}}, \tag{5.9}$$

where, σ_{f_i} defines the radial bandwidth B in octaves with

$$B = 2\sqrt{2/log2}|log(\sigma_{f_i}/f_i)|, \tag{5.10}$$

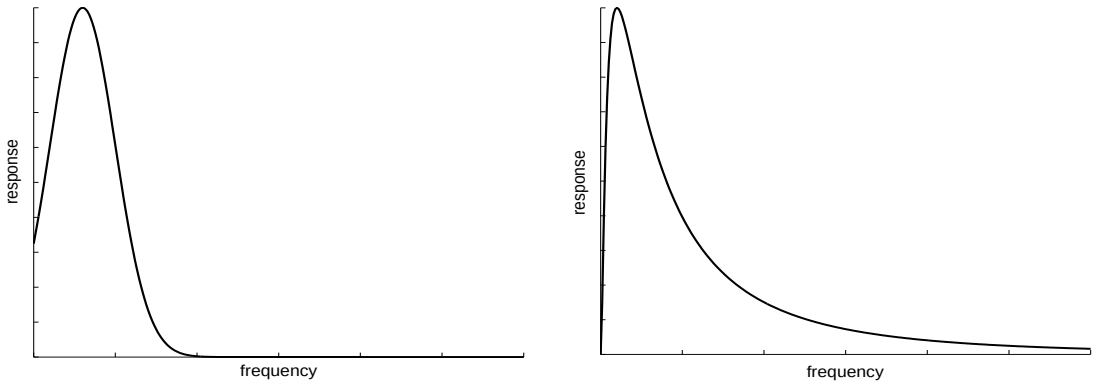

(a) (b)

Figure 5.2: Illustration of the frequency supports of 1D (a) Gabor transfer function, and (b) log-Gabor transfer function.

and σ_{θ_i} defines the angular bandwidth

$$\Delta\Omega = 2\sigma_{\theta_i}\sqrt{2log2}. \tag{5.11}$$

Here,

$$G(f) = e^{-\frac{(log(f/f_i))^2}{2(log(\sigma_{f_i}/f_i))^2}}, \tag{5.12}$$

is the radial component, which controls the frequency band that the filter responds to, and,

$$G(\theta) = e^{-\frac{(\theta-\theta_i)^2}{2\sigma_{\theta_i}^2}}, \tag{5.13}$$

is the angular component, which controls the orientation that the filter responds to. The two components are multiplied together to construct the overall filter. Fig. 5.3 shows the magnitude responses of the 2D log-Gabor filters along eight directions.

Figure 5.3: 2D log-Gabor filters at different orientations.

5.3 The proposed corner detection algorithm based on log-Gabor WT and orientation information (LGWTOI)

As corners are 2D high frequency features, they should have high values along the two principal axes corresponding to the directions of the eigenvectors of local changes. Using log-Gabor WT, we obtain first the magnitudes at every pixel along different directions at each scale. The magnitudes at different scales are averaged. For each pixel, we detect the maximum value among all the magnitudes of different orientations. This value is called the *modified wavelet transform modulus maxima* (MWTMM). This detection is reliable because the maximum value is robust to noise. Then the value along the direction that is orthogonal to the direction of the MWTMM is selected as the "cornerness" measurement. The proposed corner detection method is described as follows.

- Step 1. The input image $I(x, y)$ is first transformed using the log-Gabor wavelet along K orientations for s scales, given by

$$W_{j,k}(x, y) = \int I(x, y)\psi^*_{j,k}(x - x_1, y - y_1)dx_1dy_1, \tag{5.14}$$

for $j = 1, 2, \cdots, s$, and $k = 1, 2, \cdots, K$. In (5.14), ' * ' denotes the complex conjugate, whereas $W_{j,k}(x, y)$ represents the wavelet coefficients for the decomposition using log-Gabor wavelet.

- Step 2. Average the magnitudes obtained at different scales.

- Step 3. Select MWTMM among the magnitudes of the K directions and record the direction for each pixel. It can be denoted as $W(k_1)$. k_1 denotes the direction of the MWTMM. The value of the MWTMM is proportional to the

gradient which is along the principal axis.

• Step 4. Select the value along the direction, k_2, that is orthogonal to the gradient (i.e., k_1), which is denoted as $W(k_2)$. Here, k_2 is the other principal direction. $W(k_2)$ is proportional to the differential value along the other principal axis. The relationship between k_1 and k_2 is $|k_1 - k_2| = K/2$.

• Step 5. Apply non-maximum suppression to the result obtained in Step 4. Non-maximum suppression is a simple but efficient post processing technique in image processing. It uses a local window sliding through all the pixels in the image. If the center pixel of the window is the local maximum within the window, then the central pixel value is kept; otherwise, it would be deleted.

• Step 6. To suppress the false detection, the corners are detected by applying a threshold to the results obtained in Step 5. The threshold is selected experimentally.

Due to the inherent denoising properties of WT, this proposed detection method is less sensitive to noise. The magnitudes and orientations information obtained in Step 3 and Step 4 can be used further in other applications, such as affine invariant detection.

The flowchart of the algorithm is shown in Fig. 5.4.

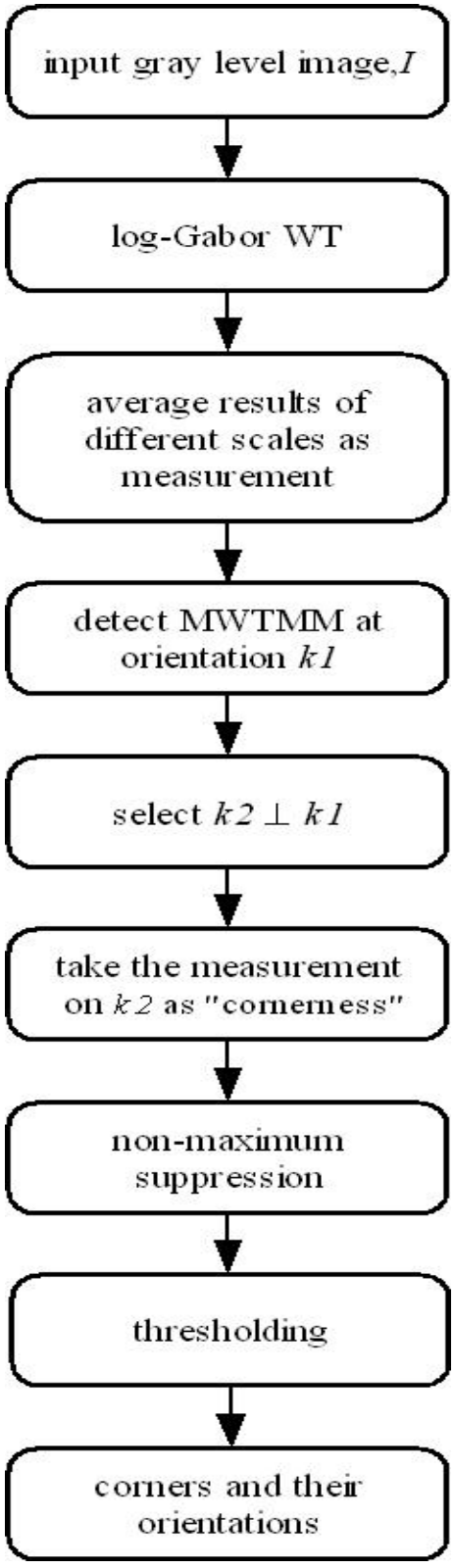

Figure 5.4: Flowchart of the proposed algorithm based on LGWTOI.

5.4 The proposed corner detection algorithm based on log-Gabor WT and second moment matrix (LGWTSMM)

The algorithm presented in section 5.3 is simple and efficient. However, the response of it is not isotropic. The resolution of the orientation is determined by the total number of orientations K applied in the algorithm. To get the isotropic response, we present an algorithm based on LGWTSMM in this section.

The input image is transformed by the log-Gabor wavelets along several directions and scales as shown in Eq.(5.14).The following measurement are computed.

$$a = \sum_j \sum_k (|W_{j,k}|cos(\theta_k))^2, \tag{5.15}$$

$$b = \sum_j \sum_k |W_{j,k}|cos(\theta_k)|W_{j,k}|sin(\theta_k), \tag{5.16}$$

$$c = \sum_j \sum_k (|W_{j,k}|sin(\theta_k))^2. \tag{5.17}$$

In Eqs. (5.15)-(5.17), $j = 1, 2, ...s$ and $k = 1, 2, ...K$ represents the scale and orientation respectively. θ_k is the angle of the orientation k. $W_{j,k}$ represents the log-Gabor WT coefficient at scale j and orientation k.

The second moment matrix is then constructed as follows.

$$M = \begin{bmatrix} a & b \\ b & c \end{bmatrix}. \tag{5.18}$$

The eigenvalues of the above matrix is

$$\lambda_{1,2} = \frac{1}{2}(a+c) \pm \frac{1}{2}\sqrt{4b^2 + (a-c)^2}. \tag{5.19}$$

We take the smaller eigenvalue as the "cornerness" measurement. The non-maximum suppression and threshold is applied as the post processing.

The flowchart of the algorithm is illustrated in Fig. 5.5.

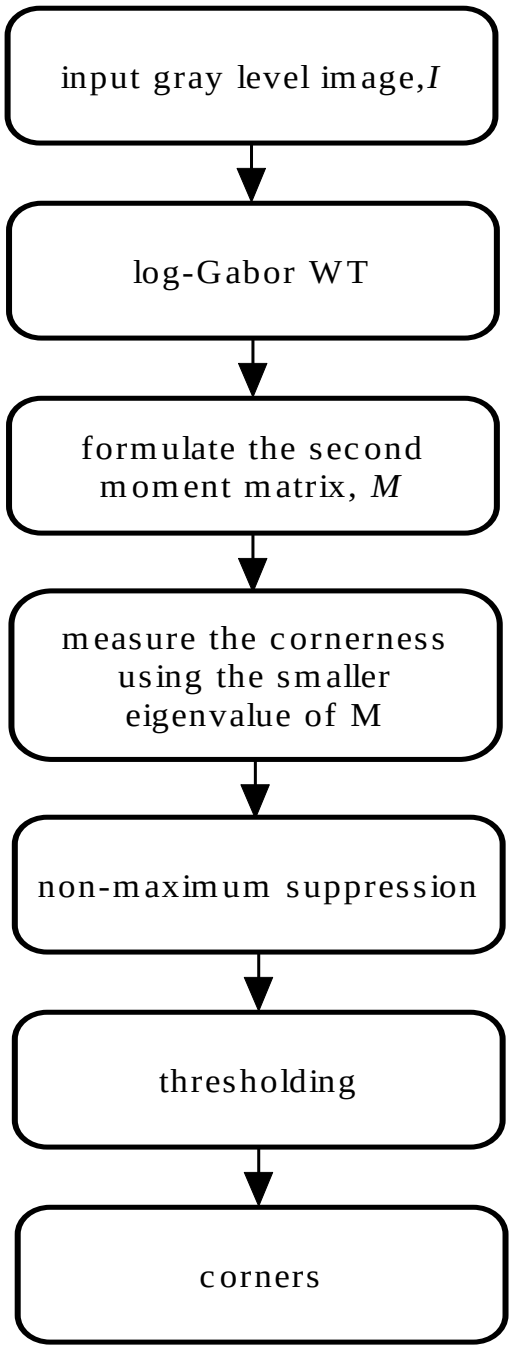

Figure 5.5: Flowchart of the proposed algorithm based on LGWTSMM.

5.5 Illustrative results and comparisons

In this section, we compare the performance of the proposed methods with Harris corner detector and Kovesi's detector visually.

In Fig. 5.6, a synthetic image called as "model" is used for evaluation. The "model" image contains corner types: "L", "Y", "T" and "X". Fig. 5.6(a) and (b) present the detection results of our proposed LGWTOI and LGWTSMM methods respectively. Both of the proposed methods achieve good results. However, the LGWTOI method needs careful adjustment of the parameters, i.e., the size of the non-maximum window, and the threshold. The LGWTSMM method can achieve good result with easy-setting parameters, which means that the parameter selection is not crucial. It further demonstrates the robustness of the LGWTSMM method. The result of Harris detector shown in Fig. 5.6 (c) treats the "T" and "X" corners as 2 and 4 separate corners, respectively. If we increase the size of the non-maximum window and the threshold, the extra detection of the "X" corners can be removed, but the extra detection of the "T" corner remains. Fig. 5.6 (d) gives the result of Kovesi's detector. Kovesi's method also shows good results for all the types of corners.

In Fig. 5.7, the "Lab" image is used for simulation. The results of the proposed methods and the Kovesi's method are obtained using the same parameters as in the simulation of the "model" image. For Harris detector, we adjust the parameters to get the best results. The proposed LGWTSMM method achieves better performance than the Harris detector. More correct corners are detected while keeping a low rate of false alarm. Although the proposed LGWTOI method detects more corners than the Harris detector, it also has a high rate of false alarm. For Kovesi's method, its performance is comparable with

the LGWTSMM method, but better than the LGWTOI method.

It is noted that the simulation results as presented in this chapter are obtained by using three scales, i.e. s=3, and the total number of orientations of 8, i.e. K=8.

For the proposed methods, the main computation is spent on the Wavelet Transform. Comparing with the existing methods (e.g. the Kovesi's method) that use the same transformation tool, the proposed methods are efficient. Fast transformation can be explored to speed up the detection in the future work. Furthermore, corner detection is a local processing, thus, parallel processing is possibly adopted in the time-critical applications.

For the third algorithm, the localization is theoretically approved to be accurate (pp.103, line 8-10). For the algorithms proposed in this chapter, the localization is analyzed on the "model" image. There are totally 19 corners in the image. From the results, we see that Kovesi's method achieves the best localization. For the proposed methods, there are 4 and 2 corners that are 2 pixels away from the true locations respectively. For Harris detector, we consider the detected point that is near the true location as the detected corner for the multiple responses. However, there are still 6 points that are 1 pixel away from the true locations and 3 points that are 2 pixels away. Although the localization of the proposed methods is improved compared to Harris detector, it still has some space to improve.

Table 5.1: Localization analysis on the "model" image: number of detected corners that are some pixels away from the true locations.

Methods	1 pixel away	2 pixels away
LGWTOI	0	4
LGWTSMM	0	2
Kovesi	0	0
Harris	6	3

5.6 Conclusions

In this chapter, we propose two multi-scale corner detection methods based on log-Gabor WT. Experimental results show that the new methods are efficient. The localization is improved by utilizing the optimal localization property of the log-Gabor WT. In the first proposed algorithm, the multi-orientation information is applied directly to detect corners. To achieve isotropic response, the second method exploits the multi-orientation decomposition of log-Gabor WT and constructed the second moment matrix. The smaller eigenvalue of the second moment matrix is used to detect corners. Both the methods provide a unique response for the higher order structure corners. Simulation results compare the proposed methods with the two existing well-known approaches and show the good performance of the proposed methods.

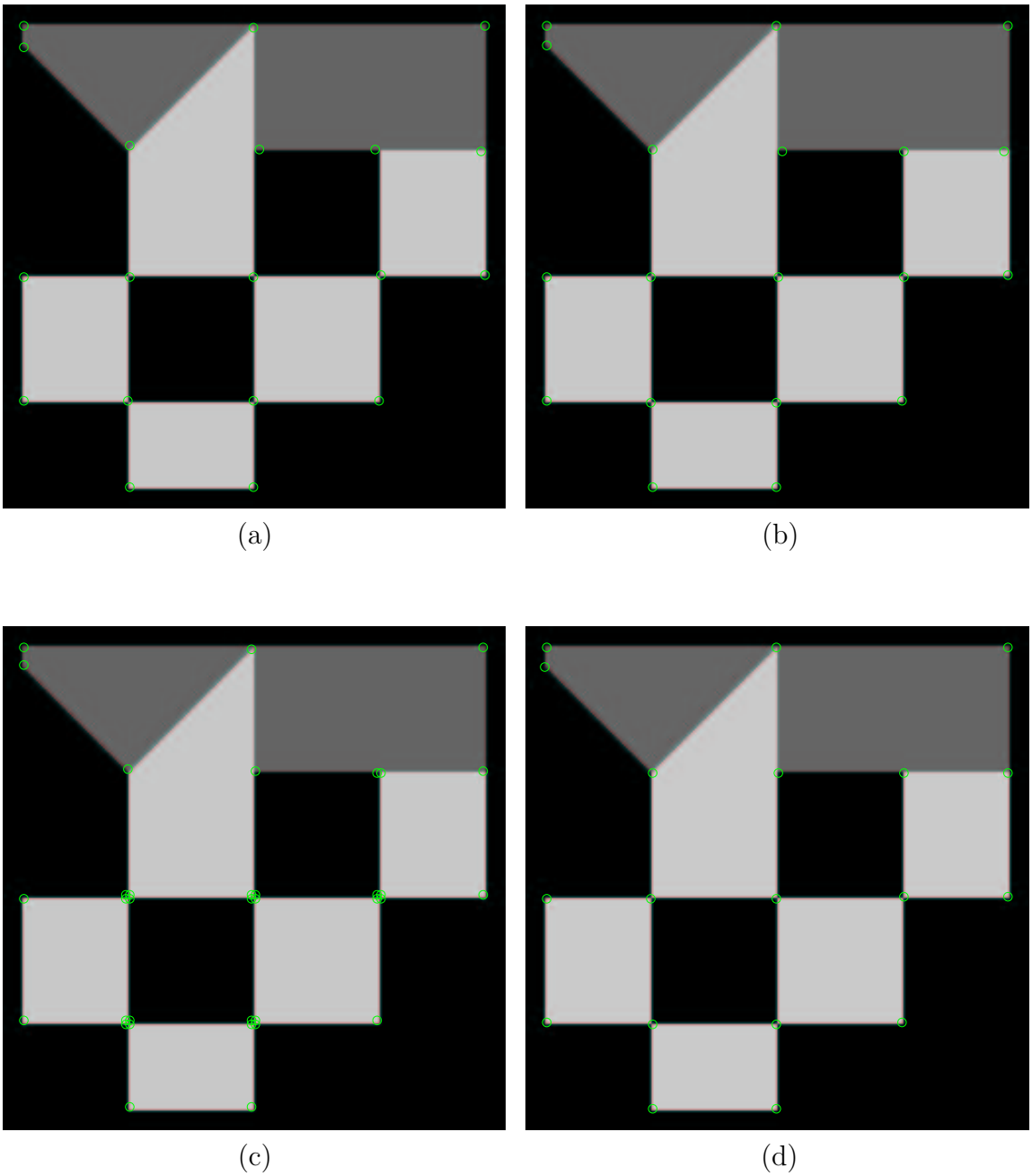

(a) (b)

(c) (d)

Figure 5.6: Results of corner detection using (a) proposed LGWTOI method, (b) proposed LGWTSMM method, (c) Harris detector, (d) Kovesi's detector.

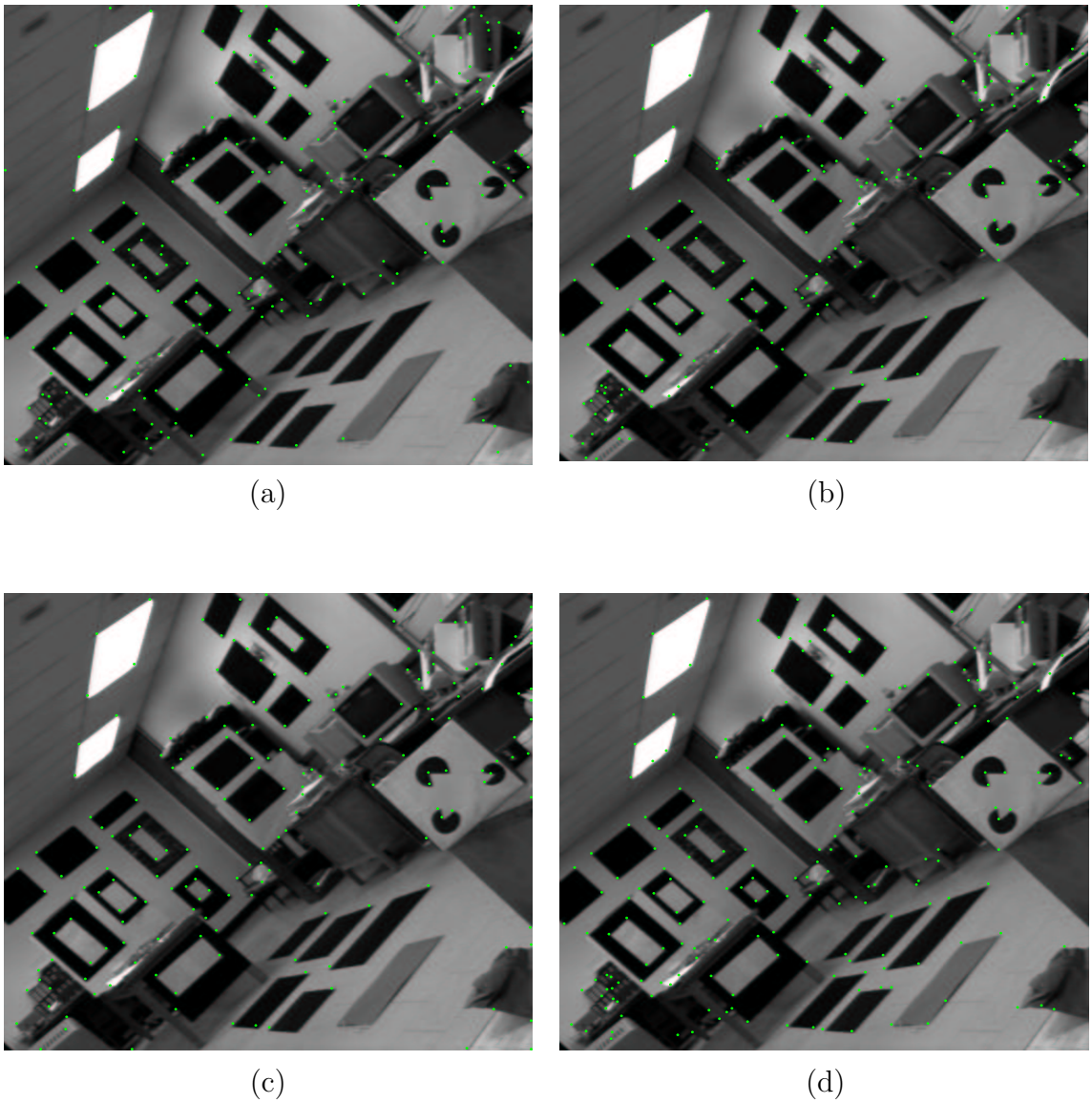

(a) (b)

(c) (d)

Figure 5.7: Results of corner detection using (a) proposed LGWTOI method, (b) proposed LGWTSMM method, (c) Harris detector, (d) Kovesi's detector.

Chapter 6

Comparison in a Stereo Matching System

Although corners are very important in many applications of computer vision and image processing, there is no benchmark or standard evaluation method for gray level corner detection algorithms. Most of the existing literatures apply the visual evaluation. Very few evaluate objectively. In [135], *receiver operating characteristic* (ROC) is applied to analyze the detection rates across all values of a detection threshold. In [110], Sojka defines the ground-truth manually. There are also some publications that focus on the performance evaluation such as in [136, 137, 138, 139, 140, 141]. However, no standard evaluation method exists yet.

In this thesis, the CCD methods have been quantitatively evaluated by Rosin's method in chapter 3. In this chapter, the algorithms proposed in chapter 4 and 5 are evaluated in a stereo matching system. This application based evaluation gives quantitative measurement of the proposed DICD methods, Harris

detector and Kovesi's detector.

As a local feature, corners are invariant to translation, rotation and scaling. This property makes it more suitable for matching problems, particularly for partial occluded object matching, while the methods based on the global features can not work in this case. Accordingly, corner detection has a wide application in stereo matching algorithms. In this thesis, we adopt a classical stereo matching system to measure the objective performance of the proposed DICD algorithms.

In the following, we apply the proposed improved Harris method, the proposed log-Gabor based methods, Harris method and Koves's method in the stereo matching applications. Based on the results of the corner detectors, the *zero-mean normalized cross correlation* (ZNCC) method is used to generate the putative matching results. Then, the normalized 8-point algorithm [11] is used to compute the fundamental matrix. The inlying matching results satisfied the fundamental matrix are verified manually. The final matching ratio is used as the evaluation index.

6.1 Introduction

Stereo vision refers to the ability to acquire information on the 3D structure and distance of a scene from two or more intensity images taken from different viewpoints [142]. The important part of the problem is to matching the points in one image to the corresponding points in another image. In this context, we focus on the matching problem of two images.

The corresponding algorithms can be classified into correlation-based (some-

times called area-based) and feature-based algorithms. Feature-based methods match the features, such as linking edges etc.. Correlation-based methods detect "corner points" in each image, then correlation measurements of the image windows centered on the corner points are computed as the score of matching. Different matching methods are reviewed in [143, 144, 145, 146]. In this chapter, we adopt the classical ZNCC algorithm.

To compute the fundamental matrix, the normalized 8-point algorithm is adopted. In the putative results obtained by the ZNCC algorithm, there still exist some outliers. To robust fit a fundamental matrix, RANSAC (Random Sample Consensus) algorithm [147] is used. Other fitting methods such as least-squares minimization or median least-squares minimization methods can be found in [148].

The inlying matching results satisfied the fundamental matrix are verified manually and the matching ratio is taken as the evaluation index.

The following of this chapter is organized as follows. In section 2, ZNCC method is briefly introduced. The RANSAC method is investigated in section 3. Section 4 describes the normalized 8-point algorithm. The simulation and evaluation results are shown in section 5. Section 6 gives the conclusion.

6.2 Zero-mean normalized cross correlation matching

Zero-mean normalized cross correlation (ZNCC) is a simple but robust method to measure the similarity between image pairs. For every feature point in the

first image, a window of the data is extracted and correlation score with a window corresponding to any feature point in the other image is computed as follows.

$$C_{I_1,I_2} = \frac{\sum_w (I_1 - \mu_1)(I_2 - \mu_2)}{\sqrt{\sum_w (I_1 - \mu_1)^2 \sum_w (I_2 - \mu_2)^2}}, \tag{6.1}$$

where I_1, I_2 represent the points in the two windows belonging to the two images respectively, whereas w is the window. μ_1 and μ_2 are the means with the two windows.

The normalization provides invariance to linear transformation of the image grey-levels [145]. The matching algorithm also rejects the idea of thresholding the correlation score. The maximum correlation is picked instead. The left-right consistency constraint is applied in the algorithm. It means that the matching from first image to second image must also be the maximum one when matching from the second image to the first image. In another words, the matching from each image independently must reinforce each other.

6.3 Random sample consensus (RANSAC) algorithm

RANSAC is a robust algorithm to fit a model of experimental data [149]. It is proposed by Fischler and Bolles in [147]. The algorithm is capable of interpreting and smoothing data containing a significant percentage of gross errors. Consequently, it is suitable for applications in automated image analysis where interpretation is based on the data provided by error-prone feature detectors.

RANSAC works as follows. First, a number of samples are drawn uniformly but at random from the input data set. Then the model is constructed. In the

following, the model is evaluated on the whole data set. The number of inliers (a commonly used cost function) is counted. The above process is repeated a number of times and the model with most support is taken as the robust fit. As the model estimated by RANSAC is correct with a certain probability, the estimated model parameters are recomputed by for example a least-squares fit to the data subset which supports the best estimate. The RANSAC algorithm is widely applied in computer vision, such as feature matching, registration etc.. The details of the algorithm can be found in [147, 149, 11].

6.4 The normalized 8-point algorithm

The normalized 8-point algorithm is first proposed by Longuet-Higgins in [150]. It is a simple but efficient method to compute the fundamental matrix [11]. The first and important step in this algorithm is to normalize the input data so that the origin is at centroid and mean distance from origin is $\sqrt{2}$.

The fundamental matrix is defined by the equation

$$X_1^T F X_2 = 0, \tag{6.2}$$

where X_1 and X_2 are the homogeneous coordinates of any pair of matching points in the two images. The solution is obtained by solving linear equations followed by a constraint enforcement [11]. Finally, a denormalization is applied to get the fundamental matrix corresponding to the original data.

6.5 Evaluation results - matching ratio

To evaluate the proposed methods in a quantitative way, the corner detection results are input in the stereo matching system described above. The matching inliers are examined manually. To compare the performance, the number of corners detected in each images is set the same. The number of correct matching is recorded. The matching ratio is used as the evaluation index.

$$r = \frac{n_2}{n_1}, \tag{6.3}$$

where n_2 is the number of correct matching, and n_1 is the number of detected corners. The illustration of the evaluation system is shown in Fig. 6.1. A set of

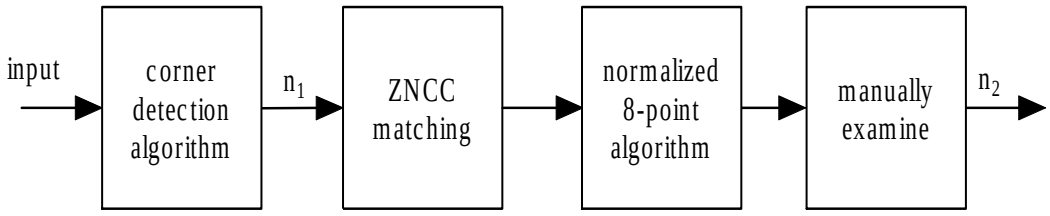

Figure 6.1: Illustration of the evaluation system.

commonly used pairs of images shown in Fig. 6.2-6.6 is used in the experiment.

Figure 6.2: Test image pairs: "Venus".

Figure 6.3: Test image pairs: "Tsukuba".

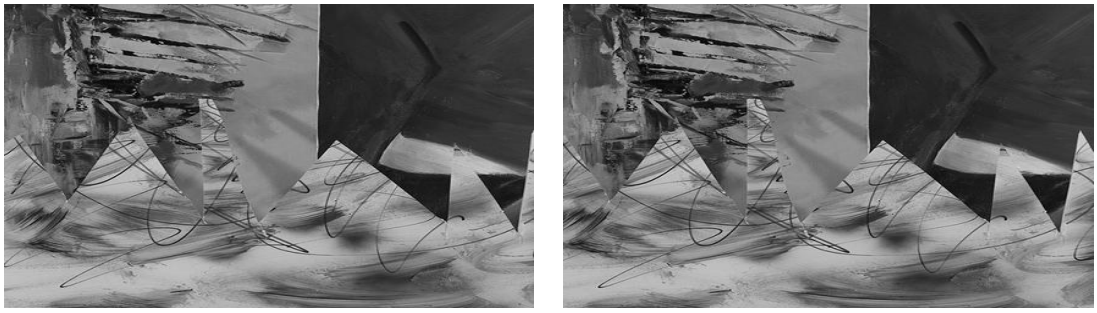

Figure 6.4: Test image pairs: "Sawtooth".

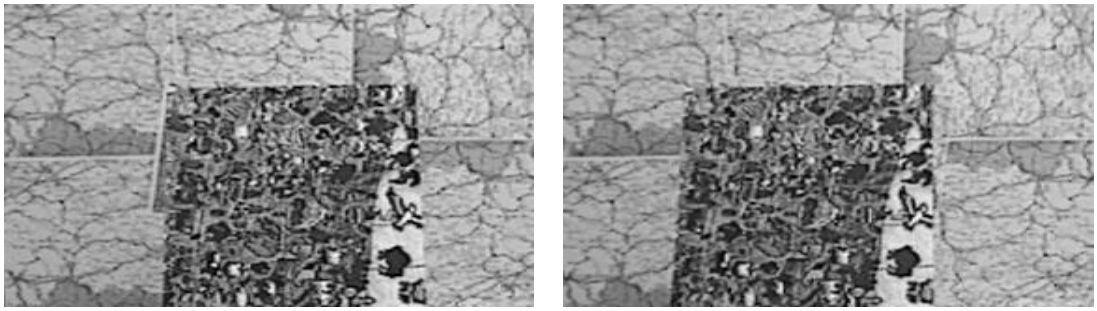

Figure 6.5: Test image pairs: "Map".

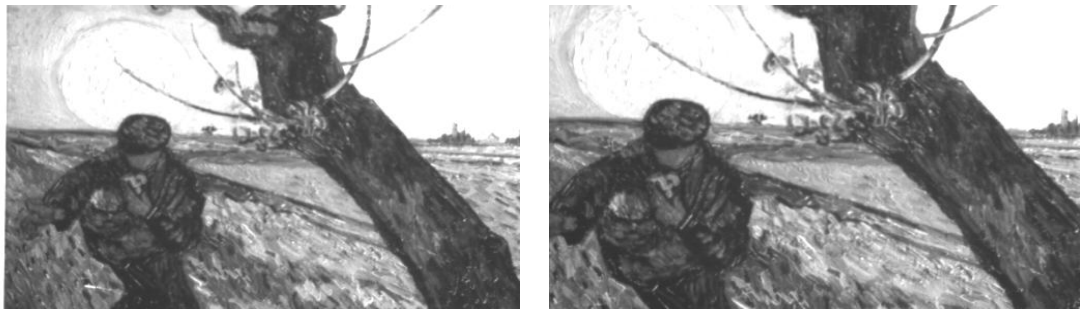

Figure 6.6: Test image pairs: "VanGogh".

The results of matching ratio are shown in Figs. 6.7-6.11. From the results, we see that the proposed LGWTSMM method achieves overwhelming advantages over the other four methods. The other four methods have comparable performance. The proposed improved Harris detector has no obvious advantages than Harris detector. There may be due to two reasons. First, it is not optimal for the proposed strategy of taking corners from different scales. Second, the adopted matching algorithm has already included a scaling factor. Thus, the advantage of the improved method is not obvious in the stereo matching system. For the proposed LGWTOI method, only the location of the detected corners is used in the evaluation. The orientation information of the detected corners could be a constraint in stereo matching system, which should be an advantage of the orientation based method.

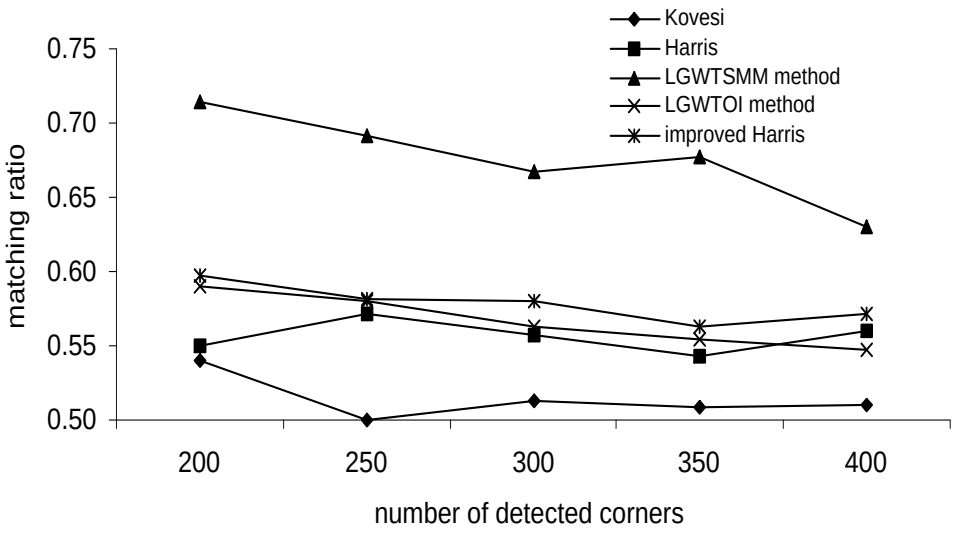

Figure 6.7: Matching results of "Venus".

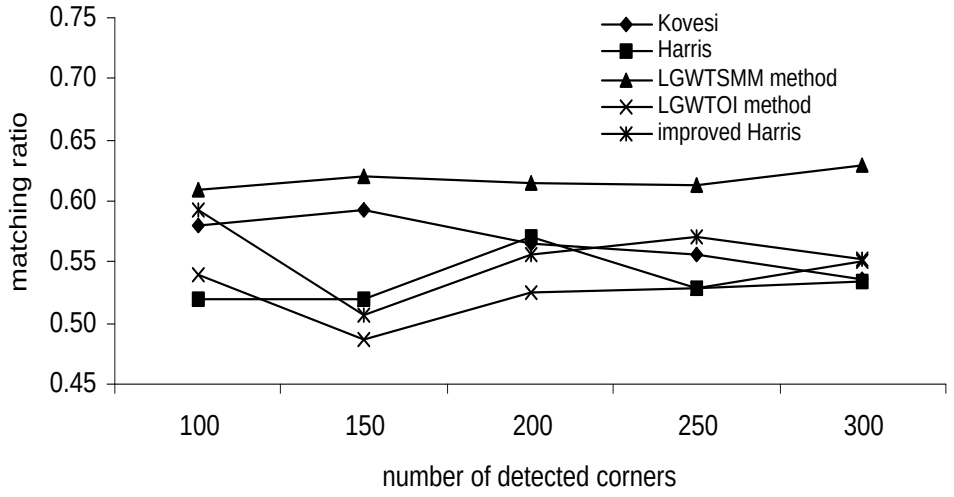

Figure 6.8: Matching results of "Tsukuba".

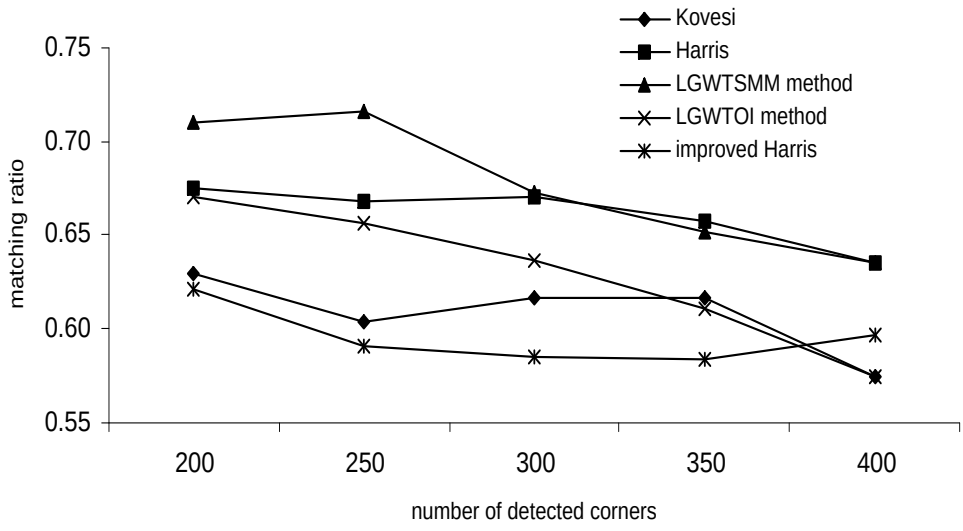

Figure 6.9: Matching results of "Sawtooth".

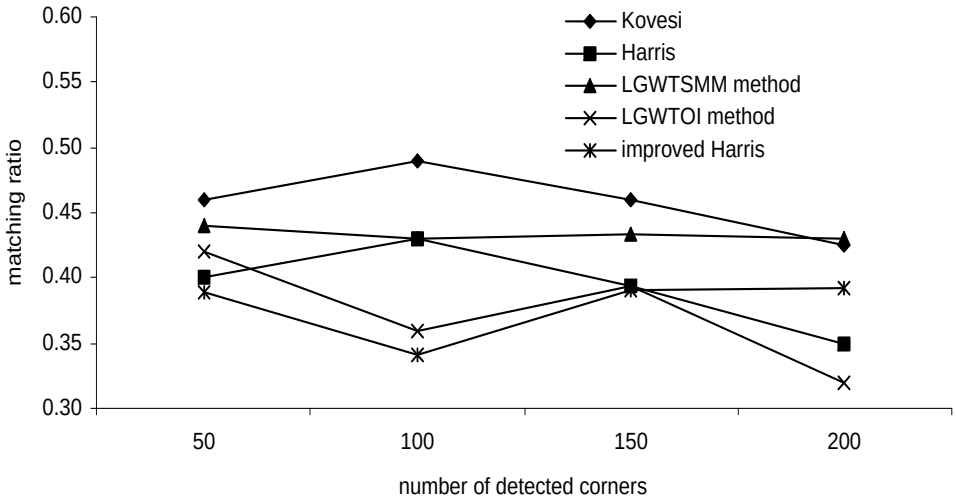

Figure 6.10: Matching results of "Map".

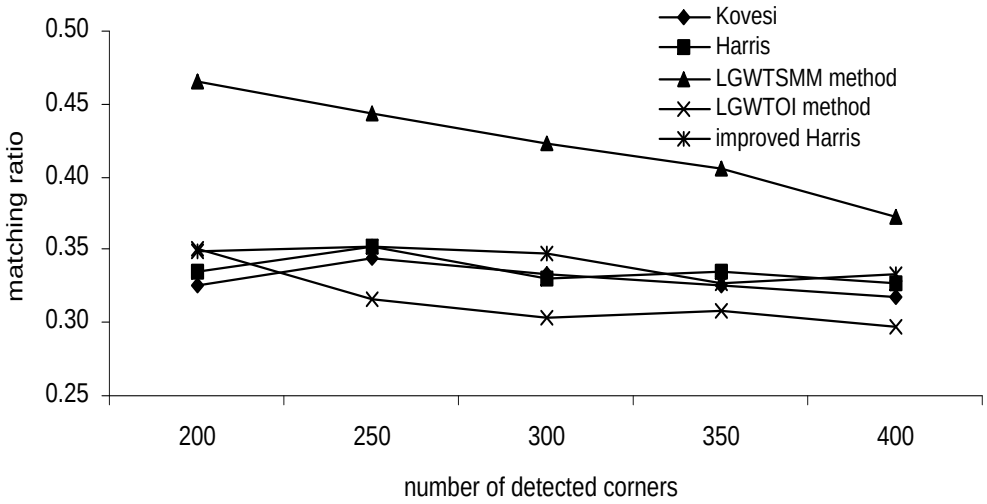

Figure 6.11: Matching results of "VanGogh".

6.6 Discussions and conclusions

As no standard objective evaluation method exists for the corner detection methods of gray level images, we adopt the application based evaluation using a classical stereo matching system. The advantage of this evaluation is that we avoid to define the ground-truth, which is not a trivial problem. However, the disadvantage of the evaluation is that it is application-dependent, which may be suitable for some specific methods.

In the chapter, the normalized 8-point stereo matching algorithm is utilized, which evaluates the proposed improved Harris detector, LGWTOI method, LGWTSMM method, Harris detector and Kovesi's detector. The matching ratio shows that the proposed LGWTSMM method achieves the best results. The proposed improved Harris detector has no obvious advantages than Harris detector in this application based evaluation. The two possible reasons can be found. For the proposed LGWTOI method, only the location of the detected corners is used in the evaluation. The orientation information of the detected corners could be an extra constraint in a stereo matching system, which could be an advantage of the orientation based method.

In this thesis, only one classical stereo matching method is used to evaluate the performance of the DICD methods. If several stereo matching methods are adopted and the results are consistent, the evaluation will be more persuasive. Considering this point, the human perception based evaluation is also applied to the DICD methods. The algorithms IV and V achieve a little better results. The details will be found in Appendix C.2.

Chapter 7

Conclusions and Future Works

7.1 Conclusions

Being a low level image processing step, corner detection is still paid much attention and has a wide applications. Based on the review, we propose five algorithms that partially or fully solve the three problems as stated in chapter 1, i.e., (1) detection based on incomplete information; (2) delocalization; (3) multiple responses to higher order structures. Our research mainly focuses on the CCD methods and DICD methods.

7.1.1 CCD methods

Although corner detection is an important issue in computer vision and image processing, the classification and comparison among various existing corner detection methods on contour images have not been addressed before. In this thesis, we provide an overview of the existing corner detection methods for contour images including classification, comparison and performance evaluation.

The advantages and disadvantages of each type of methods are also discussed. From the review, we can conclude that there are three important components in CCD methods which are inter-linked: the curvature estimation, the natural scale determination and the appropriate smoothing selection. Appropriate smoothing is necessary when determining the natural scale. The curvature estimation should be done at the natural scale with appropriate smoothing.

Based on the review, we propose two new CCD methods (**Algorithm I & II**) based on dyadic WT of the orientation function of a contour image. The maximum decomposition level of the dyadic WT is imposed by the contour length, which makes the algorithm suitable for both long and short contours. Unlike the existing methods, the information at all dyadic scales have been used for detection, which makes the proposed method independent to the type of contour images. For the global based methods, the average of the measurement at all the decomposed scales are taken as the detection measurement. For the local based methods, the local natural scale is determined more accurately and the measurement at the local natural scale is used as the detection measurement. The two methods are also computationally efficient due to the fast implementation of the dyadic WT. Both subjective and objective evaluation illustrates the better performance of the proposed corner detectors compared with the conventional methods.

CCD methods have many advantages. This kind of methods generally has high detection rate and accurate localization. Furthermore, it simplifies the 2D detection into a 1D detection. However, the simplification from 2D to 1D is also a major drawback of this kind of methods. The detection is dependent on the performance of the preprocessing steps: edge detection and contour tracing.

Moreover, even if the preprocessing steps are perfect, CCD method still cannot detect corner points that are not on an edge, e.g., a single blob or a salt-and-pepper texture. Consequently, we proposed DICD methods to overcome these problems.

7.1.2 DICD methods

In chapter 4, we propose an improvement of Harris corner detection (**Algorithm III**) . The proposed algorithm addresses the following problems existing in Harris detector.

• The proposed multiscale algorithm detects the corner points at multiscales. At small scales, details of the structure in the image are captured. At large scales, the general feature of the structure is obtained [66]. Thus, the corners detected by the proposed algorithm obtain more complete information of the images.

• The proposed algorithm simplifies the setting of parameters. As the corners are detected at different scales, we can set the size of the non-maximum suppression window according to the size of the Gaussian kernel used in scale-space transformation. We also take the number of corners expected to be detected at each scale as the threshold, which simplifies the parameter setting and is convenient for the following application.

• To address the delocalization problem, we detect the corners from small scale to large scale. Corners detected at small scale have relatively better localization. After all the detections, we track back from large scale to small scale to obtain the accurate localization.

Experimental results show that this new method is efficient. It also simplifies the parameter setting and solves the delocalization problem existed in Harris detector. Moreover, this proposed scheme can be applied to other spatial corner detection methods to improve their performances as well.

The improved method has solved the first two problems that exist in the Harris detector, i.e., detection based on incomplete information and delocalization. For the third problem (i.e., multiple responses to higher order structures), the Harris detector can not solve it, neither does the improved method.

To solve all the three problems thoroughly, we propose two multiscale corner detection methods based on log-Gabor WT (**Algorithm IV & V**). Experimental results show that the new methods are efficient. The localization is improved by utilizing the optimal localization property of the log-Gabor WT. In the first proposed algorithm, the multi-orientation information is applied directly to detect corners. To achieve isotropic response, the second method exploits the multi-orientation decomposition of log-Gabor WT and constructs the second moment matrix. The smaller eigenvalue of the second moment matrix is used to detect corners. Both of the methods keep a unique response for the higher order structure corners. Simulation results compare the proposed methods with the two existing well-known approaches and show the good performance of the proposed methods.

To evaluate the proposed DICD methods (Algorithm III, IV and V) quantitatively, we utilize a stereo matching system to do the application based evaluation. The results demonstrate the potential advantages of the proposed methods. Compared to Harris detector, the drawback of the proposed log-Gabor WT based methods is the more computational load that is mainly due to the

log-Gabor WT. However, the computational power today is enhanced much more than that of the time when Harris detector was proposed, which makes the drawback a trivial problem.

In summary, the CCD methods need prior segmentation, thus, it should be suitable for the applications where the objects in the images are easy to be segmented, such as cartoon images. It can also be applied in the computer graphics system that has the contour image as the input [8, 9]. For the DICD methods, it has wider applications in computer vision systems.

7.2 Future works

Although the work presented in this thesis achieves satisfactory results, it may be extended in different directions. Some possible future research and open questions are listed below.

• In the proposed CCD algorithms, we normalize the coefficients at each scale with the maximum value. Other normalization method could be proposed and tested. To apply the CCD methods to the gray level image, the prior segmentation and boundary tracking algorithms need to be explored further.

CCD methods can be applied directly on the contour images. So the application could be some symbol recognition based on corner points. Combine both edge detection and corner detection, CCD methods also could be used in the stereo matching problem, which could take the advantages of both the feature based matching methods and the area based matching methods.

• The evaluation in the stereo matching system shows that the improved Harris detector cannot always achieve better results. It may be due to the strategy we adopt to take the corners at different scales. Other better strategy could be explored.

• For the log-Gabor based methods, the advantage of the orientation based method is not taken in the application of stereo matching. A suitable stereo matching system that exploits the orientation information of the detected corners should improve the performance.

As the proposed orientation based method provides the magnitudes along the principal axes, this method is useful also for affine invariant detection applications. In the future work, we will exploit these information to develop an

affine invariant corner detector and apply it in some matching applications, e.g., in stereo matching.

- Evaluation of corner detection algorithms is still an open question. In this thesis, we apply Rosin's method to evaluate the CCD algorithms. For the DICD methods, we utilize the application based evaluation with a stereo matching system. However, a unique evaluation strategy and some benchmark database are still in demand.

Appendices

Appendix A

Chain code of the test contour images

Suppose that the digital curve, C, is defined as a sequence of integer-coordinate points $p_1, \cdots, p_n$, where p_{i+1} is a neighbor of p_i (modulo n), $1 \leq i \leq n$. Relative to p_i, p_{i+1} has eight possible locations, i.e., the curve at the ith point has eight possible directions. Each direction can be represented by an integer, f, $(0 \leq f \leq 7)$ as illustrated in Fig. A.1, where $f\pi/4$ is the angle between the X-axis and the direction. The Freeman chain code is the representation of the curve by the sequence of the integer that labels the direction [125].

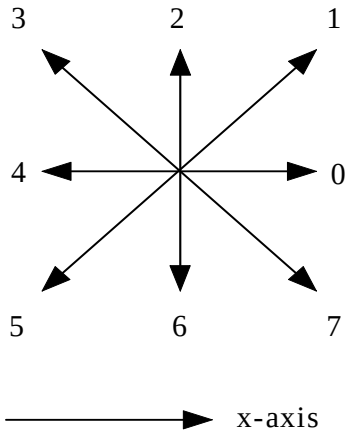

Figure A.1: Freeman code (8-directional chain code representation).

Chain code of the "figure-8" curve shown in Fig. 2.2(a) is as follows.

7 6 7 7 6 7 7 0 0 7 1 0 1 2 1 2 2 2 3 4 4 4 5 5 5 5 5 6 5 4

5 5 4 5 3 4 2 2 1 1 2 1 1 2 1

Chain code of the "chromosome" curve shown in Fig. 2.3(a) is as follows.

5 5 4 5 4 3 2 0 1 1 0 1 1 1 1 1 2 1 1 2 1 2 0 0 6 6 5 6 5 5

6 0 0 1 0 1 0 7 6 5 5 5 4 5 5 5 5 5 5 5 5 5 4 3 1 1 2 1 2 2

Chain code of the "semicir" curve shown in Fig. 2.4(a) is as follows.

0 0 0 0 7 0 0 7 7 7 7 7 6 6 7 6 6 6 6 6 6 5 7 6 7 6 6
5 6 4 5 4 4 3 4 3 6 6 6 6 5 6 5 5 4 5 4 4 4 4 3 4 3 3 2 3 2
2 2 2 5 4 5 4 4 3 4 2 3 2 2 1 2 1 3 2 2 2 2 2 2 2 1 2 2 1
1 1 1 1 1 0 0 1 0 0 0 0

Chain code of the "leaf" curve shown in Fig. 2.5(a) is as follows.

3 3 3 3 2 3 0 7 0 0 0 0 3 3 2 3 2 3 0 7 0 0 0 0 3 3 2 3 2 2
2 6 7 7 7 2 2 2 1 2 7 6 6 6 1 1 1 1 1 6 6 6 5 6 6 5 5 0 0 0
1 0 0 5 6 6 5 6 5 5 0 0 1 1 0 6 6 5 6 5 6 5 5 5 5 5 5 6 6 6 7
6 6 6 6 6 6 6 6 6 4 2 2 2 2 2 2 2 2 2 2 2 3 2 2 4 4 3 4 3 3

Appendix B

Coefficients of the mirror filters of the Quadratic Spline Wavelet

The filter coefficients of the Quadratic Spline Wavelet is shown in Table B.1. H is the low pass filter and G is the high pass filter.

Table B.1: The filter coefficients of the quadratic spline wavelet.

n	H	G
-1	0.125	
0	0.375	-2.0
1	0.375	2.0
2	0.125	

Appendix C

Perceptual Evaluation for Corner Detection

C.1 Contour Corner Detection (CCD) Evaluation based on Human Perception

We have 11 helpers to mark the fish contour images. The helpers are not familiar with corner detection field. They are just told to mark the high curvature points on the contour images. When grouping the results marked by the helpers, it is found that the results are quite diverse and some of them are just mark some minor changes in the curve, for example, in fig. C.1, a lot of minor changes (due to quantization error or noise) is marked as corners. Due to the above facts, the points that are marked by more than 2 helpers are taken as corners. The parameters in the algorithms are set to a range and the best results are selected. The best results are defined as the minimum false detection which includes both the miss and the false alarm.

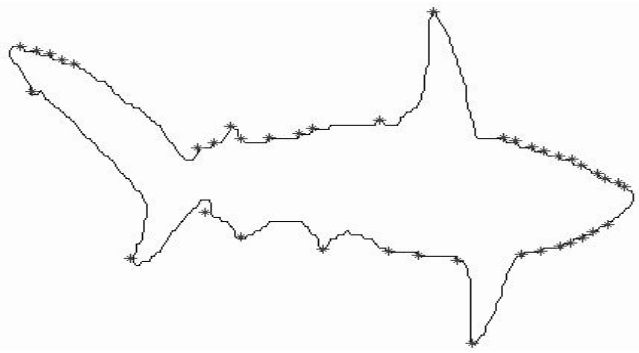

Figure C.1: One example of the corners marked by one of the helpers. The corners are indicated by '$*$'.

In Tables C.1 - C.4, the best results of the two proposed algorithms, Quddus-Gabbouj's algorithm and He-Yung's algorithm are listed. For the two proposed algorithms and Quddus-Gabbouj's algorithm, only the threshold needs to be adjusted, while for He-Yung, the 3 parameters are adjusted to get the best results. From the results, we can see that the four methods achieve comparable performance.

Table C.1: Results based on Human Perception for the proposed Algorithm I on the images shown in figure 3.9.

Images	fig. 3.9(a)	fig. 3.9(b)	fig. 3.9(c)	fig. 3.9(d)
Threshold	0.10	0.18	0.12	0.08
Marked Corner	18	22	21	60
Detected Corner	20	18	21	61
Hit	17	14	21	55
False Alarm	3	4	0	6
Miss	1	8	0	5
Total False	4	12	0	11

Table C.2: Results based on Human Perception for the proposed Algorithm II on the images shown in figure 3.9.

Images	fig. 3.9(a)	fig. 3.9(b)	fig. 3.9(c)	fig. 3.9(d)
Threshold	0.32	0.40	0.30	0.25
Marked Corner	18	22	21	60
Detected Corner	17	16	21	61
Hit	15	13	21	56
False Alarm	2	3	0	5
Miss	3	9	0	4
Total False	5	12	0	9

Table C.3: Results based on Human Perception for Quddus-Gabbouj's algorithm on the images shown in figure 3.9.

Images	fig. 3.9(a)	fig. 3.9(b)	fig. 3.9(c)	fig. 3.9(d)
Threshold	0.14	0.28	0.22	0.28
Marked Corner	18	22	21	60
Detected Corner	17	21	21	56
Hit	15	16	21	54
False Alarm	2	5	0	2
Miss	3	6	0	6
Total False	5	11	0	8

Table C.4: Results based on Human Perception for the proposed Algorithm I on the images shown in figure 3.9.

Images	fig. 3.9(a)	fig. 3.9(b)	fig. 3.9(c)	fig. 3.9(d)
T	1.3	1.5	1.3	1.1
C	165	150	150	155
Sig	3	3	3	2
Marked Corner	18	22	21	60
Detected Corner	16	20	20	57
Hit	15	16	20	55
False Alarm	1	4	0	2
Miss	3	6	1	5
Total False	4	10	1	7

C.2 Direct Intensity Based Corner Detection (DICD) Evaluation based on Human Perception

For the gray level test images, i.e., the "model" image and the "lab" image, the helpers are told to mark the high intensity variation points. The results marked by the helps are diverse too, despite the fact that the two images are full of rectangular objects. For example, for the "model" images, no points have been marked by all the 11 helpers. Thus, in this part of work, we take all the marked points as corners. As there are no minimum false detection can be found in the simulation results, the comparison is made on the selected specific number of detected points, say, 400 points. Table C.5 shows the results. The two parameters of the Harris detector, the sizes of the Gaussian window and nonmaximum suppression window, are adjusted to get the best results. From the results, we can see that the proposed algorithms IV and V achieve slightly better performance. But all the performance is not satisfactory despite the promising visual results demonstrated in the thesis. It may be due to the following possible reasons. Firstly, corners are detected for the usage of the computer, not for human being to perceive. Thus, it is hard to get a good set of "corners" from the humans. Secondly, the localization of the marked points may not be optimal. If we increase the distance threshold from 10 to 15, the performance will be better.

Table C.5: Results based on Human Perception for the DICD Algorithms on the 'lab' image shown in fig 4.5.

Algorithms	Proposed III	Proposed IV	Proposed V	Kovesi	Harris
Marked Corner	202	202	202	202	202
Detected Corner	400	400	400	400	400
Hit	76	93	93	88	78
False Alarm	324	307	307	312	322
Miss	126	109	109	114	124
Total False	450	416	416	426	446

C.3 More Comments on Perception Based Evaluation

The corners marked by the helpers are not complete both for the contour images and "lab" image. For example, in the "lab" image, there are totally 202 points that are marked as corners, but in fact, by visually examining the image, we can find some points that belong to the sharp change of rectangle are not marked, not even to say some "round/subtle" corners. False Alarm in the above evaluations is defined as the points that are detected by the algorithms but not marked by the helpers. In this point of view, the better results achieved by the algorithm VI and algorithm V may be due to the inconsistency of the human perception.

Author's Publications

Journals

1. Xinting Gao, Farook Sattar, Azhar Quddus and Ronda Venkateswarlu, Multiscale Corner detection of contour images using wavelet transform, *SPIE, Journal of Electronic Imaging.* Vol. 14, No. 4, 2005.

2. Xinting Gao, Farook Sattar, Azhar Quddus and Ronda Venkateswarlu, Contour corner detection based on local natural scale and wavelet transform, *Image and Vision Computing, in press.*

3. Xinting Gao, Farook Sattar and Ronda Venkateswarlu, An overview of corner detection methods for contour images, *IEEE Trans. Systems, Man and Cybernetics, Part A, submitted.*

4. Wenbo Zhang, Xinting Gao, Eric Sung, Farook Sattar, and Ronda Venkateswarlu, A feature-based matching system: MPCD and robust matching strategy, *Pattern Recognition Letters, accepted.*

5. Xinting Gao, Wenbo Zhang, Zhuliang Yu, Farook Sattar, Ronda Venkateswarlu and Eric Sung, An improvement of Harris corner detector based on scale-space theory, *SPIE Optical Engineering, submitted.*

6. Xinting Gao, Farook Sattar and Ronda Venkateswarlu, Log-Gabor wavelet transform based corner detection of gray level images, *IEEE Trans. on Circuits and Systems for Video Technology, resubmitted after minor revision.*

Conferences

1. Farook Sattar and Xinting Gao, "Image enhancement based on a nonlinear multiscale method using dual-tree complex wavelet transform," *IEEE Pacific Rim Conference on Communications Computers and Signal Processing (PacRim'03)*, Victoria, B.C., Canada, volume 2, pages 716 - 719, 28-30 Aug., 2003

2. Xinting Gao, Farook Sattar, Azhar Quddus and Ronda Venkateswarlu, Corner detection of contour images using continuous wavelet transform,

Proceedings of the 2003 Joint Conference of the Fourth International Conference on Information, Communications and Signal Processing and the Fourth Pacific Rim Conference on Multimedia (ICICS-PCM'03), Singapore, volume 2, Pages 724 - 728, 15-18 Dec. 2003.

3. Xinting Gao, Farook Sattar and Ronda Venkateswarlu, Corner detection of gray level images using Gabor wavelets, *IEEE International Conference on Image processing (ICIP'04)*, Singapore, pages 2669-2672, Oct., 2004.

4. Xinting Gao, Zhuliang Yu, Farook Sattar, and Ronda Venkateswarlu, Multiscale corner detection for gray level images using Plessey method, *the 8th International Conference on Control, Automation, Robotics and Vision (ICARCV'04)*, Kunming, China, pages 363-368, 6-9th, Dec. 2004.

5. Wenbo Zhang, Xinting Gao, Eric Sung, Farook Sattar, and Ronda Venkateswarlu, A robust feature-based matching of two uncalibrated images, *the 8th International Conference on Control, Automation, Robotics and Vision (ICARCV'04)*, Kunming, China, pages 1522-1527, 6-9th, Dec. 2004.

6. Xinting Gao, Farook Sattar, Azhar Quddus and Ronda Venkateswarlu, Local natural scale based contour corner detection using wavelet transform, *Fifth International Conference on Information, Communications and Signal Processing (ICICS'05)*, Bangkok, Thailand, 6-9 December 2005.

7. Xinting Gao, Wenbo Zhang, Farook Sattar, and Ronda Venkateswarlu, Scale-space based corner detection for gray level images using Plessey method, *Fifth International Conference on Information, Communications and Signal Processing (ICICS'05)*, 6-9 December 2005, Bangkok, Thailand, 6-9 December 2005.

8. Xinting Gao, Farook Sattar, and Ronda Venkateswarlu, Corner detection of gray level images based on log-Gabor wavelet transform, *2007 IEEE International Conference on Acoustics, Speech, and Signal Processing(ICASSP'07), accepted.*

Bibliography

[1] F. Chabat, G. Z. Yang, and D. M. Hansell. A corner orientation detector. *Image and Vision Computing*, 17:761–769, 1999.

[2] A. Quddus, F. A. Cheikh, and M. Gabbouj. Content-based object retrieval using maximum curvature points in contour images. In *Proc. of SPIE/EI'2000 Symposium on Storage and Retrieval for Media Databases 2000*, pages 23–28, San Jose, California, USA, Jan. 23-38 2000.

[3] P. L. Rosin. Note measuring corner properties. *Computer Vision and Image Understanding*, 73:291–307, 1999.

[4] F. Shen and H. Wang. Corner detection based on modified Hough transform. *Pattern Recognition Letters*, 23:1039–1049, 2002.

[5] K. Mikolajczyk. *Detection of Local Features Invariant to Affine Transformations: Application to matching and Recognition*. D.Phil. thesis, Institut National de Polytechniques de Grenoble, 2002.

[6] K. Rangarajan, M. Shah, and D. V. Brackle. Optimal corner detector. *Computer Vision, Graphics, and Image Processing 48*, pages 230–245, 1989.

[7] A. Singh and M. Shneier. Gray level corner detection a generalization and a robust real time implementation. *Computer Vision, Graphics, and Image Processing*, 51:54–69, 1990.

[8] V. Solachidis and I. Pitas. Watermarking polygonal lines using fourier descriptors. *IEEE Computer Graphics and Applications*, pages 44–51, May/Jun. 2004.

[9] L. F. Costa and R. M. Cesar Jr. *Shape Analysis and Classification: Theory and Practice*. CRC Press, Boca Raton, USA, 2001.

[10] P. L. Rosin. Techniques for assessing polygonal approximations of curves. *IEEE Trans. on Pattern Analysis and Machine Intelligence*, 19(6):659–666, Jun. 1997.

[11] R. Hartley and A. Zisserman. *Multiple View Geometry in Computer Vision*. Cambridge University Press, 2004.

[12] F. Mokhtarian and R. Suomela. Robust corner detection through curvature scale space. *IEEE Trans. on Pattern Analysis and Machine Intelligence*, 20:1376–1381, 1998.

[13] Z. Zheng, H. Wang, and E. K. Teoh. Analysis of gray level corner detection. *Pattern Recognition Letters*, 20:149–162, 1999.

[14] J. J. Koenderink. The structure of images. *Biological Cybernetics*, 50:363–370, 1984.

[15] F. Attneave. Some informational aspects of visual perception. *Psychological Review*, 61(3):183–193, 1954.

[16] M. Marji and P. Siy. A new algorithm for dominant points detection and polygonization of digital curves. *Pattern Recognition*, 36:2239–2251, 2003.

[17] J. P. Antoine, D. Barache, R.M. Cesar Jr., and L. F. Costa. Shape characterization with the wavelet transform. *Signal Processing 62*, pages 265–290, 1997.

[18] A. Garrido, N. Pérez de la Blanca, and M. Garcia-Silvente. Boundary simplification using a multiscale dominant-point detection algorithm. *Pattern Recognition*, 31(6):791–804, 1998.

[19] A. Quddus, F. A. Cheikh, and M. Gabbouj. Wavelet-based multi-level object retrieval in contour images. In *Proc. of the International Workshop on Very Low Bit Rate Video Coding (VLBV'99)*, Kyoto, Japan, Oct. 29-30 1999.

[20] F. A. Cheikh, A. Quddus, and M. Gabbouj. Contour-based object recognition using wavelet-transform. In *X European Signal Processing Conference, Eusipco-2000,*, Tampere, Finland, Sept. 5-8 2000.

[21] F. A. Cheikh, A. Quddus, and M. Gabbouj. Multi-level shape recognition based on wavelet-transform modulus maxima. In *Proc. of the Southwest Symposium on Image Analysis and Interpretation, SSIAI*, pages 8–12, Austin, Texas, USA, Apr. 2-4 2000.

[22] F. Mohanna and F. Mokhtarian. Fusion of corners from multiple scales for robust tracking. In *Proc. International Conference on Computer Vision Pattern Recognition and Image Processing (part of Proc. Joint Conference on Information Sciences*, volume 1, pages 765–768, Durham, North Carolina, 2002.

[23] A. M. G. Pinheiro, E. Izquierdo, and M. Ghanbari. Shape matching using a curvature based polygonal approximation in scale-space. In *International Conference on Image Processing(ICIP)*, volume 3, Vancouver, B.C., Sept. 2000.

[24] C. H. Teh and R. T. Chin. On the detection of dominant points on digital curves. *IEEE Trans. on Pattern Analysis and Machine Intelligence*, 11(8):859–872, Aug. 1989.

[25] J. Perez and E. Vidal. Optimum polygonal approximation of digitized curves. *Pattern Recognition Letters*, 15:743–750, Aug. 1994.

[26] J. Horng. Improving fitting quality of polygonal approximation by using the dynamic programming technique. *Pattern Recognition Letters 23*, pages 1657–1673, 2002.

[27] P. Cornic. Another look at the dominant point detection of digital curves. *Pattern Recognition Letters 18*, pages 13–25, 1997.

[28] F. Mokhtarian and A. Mackworth. Scale-based description and recognition of planar curves and two-dimensional shapes. *IEEE Trans. on Pattern Analysis and Machine Intelligence*, 8(1):34–43, Jan. 1986.

[29] W. Wu. A dynamic method for dominant point detection. *Graphical Models*, 64:304–315, 2003.

[30] K. Sohn, W. E. Alexander, J. H. Kim, and W. E. Snyder. A constrained regularization approach to robust corner detection. *IEEE Trans. on Systems, Man, and Cybernetics*, 24(5):820–828, May 1994.

[31] M. Worring and A. W. M. Smeulders. Digital curvature estimation. *Computer Vision, Graphics and Image Processing (CVGIP): Image Understanding*, 58(3):366–382, Nov. 1993.

[32] P. L. Rosin. Determining local natural scales of curves. *Pattern Recognition Letters*, 19:63–75, 1998.

[33] P. L. Rosin. Representing curves at their natural scales. *Pattern Recognition*, 25(11):1315–1325, 1992.

[34] A. Quddus and M. Gabbouj. Wavelet-based corner detection technique using optimal scale. *Pattern Recognition Letters*, 23:215–220, 2002.

[35] A. Rosenfeld and E. Johnston. Angle detection on digital curves. *IEEE Trans. Computers*, 22:875–878, 1973.

[36] A. Rosenfeld and J. S. Weszka. An improved method of angle detection on digital curves. *IEEE Trans. Computers*, 24:940–941, 1975.

[37] H. Freeman and L. S. Davis. A corner finding algorithm for chain-coded curves. *IEEE Trans. Computers*, 26:297–303, 1977.

[38] H. L. Beus and S. S. H. Tiu. An improved corner detection algorithm based on chain-coded plane curves. *Pattern Recognition*, 20:291–296, 1987.

[39] D. Chetverikov and Z. Szabo. A simple and efficient algorithm for detection of high curvature points in planar curves. In *Proc. 23rd Workshop of the Australia Pattern Recognition Group*, pages 175–184, Steyr, Australia, 1999.

[40] I. M. Anderson and J. C. Bezdek. Curvature and tangential deflection of discrete arcs: a theory based on the commutator of scatter matrix pairs and its application to vertex detection in planar shape data. *IEEE Trans. on Pattern Analysis and Machine Intelligence*, 6(1):27–40, Jan. 1984.

[41] Q. Ji and R. M. Haralick. Breakpoint detection using covariance propagation. *IEEE Trans. on Pattern Analysis and Machine Intelligence*, 20(8):845–851, Aug. 1998.

[42] D. Tsai, H. Hou, and H. Su. Boundary-based corner detection using eigenvalues of covariance matrices. *Pattern Recognition Letters*, 20:31–40, Jan. 1999.

[43] C. Yeh. Wavelet-based corner detection using eigenvectors of covariance matrices. *Pattern Recognition Letters*, 24:2797–2806, Nov. 2003.

[44] M. J. Wang, W. Wu, L. Huang, and D. Wang. Corner detection using bending value. *Pattern Recognition Letters 16*, pages 575–583, 1995.

[45] J. Basak and D. Mahata. A connectionist model for corner detection in binary and gray images. *IEEE Transactions on Neural Networks*, 11(5):1124–1132, Sept. 2000.

[46] X. Zhang and D. Zhao. A parallel algorithm for detecting dominant points on multiple digital curves. *Pattern Recognition*, 30(2):239–244, 1997.

[47] L. Li and W. Chen. Corner detection and interpretation on planar curves using fuzzy reasoning. *IEEE Trans. on Pattern Analysis and Machine Intelligence*, 21(11):1204–1210, Nov. 1999.

[48] M. A. Fischler and H. C. Wolf. Locating perceptually salient points on planar curves. *IEEE Trans. on Pattern Analysis and Machine Intelligence*, 16(2):113–129, Aug. 1994.

[49] A. P. Witkin. Scale space filtering: a new approach to multi-scale description. *Chapter 3 of the book: Image Understanding*, pages 79–95, 1984.

[50] D. Langridge. On the computation of shape. *Frontiers of Pattern Recognition, S. Watanabe, Ed. New York: Academic*, pages 347–365, 1972.

[51] B. K. Ray and K. S. Ray. Detection of significant points and polygonal approximation of digitized curves. *Pattern Recognition Letters*, 13:443–452, Jun. 1992.

[52] B. K. Ray and K. S. Ray. An algorithm for detection of dominant points and polygonal approximation of digitized curves. *Pattern Recognition Letters*, 13:849–856, Dec. 1992.

[53] A. Bandera, C. Urdiales, F. Arrebola, and F. Sandoval. Corner detection by means of adaptively estimated curvature function. *Electronics Letters*, 36(2):124–126, Jan. 2000.

[54] P. Reche, C. Urdiales, A. Bandera, C. Trazegnies, and F. Sandoval. Corner detection by means of contour local vectors. *Electronics Letters*, 38(14):699–701, 4 Jul. 2002.

[55] C. Urdiales, C. Trazegnies, A. Bandera, and F. Sandoval. Corner detection based on adaptively filtered curvature function. *Electronics Letters*, 39(5):426–428, Mar. 2003.

[56] W. Wu. Dominant point detection using adaptive bending value. *Image and Vision Computing 21*, pages 517–525, 2003.

[57] D. S. Guru and R. Dinesh. Non-parametric adaptive region of support useful for corner detection: A novel approach. *Pattern Recognition*, 37(1):165–168, 2004.

[58] W. Wu. An adaptive method for detecting dominant points. *Pattern Recognition*, 36:2231–2237, 2003.

[59] N. Ansari and K. Huang. Non-parametric dominant point detection. *Pattern Recognition*, 24(9):849–862, 1991.

[60] N. Ansari and E. J. Delp. On detecting dominant points. *Pattern Recognition*, 24(5):441–451, 1991.

[61] P. Saint-Marc, J. Chen, and G. Medioni. Adaptive smoothing: A general tool for early vision. *IEEE Trans. on Pattern Analysis and Machine Intelligence*, 13(6):514–529, Jun. 1991.

[62] M. Chen and R. T. Chin. Partial smoothing splines for noisy boundaries with corners. *IEEE Trans. on Pattern Analysis and Machine Intelligence*, 15(11):1208–1216, Nov. 1993.

[63] K. Sohn, J. H. Kim, and W. E. Alexander. A mean field annealing approach to robust corner detection. *IEEE Trans. on Systems, Man, and Cybernetics-Part B: Cybernetics*, 28(1):82–90, Feb. 1998.

[64] G. Cong and S. Ma. Corner enhancement in curvature scale space. *Pattern Recognition*, 31(10):1491–1501, 1998.

[65] B. K. Ray and R. Pandyan. Acord−an adaptive corner detector for planar curves. *Pattern Recognition*, 36:703–708, 2003.

[66] J. Babaud, A. P. Witkin, M. Baudin, and R. O. Duda. Uniqueness of the gaussian kernel for scale-space filtering. *IEEE Trans. on Pattern Analysis and Machine Intelligence*, PAMI-8(1):26–33, Jan. 1986.

[67] I. Asada and M. Brady. The curvature primal sketch. In *Proc. 2nd IEEE Workshop Computer Vision: Representation and Control*, 1984.

[68] A. K. Mackworth and F. Mokhtarian. The renormalized curvature scale space and the evolution properties of planar curves. In *Proc. IEEE CVPR*, pages 318–326, Ann Arbor, MI, 1988.

[69] F. Mokhtarian and A. K. Mackworth. A theory of multiscale, curvature-based shape representation for planar curves. *IEEE Trans. on Pattern Analysis and Machine Intelligence*, 14(8):789–805, Aug. 1992.

[70] N. Ansari and E. J. Delp. Partial shape recognition: A landmark-based approach. *IEEE Trans. on Pattern Analysis and Machine Intelligence*, 12(5):470–483, May 1990.

[71] A. Rattarangsi and R. T. Chin. Scale-based detection of corners of planar curves. *IEEE Trans. on Pattern Analysis and Machine Intelligence*, 14(4):430–449, Apr. 1992.

[72] S. Pei and C. Lin. The detection of dominant points on digital curves by scale-space filtering. *Pattern Recognition*, 25(11):1307–1314, 1992.

[73] B. K. Ray and K. S. Ray. Corner detection using iterative gaussian smoothing with constant window size. *Pattern Recognition*, 28(11):1765–1781, 1995.

[74] K. Xin, K. B. Lim, and G. S. Hong. A scale-space filtering approach for visual feature extraction. *Pattern Recognition*, 28(8):1145–1158, 1995.

[75] B. Li. Repeatedly smoothing, discrete scale-space evolution and dominant point detection. *Pattern Recognition*, 29(6):1049–1059, 1996.

[76] Y. Wang, S. L. Lee, and K. Toraichi. Multiscale curvature based shape representation using b-spline wavelets. preprint, Wavelets Strategic Research Programme, NUS, 1997. Available at http://wavelets.math.nus.edu.sg/∼wyp/download papers/shape2.ps.gz.

[77] F. Mokhtarian and F. Mohanna. Enhancing the curvature scale space corner detector. *Proc. Scandinavian Conference on Image Analysis*, pages 145–152, 2001.

[78] C. Fermüller and W. Kropatsch. A syntactic approach to scale-space-based corner description. *IEEE Trans. on Pattern Analysis and Machine Intelligence*, 16(7):748–751, Jul. 1994.

[79] P. V. Sankar and C. V. Sharma. A parallel procedure for the detection of dominant points on a digital curve. *Comput. Graphics Image Processing*, 7:403–412, 1978.

[80] A. Held, K. Abe, and C. Arcelli. Towards a hierarchical contour description via dominant point detection. *IEEE Trans. on Systems, Man, and Cybernetics*, 24(6):942–949, Jun. 1994.

[81] P. Zhu and P. M. Chirlian. On critical point detection of digital shapes. *IEEE Trans. on Pattern Analysis and Machine Intelligence*, 17(8):737–748, Aug. 1995.

[82] X. C. He and N. H. C. Yung. Curvature scale space corner detector with adaptive threshold and dynamic region of support. In *Proc. 17th International Conference on Pattern Recognition (ICPR04)*, volume 2, pages 791–794, August, 2004.

[83] J. Lee, Y. Sun, C. Chen, and C. Tsai. Wavelet based corner detection. *Pattern Recognition*, 26(6):853–865, 1993.

[84] J. Lee, Y. Sun, and C. Chen. Multiscale corner detection by using wavelet transform. *IEEE Trans. on Image Processing*, 4:100–104, 1995.

[85] Y. Nakamura and T. Yoshida. Learning two-dimensional shapes using wavelet local extrema. In *12th ICPR*, volume 3, pages 48–52, 1994.

[86] E. Hussein, Y. Nakamura, and Y. Ohta. Analysis of detailed patterns of contour shapes using wavelet local extrema. In *Proceedings of the 13th International Conference on Pattern Recognition*, volume 2, pages 335 – 339, Aug. 1996.

[87] J. Hua and Q. Liao. Wavelet-based multiscale corner detection. In *WCCC-ICSP 2000. 5th International Conference on Signal Processing Proceedings, 2000.*, volume 1, pages 341–344, 21-25 Aug. 2000.

[88] A. Quddus and M. M. Fahmy. Corner detection using various wavelets. In *Second International Conference on Information, Communications & Signal Processing (ICICS'99),Singapore*, Dec. 1999.

[89] A. Quddus and M. M. Fahmy. Fast wavelet-based corner detection technique. *Electronics Letters*, 35(4):287–288, Feb. 1999.

[90] M. K. Leung and Y. Yang. Dynamic two-strip algorithm in curve fitting. *Pattern Recognition*, 23(1/2):69–79, 1990.

[91] F. Shen. *Camera Self-Calibration From Corner Correspondences*. D.Phil. thesis, Nanyang Technological University of Singapore, 2003.

[92] C. Harris and M. Stephens. A combined corner and edge detector. In *Proceedings of the Fourth Alvey Vision Conference*, pages 147–151, Manchester, 1988.

[93] S. M. Smith and J. M. Brady. Susan-a new approach to low level image processing. *International Journal of Computer Vision 23(1)*, pages 45–78, 1997.

[94] S. M. Smith. *Feature Based Image Sequence Understanding*. D.Phil. thesis, Robotics Research Group, Department of Engineering Science, Oxford University, 1992.

[95] E. R. Davies. *Machine Vision: Theory, Algorithms,Practicalities*. Morgan Kaufmann, 2004.

[96] P. R. Beaudet. Rotational invariant image operators. In *Fourth International Conference on Pattern Recognition*, pages 579–583, 1978.

[97] R. Deriche and G. Giraudon. A computational approach for corner and vertex detection. *The International Journal of Computer Vision*, 10(2):101–124, 1993.

[98] L. Kitchen and A. Rosenfeld. Grey level corner detection. *Pattern Recognition Letters*, pages 95–102, 1982.

[99] Z. O. Wu and A. Rosenfeld. Filtered projections as an aid to corner detection. *Pattern Recognition*, 16(31), 1983.

[100] H. P. Moravec. Towards automatic visual obstacle avoidance. In *In Proceedings of the 5th International Joint Conference on Artificial Intelligence*, page 584, Cambridge, Massachusetts, USA, 1977.

[101] J. A. Noble. Finding corners. *Image and Vision Computing*, 6(2):121–128, May 1988.

[102] A. K. Chan, C. K. Chui, J. Zha, and Q. Liu. Corner detection using spline-wavelets. In *SPIE Proceedings, Curves and Surfaces in Computer Vision and Graphics II*, volume 6610, pages 211–322, Boston, MA, USA, 19-24 Nov. 1991.

[103] P. Fransson. *Using Wavelet to Detect Corner Points in Images*. Master Thesis of Department of Mathematics of Lund Institute of Technology, 1992.

[104] C. Chen, J. Lee, and Y. Sun. Wavelet transformation for gray-level corner detection. *Pattern Recognition*, 28(6):853–861, Jun. 1995.

[105] A. Quddus and M. M. Fahmy. Corner detection using gabor-type filtering. In *Proceedings of the 1998 IEEE International Symposium on Circuits and Systems, ISCAS '99.*, volume 4, pages 150–153, 04 May-3 Jun. 1998.

[106] F. Pedersini, E. Pozzoli, A. Sarti, and S. Tubaro. Multi-resolution corner detection. In *Proceedings of the International Conference on Image Processing*, volume 3, pages 881 – 884, Sept. 2000.

[107] P. Kovesi. Phase congruency detects corners and edges. In *the Australian Pattern Recognition Society Conference: DICTA 2003*, pages 309–318, Sydney, Dec. 2003.

[108] J. Cooper, S. Venkatesh, and L. Kitchen. Early jump-out corner detectors. *IEEE Trans. on Pattern Anal. and Machine Intell.*, 15(8):823–828, Aug. 1993.

[109] S. Ando. Image field categorization and edge/corner detection from gradient covariance. *IEEE Trans. on Pattern Analysis and Machine Intelligence*, 22(2):179–190, Feb. 2000.

[110] E. Sojka. A new algorithm for detecting corners in digital images. In *Proceedings of the 18th Spring Conference on Computer graphics (SCCG)*, pages 55 – 62, New York, 2002.

[111] K. Kohlmann. Corner detection in natural images based on the 2-d Hilbert transform. *Signal Processing*, 48:225 – 234, 1996.

[112] M. A. Ruzon and C. Tomasi. Edge, junction, and corner detection using color distributions. *IEEE Trans. on Pattern Analysis and Machine Intelligence*, 23(11):1281 – 1295, Nov. 2001.

[113] L. Alvarez and F. Morales. Affine morphological multiscale analysis of corners and multiple junctions. *International Journal of Computer Vision*, 25(2):95 – 107, Nov. 1997.

[114] M. Fidrich and J. P. Thirion. Stability of corner points in scale space: the effect of small non-rigid deformations. *Computer Vision and Image Understanding*, 72(1):72 – 83, Oct. 1998.

[115] B. Luo and D. Pycock. Unified multi-scale corner detection. *Proc. Visualization, Imaging and Image Processing*, 2004.

[116] T. Lindeberg. Feature detection with automatic scale selection. *International Journal of Computer Vision*, 30(12):79 – 116, 1998.

[117] K. Mikolajczyk and C. Schmid. Scale and affine invariant interest point detectors. *International Journal of Computer Vision*, 60(1):63–86, 2004.

[118] D. G. Lowe. Distinctive image features from scale-invariant keypoints. *International Journal of Computer Vision*, 60(2):91–110, 2004.

[119] T. Lindeberg. *Scale-Space Theory in Computer Vision*. Kluwer Academic Publishers, 1994.

[120] N. M. Temme. Wavelets: first steps. *in the book edited by Tom H. Koornwinder, Wavelets: An Elementary Treatment of Theory and Applications*, 1993.

[121] S. Mallat. *A Wavelet Tour of Signal Processing*. Academic Press, 1999.

[122] S. Mallat and W. L. Hwang. Singularity detection and processing with wavelets. *IEEE Trans. on Information Theory*, 38(2):617–643, Mar. 1992.

[123] S. Mallat and S. Zhong. Characterization of signal from multiscale edges. *IEEE Trans. on Pattern Anal. and Mach. Intell.*, 14(7):710–732, Jul. 1992.

[124] D. J. Field. Relations between the statistics of natural images and the response properties of cortical cells. *Journal of the Optical Society of America A*, 4(12):2379–2394, Dec. 1987.

[125] H. Liu and M. D. Srinath. Corner detecting from chain-code. *Pattern Recognition*, 23(1/2):51–68, 1990.

[126] L. Florack. *The Syntactical Structure of Scalar Images*. D.Phil. thesis, Universiteit Utrecht, 1993.

[127] J. J. Koenderink and A. Doorn. Receptive field assembly specificity. *J. Vis. Comm. and Im. Process*, 3(1):1–12, 1992.

[128] J. J. Koenderink. What is a feature? *J. Intell. Syst.*, 3(1):49–82, 1993.

[129] J. S. Walker. *A Primer on Wavelets and their Scientific Applications*. Chapman & Hall/CRC, 1999.

[130] J. Fdez-Valdivia, J. A. Garcia, J. Martinez-Baena, and X. R. Fdez-Vidal. The selection of natural scales in 2d images using adaptive gabor filtering. *IEEE Trans. on Pattern Analysis and Machine Intelligence*, 20(5):458–469, May 1998.

[131] B. S. Manjunath and W. Y. Ma. Texture features for browsing and retrieval of image data. *IEEE Trans. on Pattern Analysis and Machine Intelligence*, 18(8):837–842, Aug. 1996.

[132] P. D. Kovesi. MATLAB functions for computer vision and image analysis. School of Computer Science & Software Engineering, The University of Western Australia. Available from: <http://www.csse.uwa.edu.au/∼pk/research/matlabfns/>.

[133] R. Rodriguez-Sanchez, J. A. Garcia, J. Fdez-Valdivia, and X. R. Fdez-Vidal. How to define the notion of microcalcifications in digitized mammograms. In *15th International Conference on Pattern Recognition (ICPR'00)*, volume 1, pages 494 – 499, 2000.

[134] C. Mancas-Thillou and B. Gosselin. Character segmentation-by-recognition using log-gabor filters. In *Proc. of IAPR International Conference on Pattern Recognition (ICPR'06)*, Hong Kong, China, 2006.

[135] T. Hansen. *A Neural Model of Early Vision: Contrast, Contours, Corners and Surfaces— Contributions toward an Integrative Architecture of Form and Brightness Perception.* Ph.D Thesis, University of Ulm, 2002.

[136] P. K. Rajan and J. M. Davidson. Evaluation of corner detection algorithms. In *Twenty-First Southeastern Symposium on System Theory*, pages 29–33, 26-28 March 1989.

[137] K. Rohr. Localization properties of direct corner detectors. *Journal of Mathematical Imaging and Vision*, 4:139–150, 1994.

[138] A. Heyden and K. Rohr. Evaluation of corner extraction schemes using invariance methods. In *International Conference on Pattern Recognition (ICPR)*, pages 895–899, 1996.

[139] C. Schmid, R. Mohr, and C. Bauckhage. Evaluation of interest point detectors. *International Journal of Computer Vision*, 37(2):151–172, 2000.

[140] P. Tissainayagam and D. Suter. Assessing the performance of corner detectors for point feature tracking applications. *Image and Vision Computing*, 22(8):663–679, August 2004.

[141] F. Mokhtarian and F. Mohanna. Performance evaluation of corner detectors using consistency and accuracy measures. *Computer Vision and Image Understanding*, 102(1):81–94, April 2006.

[142] J. Banks, M. Bennamoun, K. Kubik, and P. Corke. An accurate and reliable stereo matching algorithm incorporating the rank constraint. *Symposium on Intelligent Robotic Systems*, pages 23–32, 1999.

[143] S. T. Barnard and M. A. Fischler. Computational stereo. *ACM Computing Surveys (CSUR)*, 14(4):553–572, Dec. 1982.

[144] U. R. Dhond and J. K. Aggarwal. Structure from stereo-a review. *IEEE Trans. on Systems, Man and Cybernetics*, 19(6):1489–1510, Nov.-Dec. 1989.

[145] R. A. Lane and N. A. Thacker. Tutorial: Overview of stereo matching research. Technical report, Tina Memo No.1994-001, Imaging Science and Biomedical Engineering Division, Medical School, University of Manchester, 1994.

[146] D. Scharstein and R. Szeliski. A taxonomy and evaluation of dense two-frame stereo correspondence algorithms. *International Journal of Computer Vision*, 47(1/2/3):7–42, Apr.-Jun. 2002.

[147] M. A. Fischler and R. C. Bolles. Random sample consensus: A paradigm for model fitting with applications to image analysis and automated cartography. *Communications of the ACM*, 24:381–395, Jun. 1981.

[148] G. Xu and Z. Zhang. *Epipolar Geometry in Stereo, Motion and Object Recognition: A Unified Approach*. Kluwer Academic Publishers, 1996.

[149] H. Cantzler. Random sample consensus (ransac). http://homepages.inf.ed.ac.uk/rbf/CVonline/LOCAL_COPIES/CANTZLER2/ransac.pdf.

[150] H. C. Longuet-Higgins. A computer algorithm for reconstructing a scene from two projections. *Nature*, 293:133–135, Sept. 1981.